Structural and functional analysis of the MHC I–tapasin–ERp57 multi-chaperone complex in antigen processing and presentation

Dissertation

zur Erlangung des Doktorgrades

der Naturwissenschaften

vorgelegt dem Fachbereich 14

Biochemie, Chemie und Pharmazie

der Johann Wolfgang Goethe-Universität

in Frankfurt am Main

von

Ines Katharina Müller

aus Marburg an der Lahn

Frankfurt, 2022

(D30)

Vom Fachbereich Biochemie, Chemie und Pharmazie der Johann Wolfgang Goethe-Universität als Dissertation angenommen.

Dekan: Prof. Dr. Clemens Glaubitz

Gutachter: Prof. Dr. Tampé
Zweitgutachter: Prof. Dr. Nina Morgner

Datum der Disputation: 15.12.22

Results and parts of this work were published in:

Mueller I. K., Winter C., Thomas C., Trowitzsch S., Tampé R., Structure of an MHC I–tapasin–ERp57 complex defines chaperone promiscuity. *Nat Commun* **13**, 5383 (2022).

1 Table of contents

2 Declaration

Except where stated otherwise by reference or acknowledgment, the work presented was generated by myself under the supervision of my advisors during my doctoral studies. All contributions from colleagues are explicitly referenced in the thesis. The material listed below was obtained in the context of collaborative research:

TAPBPR$^{\Delta TMD}$ was expressed and purified by Felix Hennig, Tampé laboratory, Institute of Biochemistry, Goethe-University Frankfurt.

Figure 8: Intermolecular disulfide bond and sample quality of tapasin$^{\Delta TMD}$–ERp57^{C36A}. Tapasin$^{\Delta TMD}$–ERp57^{C36A} heterodimer was expressed and purified by me. LC-MS experiments of tapasin$^{\Delta TMD}$–ERp57^{C36A} sample (b-e) were carried out by Christian Winter, Tampé laboratory, Institute of Biochemistry, Goethe-University Frankfurt.

Figure 12: Tapasin$^{\Delta TMD, His6}$–ERp57^{C36A}/calreticulin^{WT} form a trimeric complex. I expressed and purified tapasin$^{\Delta TMD}$–ERp57^{C36A} and both calreticulin samples. LILBID-MS experiments were performed by Dr. Janosch Martin, Morgner laboratory, Institute of Physical and Theoretical Chemistry, Goethe-University Frankfurt.

Figure 18: UV illumination of p*MHC I results in almost complete cleavage of peptide. The refolding and isolation of p*MHC I was carried out by me. Christian Winter, Tampé laboratory, Institute of Biochemistry, Goethe-University Frankfurt, conducted the SEC-coupled MS experiments.

Whenever a figure, table or table is adopted from a previous publication it is explicitly stated.

The following parts of this thesis have been previously published:

Section	Figure	Publication
9.1.1 – 9.2.16	Figure 8a-e, Figure 18, Figure 26, Figure 31-33, Figure 34a-f, Figure 35-40	Müller *et al.* 2022 *Nat Commun*

3 Abstract

The health status of every nucleated cell in the human body is monitored through peptides presented by major histocompatibility complex class I (MHC I) to T-cell receptors of $CD8^+$ T-cells[1,2]. Thereby, the adaptive immune system ensures the recognition and elimination of infected or cancerous cells. MHC I molecules comprise the polymorphic heavy chain (hc) and the light chain β_2-microglobulin (β_2m). More than 13,000 allomorphs of the MHC I hc have been identified. All MHC I hcs associate with β_2m but differ in their binding preferences for peptides, ensuring the presentation of a large peptide pool. After maturation of MHC I hc/β_2m heterodimers in the endoplasmic reticulum (ER), most of the peptide-deficient MHC I molecules are recruited to the peptide-loading complex (PLC)[3]. There, they go through peptide loading and editing before they are released as stable peptide-MHC I (pMHC I) complexes and traffic to the cell surface for antigen presentation[3–5].

During the stringent quality control of MHC I peptide loading and editing within the PLC, the chaperone tapasin in conjunction with the oxidoreductase ERp57 stabilizes peptide-receptive MHC I molecules and alters the peptide cargo for high immunogenicity by catalyzing peptide-exchange[4,6,7]. The tapasin-homologue TAP-binding protein related (TAPBPR) is involved in downstream quality control, editing the peptide repertoire of MHC I molecules that slipped through peptide proofreading by tapasin. Both chaperones were shown to adopt similar binding-modes for MHC I, suggesting related mechanisms of peptide editing[8–12]. Nevertheless, the MHC I specific chaperones operate in different subcellular locations with differing assistance. While TAPBPR mediates peptide-exchange solely in the peptide-poor environment of the *cis*-Golgi and ER-Golgi intermediate compartment (ERGIC)[13], tapasin functions mainly within the PLC together with ERp57 and the lectin-like chaperone calreticulin[3,12]. Calreticulin with its lectin-, arm- and C-terminal domain contacts the MHC I heterodimer, ERp57 and the C-terminal domain of tapasin, respectively[12]. Notably, the interaction site between calreticulin and tapasin has not yet been elucidated experimentally at molecular detail[12]. The depletion of tapasin leads to a compromised immune response and a change in the pool of peptide cargo[14,15]. The numerous MHC I allomorphs vary in their plasticity and their dependence on tapasin for the loading of optimal peptides[16,17]. Moreover, the conformational plasticity of MHC I correlates with their dependence on tapasin[18–21]. However, the molecular basis on how tapasin edits the various MHC I allomorphs and the structural features that are essential for peptide exchange catalysis at atomic resolution remained elusive.

In the first part of this thesis, the trimeric complex of tapasin–ERp57/calreticulin was analyzed. To this end, laser induced liquid bead ionization mass spectrometry (LILBID-MS) was performed as part of a collaboration and revealed the trimeric assembly for tapasin–ERp57

and calreticulin. Furthermore, additional to a wildtype construct of calreticulin, a second construct, lacking the acidic helix of calreticulin that was found to come to close contact with tapasin, was utilized for isothermal titration calorimetry (ITC). A micromolar affinity of wildtype calreticulin to tapasin–ERp57 was determined. Previous biochemical and NMR studies utilizing the P-domain of calreticulin and solely ERp57 provided a micromolar affinity for the complex of calreticulin and ERp57 (ref.[22]). In this study, no interaction of calreticulin lacking the acidic helix with tapasin–ERp57 could be measured by ITC. However, these results undergo with findings that calreticulin lacking the acidic helix impairs the function of the PLC[23]. Most likely, the negatively charged acidic helix is located in a groove of tapasin, carrying a more positive charge[12]. Taken together, the functional data demonstrates the importance of the acidic helix of calreticulin for assembly of the trimeric subunit of calreticulin/tapasin–ERp57.

In the main part of this study an MHC I–tapasin–ERp57 complex was structurally analyzed. Therefore, a photo-triggered approach was chosen to assemble the transient complex of MHC I–tapasin–ERp57. Various allomorphs were screened for complex formation with the tapasin–ERp57 heterodimer after photocleavage by size exclusion chromatography (SEC), resulting in mouse MHC I H2-D^b as the suited allomorph. Microseed matrix screening[24] was performed. Crystals diffracting X-rays to a resolution of 2.7 Å were obtained showing one tetrameric tapasin–ERp57–MHC I complex per asymmetric unit.

The MHC I-chaperone structure shows molecular rearrangements upon MHC I engagement and unveils structural features of tapasin, involved in peptide-exchange catalysis. The N-terminal domain of tapasin embraces the α2-1 helix region of MHC I and the C-terminal domain of tapasin comes to close contact to the α3 domain of MHC I and β_2m. A loop, named editing loop, rigidifies, and is placed on top of the MHC I F-pocket and a β hairpin motif, which swings up towards the β-sheet floor of the MHC I peptide-binding pocket. The F-pocket of MHC I is widened by rearrangements of the α1, and α2-1 helices and the β-sheet floor is distorted.

Furthermore, a flow-cytometry cell-based assay that monitored different levels of MHC I surface expression of cells, expression wildtype tapasin or mutants of tapasin, whereas residues of interaction sites to MHC I or β_2m were exchanged to abrogate binding, was established. Combining the structural and functional data, a dual function for the editing loop was proposed. In a peptide-deficient MHC I state, the loop is involved in widening the F-pocket of MHC I and in an intermediate peptide-chaperone complex the loop might shield the C-terminus of the peptide. The crystal structure of the MHC I–tapasin–ERp57 complex elucidates that both tapasin-dependent and -independent MHC I allomorphs possess the structural requirements to interact with tapasin. The degree of plasticity of MHC I thus their capability to pick up optimal peptides correlates with their association to tapasin.

Taken together, this study provides molecular details and structural features of MHC I recognition and peptide editing of the main chaperone tapasin in conjunction with ERp57. Furthermore, the structure reveals how tapasin engages the numerous MHC I allomorphs and stabilizes them during peptide loading and proofreading.

4 Deutsche Zusammenfassung

Der „Gesundheitszustand“ jeder menschlichen, zellkernhaltigen Zelle wird durch Oberflächen-Präsentation von Peptiden über Klasse I Haupthistokompatibilitätskomplexe (*major histocompatibility complex class I*, MHC I) an T-Zell-Rezeptoren von $CD8^+$ T-Zellen vermittelt[1,2]. Auf diese Weise kann das adaptive Immunsystem infizierte oder krebsartige Zellen erkennen und eliminieren. MHC I Moleküle setzen sich aus einer polymorphen, schweren Kette (*heavy chain*, hc) und einer invarianten, leichten Kette, dem β_2-Mikroglobulin (*β_2-microglobulin*, β_2m), zusammen. Bisher wurden bereits mehr als 13.000 hcs, auch Allomorphe genannt, identifiziert. Sie assoziieren mit β_2m, weisen aber unterschiedliche Bindungspräferenzen für Peptide auf, wodurch die Präsentation eines großen Peptidpools in einer Population gewährleistet wird. Nach der Reifung von MHC I hc/β_2m-Heterodimeren im Endoplasmatischen Retikulum (ER) werden MHC I Moleküle, die über keine Peptide verfügen, zum Peptidbeladungskomplex (*peptide loading complex*, PLC) rekrutiert[3]. Im PLC führt der Prozess des sogenannten Peptideditierens (*peptide editing*) dazu, dass MHC I Moleküle mit optimalen Peptiden beladen werden, welche dann als Peptid-MHC I Komplexe den PLC verlassen und zur Antigenpräsentation an die Zelloberfläche gelangen[3–5].

Während der strengen Qualitätskontrolle der MHC I Peptidbeladung und -bearbeitung innerhalb des PLC, stabilisiert das Hilfsprotein Tapasin, als Disulfid-verbrückter Heterodimer mit der Oxidoreduktase ERp57, unbeladene MHC I Moleküle. Tapasin katalysiert ferner das *peptide editing* und sorgt so für die Selektion und Beladung von MHC I Molekülen mit hochaffinen und immunogenen Peptiden[4,6,7]. Das Homolog von Tapasin, TAPBPR (engl. *TAP-binding protein related*, TAPBPR), ist wahrscheinlich in ähnlicher Weise wie Tapasin an der Qualitätskontrolle von MHC I Molekülen beteiligt, indem es die Peptide von MHC I Molekülen, die dem Editierungsprozess von Tapasin entkommen sind, bearbeitet. Es wurde gezeigt, dass beide Hilfsproteine MHC I Komplexe in ähnlichen Konformationen binden, weshalb vermutet wird, dass sie auch einen ähnlichen Mechanismus für das *peptide editing* anwenden[8–12]. Die beiden Hilfsproteine weisen jedoch unterschiedliche subzelluläre Lokalisierungen auf. Während TAPBPR den Peptidaustausch ausschließlich in der peptidarmen Umgebung des *cis*-Golgi und des ER-Golgi Zwischenkompartiments (*ER/Golgi intermediate compartment, ERGIC*)[13] katalysiert, arbeitet Tapasin hauptsächlich innerhalb des PLC zusammen mit ERp57 und dem Hilfsprotein Calreticulin[3,12]. Calreticulin hat eine zentrale, Lektin-ähnliche Domäne, welche für den Kontakt zum MHC I-Glykan wichtig ist und kontaktiert mit seiner Prolin-reichen Arm-Domäne die Oxidoreduktase ERp57 und mit seiner sauren C-terminalen Domäne das Hilfsprotein Tapasin[12]. Zu erwähnen ist, dass die Interaktion zwischen Calreticulin und Tapasin bisher noch nicht im molekularen Detail beschrieben werden konnte[12].

Die Depletion von Tapasin führt zu einer Beeinträchtigung der Immunantwort und zu einer Veränderung des präsentierten Peptidpools[14,15]. Die zahlreichen MHC I Allomorphe unterscheiden sich in ihrer Plastizität und ihrer Abhängigkeit von Tapasin für die Beladung mit optimalen Peptiden. Darüber hinaus korreliert die konformationelle Plastizität von MHC I mit ihrer Abhängigkeit von Tapasin. Der molekulare Mechanismus des Editierens der verschiedenen Peptid/MHC I-Allomorphe durch Tapasin, sowie die hierzu verwendeten strukturellen Elemente des Hilfsprotein, sind jedoch nicht vollständig beschrieben.

Im ersten Teil dieser Arbeit wurde der Komplex bestehend aus einem disulfidvernetzten Tapasin–ERp57-Heterodimer und dem Protein Calreticulin analysiert. Im Rahmen einer Kollaboration wurde der Aufbau des trimeren Komplexes mittels *laser-induced-liquid-bead ionization* (LILBID)-Massenspektroskopie (MS) bestimmt. Für isothermische Titrationskalorimetrie (ITC) wurde neben dem Wildtyp-Calreticulin eine Deletionsmutante verwendet, bei welcher die saure C-terminale Helix, die die Bindung zu Tapasin vermittelt, entfernt wurde. Es wurde eine mikromolare Affinität von Wildtyp (WT)-Calreticulin zu Tapasin–ERp57 bestimmt. In biochemischen und NMR-Studien, bei denen die Arm-Domäne von Calreticulin und ERp57 (ref.[22]) verwendet wurden, konnte eine Affinität im mikromolaren Bereich zwischen der Arm-Domäne von Calreticulin und ERp57 festgestellt werden[22]. In dieser Arbeit wurde keine Interaktion zwischen der Calreticulin-Deletionsmutante ohne die saure Helix mit Tapasin–ERp57 mittels ITC nachgewiesen. Diese Ergebnisse stehen im Einklang mit den Erkenntnissen, dass Calreticulin, dem die saure Helix fehlt, die Funktion des PLCs beeinträchtigt[23]. Wahrscheinlich befindet sich die negativ geladene Helix in einer Furche von Tapasin, die eine überwiegend positive Ladung trägt[12]. Zusammengefasst zeigen die funktionellen Daten die Bedeutung der sauren Helix von Calreticulin für den Aufbau des trimeren Calreticulin/Tapasin–ERp57 Komplex.

Im Hauptteil dieser Arbeit wurde die Struktur des MHC I–Tapasin–ERp57-Komplex bestimmt. Um den transienten Komplex aufzubauen, wurde ein photoaktivierbarer Ansatz gewählt[11,25]. Verschiedene Allomorphe wurden auf eine Komplexbildung mit dem Tapasin–ERp57 Heterodimer nach Photospaltung durch Größenausschlusschromatographie (*size exclusion chromatography*, SEC) untersucht. Dabei hat sich das Maus-MHC I H2-D^b als geeignetes Allomorph herausgestellt. Da eine homogene Population eines kinetisch stabilen MHC I–Tapasin–ERp57-Komplexes nicht isoliert werden konnte, wurde direkt eine photoaktivierte Mischung aus rückgefaltetem pMHC I und Tapasin–ERp57 für die Kristallisation verwendet. Größenausschlusschromatographie-gekoppelte Massenspektrometrie (SEC-MS) zeigte eine fast vollständige photoinduzierte Spaltung (>96%) des an MHC I gebundenen Peptids. Initial konnten Kristalle der Raumgruppe $P2_12_12_1$ gezüchtet werden, welche zwei heterotetramere Komplexe pro asymmetrische Einheit aufwiesen. Diese Kristalle zeigten allerdings nur eine Auflösung von 4,0 Å. Daraufhin wurde die *microseed matrix screening* (MMS) Methode[24]

angewandt, die zu Kristallen der Raumgruppe $P22_12_1$ führten und einen tetrameren Tapasin–ERp57–MHC I-Komplex pro asymmetrische Einheit zeigten. Diese Kristalle beugten Röntgenstrahlen bis zu einer Auflösung von 2,7 Å.

Wie in der Klienten-freien Struktur von Tapasin–ERp57 (ref.[8]) sind die vier Thioredoxin-ähnlichen Domänen von ERp57 (a-b-b'-a') in ihrer charakteristisch verdrehten U-Form angeordnet, während Tapasin seine typische L-förmige Struktur annimmt. Die a- und a'-Domänen von ERp57 interagieren mit der N-terminalen Region von Tapasin, die aus einer Fusion zwischen einem siebensträndigen β-Fass und einer Immunoglobulin (Ig)-artige Faltung besteht. Im Gegensatz zur Struktur des Klienten-freien Tapasin–ERp57 (ref.[8]) konnte die Disulfidbrücke zwischen Cys95 von Tapasin und Cys33 von ERp57 nicht modelliert werden. Da die Reduktion der Disulfidbrückenbindung nicht durch UV-Bestrahlung erfolgt, die für die Photospaltung des Peptids eingesetzt wird, kann die Reduktion entweder durch die Röntgenbestrahlung begünstigt worden sein oder entsteht durch den MHC I-Editierungsprozess selbst.

Die MHC I-Chaperon-Klienten-Struktur zeigt molekulare Umstrukturierungen durch die MHC I-Bindung und enthüllt strukturelle Merkmale von Tapasin, die an der Peptidaustauschkatalyse beteiligt sind. Die konkave N-terminale Domäne von Tapasin schließt die α2-1-Helix-Region von MHC I ein wie eine Klammer. Auf der einen Seite der Klammer befindet sich ein Loop, der sogenannte Editierloop. Dieser ist oben auf der F-Tasche der MHC I Peptid-Binde-Region platziert, während ein β-Haarnadel Element von unten den Boden der MHC I Bindetasche kontaktiert. Eine Superposition der atomaren Modelle des Klient-freien Tapasin–ERp57 (ref.[8]) und dem Peptid-gebundenen MHC I (ref.[26]) zeigen, dass die Bindung von MHC I zu strukturellen Umlagerungen der α1 und α2-1 Helices von MHC I führt und eine Weitung der F-Tasche resultiert. Diese Weitung wird durch ein Wasserstoffbrücken-Netzwerk zwischen His70 und Glu72 von Tapasin, welche die Seitenkette von Tyr84 der MHC I hc anziehen, herbeigeführt. Dabei unterstützt die Seitenkette von Lys20 von Tapasin die Positionierung des Tyr84, indem es Wasserstoffbrückenbindungen mit dem Sauerstoff der Hauptkette bildet. Bemerkenswerterweise entspricht das Glu72 strukturell dem Glu105 von TAPBPR, welches das Tyr84 von MHC I in einer ähnlichen Weise kontaktiert[10,11]. Der β-Faltblatt-Boden der MHC I-Peptid-Binde-Region nahe der F-Tasche verzerrt sich bei der Bindung von Tapasin, vermutlich wird dies durch das Engagement der β-Haarnadel von Tapasin ausgelöst. Außerdem wird die β-Haarnadel von Tapasin nach oben verschoben um der α2-1 Region von MHC I entgegenzukommen und die C-terminale Ig-artige Domäne von Tapasin schwingt der α3 Domäne von MHC I und β_2m entgegen.

Der sogenannte Editierloop wird durch die Seitenketten von Asn80 des MHC I stabilisiert, die eine Wasserstoffbrücke mit dem Rückgrat-Carbonylsauerstoff von Lys16 des Tapasin bildet. Die Seitenkette von Asp12 von Tapasin befindet sich in Salzbrückenabstand zur ε-

Aminogruppe von Lys146 der MHC I hc und trägt vermutlich zur Verbreiterung der Peptidbindetasche und zur Stabilisierung der Editierschleife von Tapasin bei. Die Seitenkette von Leu18 des Editierloops hat sich in früheren Studien als relevant für die MHC I-Oberflächen-Expression erwiesen[27–29]. Darüber hinaus kompensiert sie in der peptidfreien MHC I F-Tasche das Fehlen einer C-terminalen hydrophoben Seitenkette des Peptids und trägt vermutlich ebenfalls zur Weitung der Bindetasche bei. In Übereinstimmung mit dieser Annahme hat die Substitution von Leu18 durch eine sperrige hydrophobe Seitenkette (Trp) keine negativen Auswirkungen auf die MHC I-Oberflächen-Expression in einem zellulären Durchflusszytometrie-Assay verglichen mit dem Wildtyp. Jedoch wurde gezeigt, dass die Substitution von Leu18 durch Glycin die Peptidaustauschaktivität von Tapasin nahezu aufhebt. Überraschenderweise wirkte sich die Aufhebung der Wasserstoffbrückenbindung zwischen Tyr84 von MHC I und Glu72 von Tapasin nicht auf die MHC I-Oberflächen-Präsentation aus, wie ein *In-vitro*-Peptid-Beladungs-Assay zeigte[8]. Die Einführung einer Ladungsrepulsion durch die Mutation von Lys20 von Tapasin, das bei der Positionierung der α1-Helix von MHC I über Wasserstoffbrückenbindungen an den Rückgrat-Carbonylsauerstoff von Tyr84 beteiligt ist, führte nicht zu einer wesentlichen Verringerung der Oberflächen-MHC I-Molekülen. Deshalb stabilisiert der Editierloop von Tapasin die leere F-Tasche hauptsächlich vermutlich durch hydrophobe Wechselwirkungen. Die Reste, die sich in der MHC I F-Tasche befinden und die terminale Carboxylgruppe der gebundenen Peptide koordinieren, interagieren mit Tapasin und seinem Editierloop. Die Daten deuten darauf hin, dass Tapasin zwei Rollen einnimmt, indem es die Peptidbindetasche öffnet und die leere F-Tasche der MHC I hc stabilisiert.

Die *interface loop*-Region von Tapasin ist nicht an spezifischen Interaktionen beteiligt und spielt daher eine geringe Rolle bei der MHC I-Oberflächen-Präsentation. Im Gegensatz dazu führt die Mutation des benachbarte Gln261 von Tapasin, das an mehreren Wasserstoffbrückenbindungen mit der α2-1-Helixregion beteiligt ist, zu einer Verringerung der Oberflächen-Präsentation von MHC I. Einen noch stärkeren Rückgang der Oberflächen-Präsentation wurde beobachtet, wenn die Interaktionen zwischen der β-Haarnadel von Tapasin und der α2-Domäne der MHC I hc unterbrochen wurden. Mutationen sowohl in der *interface loop*-Region als auch in der β-Haarnadel reduzierten die MHC I-Oberflächen-Präsentation synergistisch. Interessanterweise besteht, wie bei freiem Tapasin–ERp57, ein intermolekularer Kontakt zwischen den Seitenketten Arg333 von Tapasin und Glu229 von MHC I hc. Eine Störung dieses Kontakts, durch eine Ladungsabstoßung, reduziert die MHC I-Oberflächen-Präsentation auf 37 ± 3%.

Die IgC-Domäne von Tapasin wird durch Kontakte zu β_2m stabilisiert, wobei Rückgrat-Wechselwirkungen zwischen Ile92 von β_2m und Leu329 von Tapasin und eine Seitenketten-Wasserstoffbindung zwischen Ser88 von β_2m und Glu307 von Tapasin bestehen.

Im MHC I–Tapasin–ERp57-Komplex ist die Position von β_2m in Bezug auf die MHC I hc ähnlich (RMSD 1,3 Å) wie im peptidgebundenen Zustand, während die Bindung von TAPBPR zu einer Neupositionierung von β_2m führt.

Auffallend ist, dass Sequenzabgleiche von klassischen MHC I-Allomorphen zeigen, dass die Interaktionsstellen für Tapasin zwischen Tapasin-abhängigen und -unabhängigen Allomorphen konserviert sind. Sie werden von Tapasin und TAPBPR gemeinsam genutzt, mit Ausnahme des Rests Trp73 von H2-D^b. Die Analyse der nicht-klassischen MHC I-Moleküle HLA-E, -F und -G zeigte, dass nicht alle potenziell interagierenden Reste konserviert sind. Die meisten der alternativen Reste sind aber immer noch in der Lage Wasserstoffbrückenbindungen zu bilden. Im Wesentlichen zeigt die Kristallstruktur des MHC I–Tapasin–ERp57-Komplexes, dass sowohl Tapasin-abhängige als auch -unabhängige Allomorphe die strukturellen Voraussetzungen für eine Interaktion mit dem Chaperon besitzen. Ihr Grad an Plastizität und damit ihre Fähigkeit, hochaffine Peptide aufzunehmen, bestimmt die Assoziation mit Tapasin, die durch zentrale Strukturelemente von Tapasin stabilisiert wird.

Da Tapasin in erster Linie als Teil des PLC-Multichaperon-Netzwerks agiert, könnte die Assoziation von ERp57 mit Tapasin nicht nur für die Koordination des Glykan-Chaperons Calreticulin notwendig sein. Die molekulare Dynamik dieser Interaktion könnte zusätzlich dazu beitragen, dass Tapasin für die Bindung und die Katalyse der Peptid-Editierung entriegelt wird. Durch die Kombination der strukturellen und funktionellen Daten wurde eine Doppelfunktion für die Editierschleife vorgeschlagen. In einem Peptid-defizienten MHC I-Zustand ist der Editierloop an der Verbreiterung der F-Tasche von MHC I beteiligt, und in einem intermediären Peptid-Chaperon-Komplex könnte der Loop den C-Terminus des Peptids abschirmen. Die Kristallstruktur des MHC I–Tapasin–ERp57-Komplexes verdeutlicht, dass sowohl Tapasin-abhängige als auch -unabhängige MHC I-Allomorphe die strukturellen Voraussetzungen für eine Interaktion mit Tapasin besitzen. Der Grad der Plastizität von MHC I und damit ihre Fähigkeit, optimale Peptide aufzunehmen, korreliert mit ihrer Verbindung zu Tapasin.

Insgesamt liefert diese Studie molekulare Details und strukturelle Merkmale der MHC I-Erkennung und des Peptid-Editierens durch das Hauptchaperon Tapasin in Verbindung mit ERp57. Darüber hinaus zeigt die Struktur, wie Tapasin die zahlreichen MHC I-Allomorphe erkennt und sie während des Peptidladens und der Korrekturlesung stabilisiert.

5 Introduction

5.1 The immune system – innate and adaptive immunity

Every day, the human body is exposed to a variety of pathogens through the respiratory tract, the skin, and oral exposition. Therefore, the immune system evolved as a highly developed defense system, recognizing, and eliminating non-self cells. It can be classified into innate and adaptive immunity. The innate immunity serves as a first effective defense against many pathogens, comprising physical and chemical barriers as epithelia and antimicrobial chemicals produced at epithelial surfaces[30]. Innate immune cells such as phagocytes, natural killer (NK) cells, dendritic cells (DC), and blood proteins, including members of the complement system and other inflammatory mediators are involved. Pathogens are recognized by specific pattern recognition receptors (PRRs), which identify pathogen-associated molecular patterns (PAMPs) and upon recognition, macrophages, monocytes, and granulocytes can phagocytose microbes and infected cells[31]. Degradative enzymes or reactive oxygen intermediates are produced, and the antigen can be presented to other immune cells for elimination of the pathogens. Dendritic cells (DC) are also phagocytic cells and play an essential role by linking the innate and adaptive immunity[32].

The adaptive immune system recognizes pathogen-specific molecules known as antigens and develops an immunological memory, allowing rapid detection and elimination of recurring pathogens. The immune response in adaptive immunity consists of antigen-specific reactions through lymphocytes. There are two types of adaptive immune response, depending on the type of lymphocytes. The humoral immunity is mediated by B-lymphocytes that express antigen-specific receptors on their cell surfaces, B-cell receptors (BCR)[30]. The BCRs recognize antigens and upon antigen binding activate B-cells, which proliferate and differentiate into antibody producing plasma cells. In turn, antibodies help neutralize the infection and activate further mechanisms to eliminate the extracellular invasion. The cell-mediated immune response is mainly carried out by T-lymphocytes. T-cells can be activated by presentation of antigenic peptides via major histocompatibility complexes (MHC) to their T-cell receptors (TCR)[30]. T-cells can be divided into cytotoxic T-cells (CTL), helper T-cells, and regulatory T-cells. CTLs express CD8 molecules on their cell surface, which are required for peptide-MHC (pMHC I) complex interaction and are therefore also known as $CD8^+$ T-cells. They are capable of directly killing infected cells and elimination of reservoirs of infection. Helper T-cells are also called $CD4^+$ T-cells because they express CD4 molecules, which are important for recognition of pMHC II complexes. Once helper T-cells are activated, secretion

of different cytokines further activates an immune response with other immune cells. The downregulation of immune response is mediated by regulatory T-cells.

5.2 Major histocompatibility complex class I and II

In antigen-presenting cells, MHC molecules present peptides to TCRs of T-cells on the cell surface. As noted above, there are two main types of MHC molecules: MHC class I (MHC I) and MHC class II (MHC II)[1]. While MHC I molecules present endogenous peptides and are recognized by $CD8^+$ T-cells, MHC II molecules generally present exogenous peptides to $CD4^+$ T-cells. MHC II molecules are predominantly expressed in dendritic cells, macrophages, and B-cells. They are composed of four domains α1, α2, β1 and β2. The α- and β-subunits each comprise transmembrane domain at their C terminus and together form the peptide-binding groove with their α1 and β1 domain. Human MHC molecules are encoded by the human leucocyte antigen (HLA) located on chromosome 6. Classical MHC II molecules are encoded by HLA-DR, -DQ and -DP[1] loci. The three classical MHC I-genes are encoded at the so-called HLA-A, -B and -C loci[1]. Both MHC I and MHC II genes are highly polymorphic, especially in the peptide-binding region, ensuring the binding of a wide variety of peptides. More than 24,000 classical HLA-A, -B and -C alleles encoding MHC I have been identified so far. The MHC I heterodimer is composed of the MHC I heavy chain (hc) and the light chain β_2-microglobulin (β_2m), whereby the hc is further divided into an α1, α2 and α3 domain and carries a transmembrane domain at its C terminus[33]. The peptide-binding groove is formed by the α1 and α2 domains. Peptides presented by MHC I are usually in the range of eight to ten amino acid and are stabilized by their N and C termini[1].

5.3 MHC I antigen-processing pathway

The adaptive immune system relies on the presentation of antigenic peptides by MHC I molecules to TCRs of $CD8^+$ T-cells[1,2]. The antigen presentation ensures the permanent information of the cell status of every nucleated cell to detect and eliminate infected or malignantly transformed cells. The antigen is presented in form of short peptides that are derived from two major sources: defective ribosomal products (DRiPs) and peptides generated by the ubiquitin proteasome system (UPS)[34]. DRiPs are polypeptides that were directly degraded after synthesis because of defects in sequence or folding[35]. They enable the quick recognition of virus-infected cells even before newly assembled viral particles are ejected from infected cells. However, the majority of antigenic peptides presented by MHC I molecules are generated by the proteasome. The proteasome targets ubiquitinated endogenously produced antigens and degrades them into peptides thereby defining their C-terminus[36–38]. The stimulation with interferon-γ leads to the expression of an alternative

proteasome, the immune-proteasome. This enzyme generates antigens, which are more suitable for MHC I presentation by favoring altered cleavage sites[39].

The produced peptides are translocated by the transporter associated with antigen processing (TAP) from the cytosol into the endoplasmic reticulum (ER) lumen[40]. TAP belongs to the superfamily of ATP-binding cassette (ABC) transporters and the heterodimer comprises the half-transporters TAP1 (ABCB2) and TAP2 (ABCB3). The core of each half-transporter is composed of a transmembrane domain (TMD) and a cytosolic nucleotide-binding domain (NBD). The TMDs are connected to a N-terminal extension of a four helical transmembrane domain, TMD0[41,42] (Fig. 1a). Heterodimeric core TAP lacking the TMD0s is sufficient to transport peptides[43]. However, the TMD0´s are essential for the assembly of the peptide-loading complex (PLC)[44–46]. TAP translocates peptides with a length up to 40 amino acids, preferring peptides with a length from eight to twelve amino acids[47–49]. It was shown that the three N- and C-terminal residues of the peptide are important for substrate recognition by TAP[50–52].

Peptides that underwent translocation into the ER lumen are further trimmed by the ER-associated aminopeptidases (ERAP) to generate peptides with an optimal length for MHC I-loading[53–55]. Peptide translocation and subsequent loading onto MHC I molecules is accomplished by the ER-resident supramolecular PLC (Fig. 1b)[40,56]. The PLC assembles around the heterodimeric transporter TAP and comprises two editing modules, each of which is composed of the lectin-like chaperone calreticulin, the oxidoreductase ERp57 in conjunction with the peptide-editor tapasin and the heterodimer MHC I hc/β_2m[12].

During maturation of MHC I, the MHC I hc is cotranslational translocated into the ER lumen where it is stabilized by the chaperone binding immunoglobulin protein (BiP). Asn86 within the NxS/T (x, any amino acid) motif of the hc is N-glycosylated with an $Glc_3Man_9GlcNAc_2$ glycan by the oligosaccharyltransferase (OST)[57–59]. Trimming by glucosidases I and II results in the monoglucosylated glycan $Glc_1Man_9GlcNAc_2$, generating a substrate suitable for calnexin that together with ERp57 and PDIs assist MHC I hc in further folding[59–62]. Upon initial folding, β_2m associates[63,64], and the MHC I hc/β_2m heterodimer is generated. Calreticulin recognizes empty or suboptimally loaded MHC I molecules by their N-linked $Glc_1Man_9GlcNAc_2$ glycan and recruits them to the PLC[65,66], where they are engaged by the MHC I chaperone tapasin. Tapasin forms a disulfide-linked heterodimer with ERp57, which is contacted by calreticulin, resulting in a further stabilized complex[67,68]. Peptide-loading and proofreading within the PLC is catalyzed by tapasin, ensuring the loading of high-affinity peptides to MHC I[4–7,14,69–71]. Stable pMHC I complexes are released from the PLC and are subjected to a second round of quality control by the tapasin-homologue TAP-binding protein related (TAPBPR) and uridine diphosphate (UDP)-glucose:glycoprotein glucosyltransferase 1 (UGGT1)[3]. TAPBPR acts as a peptide-editor in a peptide-depleted environment outside of the PLC[24,72,73]. UGGT1 is the main

folding sensor of glycoproteins in the ER and *cis-Golgi*, preventing misfolded proteins from leaving the ER by reglucosylating them[74]. Additionally, to the peptide-proofreading function, TAPBPR has been shown to support UGGT1 in identifying peptide-deficient MHC I complexes for reglucosylation and recycling of MHC I to the PLC[75,76]. Complexes of pMHC I that have passed these two quality control steps traffic via the secretory pathway to the cell surface, where they present their peptide cargo to CTLs (Fig. 1b)[1].

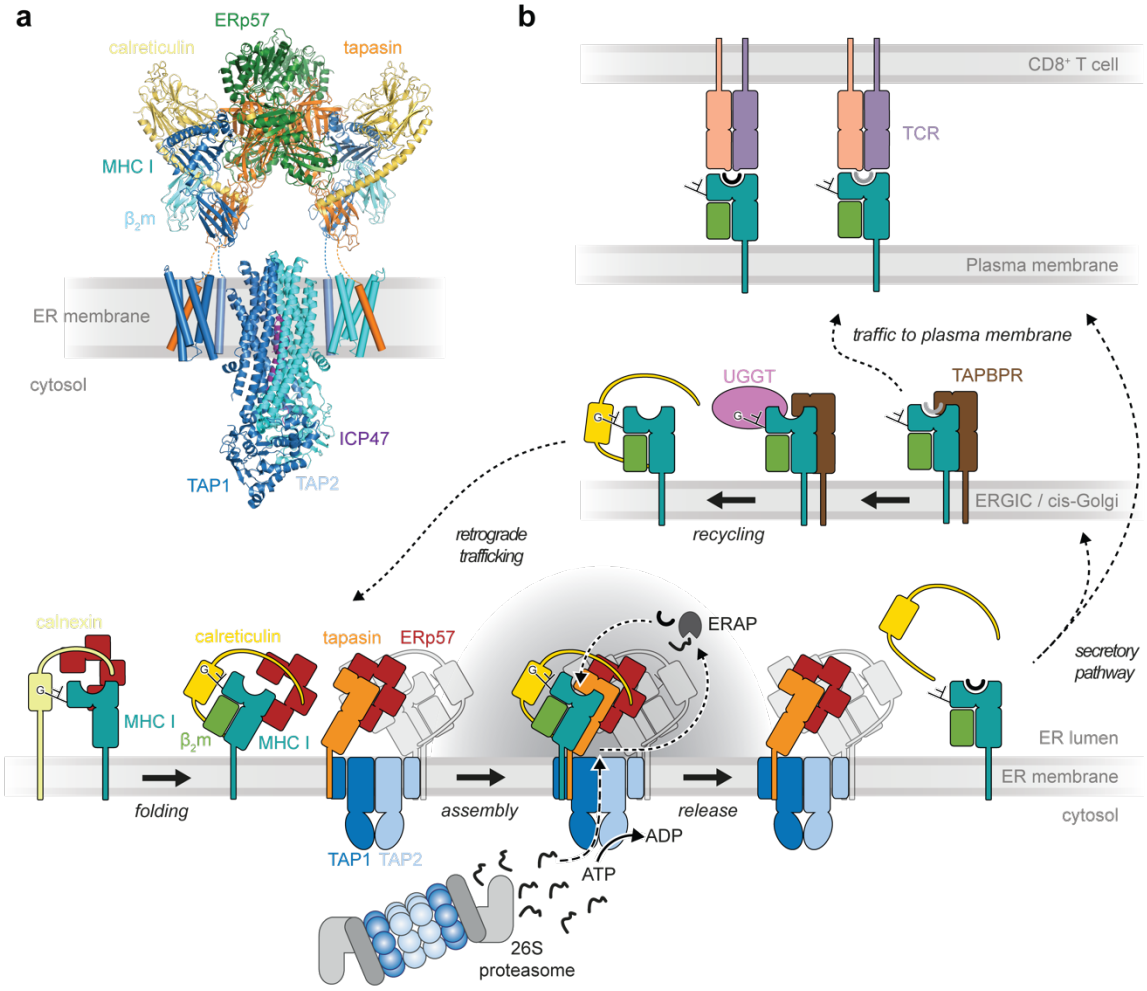

Figure 1: Antigen presentation pathway of MHC I[3]. a, Cartoon representation of the ER-resident multi-subunit PLC that is built by the heterodimeric transporter TAP (Protein Data Bank (PDB) ID 5U1D) and two editing modules, which are composed of the oxidoreductase ERp57 in conjunction with tapasin, the lectin-like chaperone calreticulin and MHC I hc/β_2m heterodimer (PDB ID 6ENY). The TMDs of MHC I hc, tapasin, TAP1 and TAP2 were not resolved in the cryo-EM structure and are illustrated as cylinders in the ER membrane. They are connected by dashed lines to their luminal domains[12,44]. **b**, MHC I hc is stabilized by calnexin and most likely ERp57 before association to the editing modules, forming a fully assembled PLC. Endogenous peptides, which were generated by the proteasome are translocated by TAP from the cytosol into the ER lumen, where they are further trimmed by ERAP. Then they are loaded onto MHC I molecules within the PLC and after trimming of the terminal glucose-residue, pMHC I complexes are released from the PLC and traffic via secretory pathway to the cell surface, where they present their antigenic cargo to TCRs of $CD8^+$ cells. TAPBPR performs a second step of quality control in peptide-depleted environments. MHC I complexes that bypassed peptide-proofreading by tapasin, are identified by TAPBPR and reglucosylated by UGGT1. The figure was adapted from Trowitzsch and Tampé, 2020.

5.4 The peptide-loading complex – first quality control in the MHC I antigen presentation pathway

The peptide-loading complex orchestrates peptide loading onto MHC I and performs the first quality control step during proofreading of pMHC I complexes. The tasks are essential for MHC I antigen presentation, thus making the PLC the key player in adaptive immunity. Within the PLC, the MHC I chaperone tapasin builds the core of the editing modules[12] and forms a disulfide-linked heterodimer with ERp57 that is contacted by calreticulin[3,8,12,77]. The MHC I hc/β_2m heterodimer is embraced by calreticulin and contacts tapasin (Fig. 2).

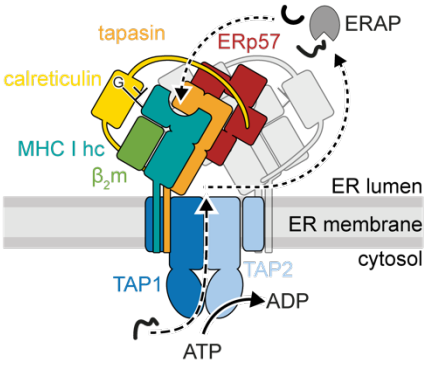

Figure 2: Schematic representation of the PLC[12]. Peptides are translocated by TAP from the cytosol into the ER lumen, where they are further trimmed by ERAP and loaded onto MHC I hc/β_2m heterodimers. Tapasin functions as peptide-editor to ensure the generation of stable pMHC I complexes. The figure is adapted from Blees *et. al.*, 2017.

5.5 Heterodimer tapasin–ERp57

Tapasin is a type-I membrane glycoprotein that forms the core of each editing module of the PLC. The transmembrane helix of tapasin binds the TMD0s of TAP1 and TAP2 and thereby bridges the translocation unit to the editing modules[7,12,44,78]. Tapasin stabilizes TAP and forms intermolecular salt bridges to each TAP protomer within the membrane bilayer. These salt bridges are required for the assembly of the PLC and for efficient pMHC I surface presentation[44]. Additionally, tapasin mediates peptide loading and editing of MHC I molecules by stabilizing peptide-receptive MHC I molecules and catalyzing the exchange of peptides[4,6,7,79]. The deletion of tapasin leads to a strong reduction of MHC I surface expression[7,14,15,78,80,81]. Mutational analysis of tapasin identified several interaction sites, which were found to be essential for MHC I surface presentation[8]. However, due to the transient interaction of tapasin and MHC I, structural data of an MHC I–tapasin complex are lacking to date.

Tapasin forms a mixed disulfide with ERp57, which involves Cys95 of tapasin and Cys33 of ERp57 (Cys57 in immature ERp57) (Fig. 3)[3,8,12,77]. In the ER, Cys33 of ERp57 switches between an intermolecular, mixed disulfide bond with Cys95 of tapasin and an intramolecular disulfide bond with Cys36 (Cys60 in immature ERp57)[8]. This switch is known as the escape pathway and has been shown for protein-disulfide-isomerase-assisted protein folding[82]. Usually, the second cysteine at the active site is utilized to release substrates after catalysis of disulfide rearrangement by displacing the intermolecular disulfide bond to the substrate with the intramolecular disulfide bond[82]. It is unclear whether this mechanism plays a role for the tapasin–ERp57 in the PLC.

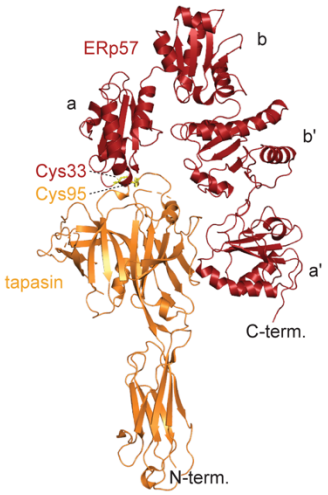

Figure 3: Structure of heterodimer tapasin–ERp57. Cartoon representation of tapasin–ERp57 (PDB ID 3F8U). The residues involved in the mixed disulfide between tapasin and ERp57, Cys95 and Cys33 respectively, are represented in yellow sticks.

The structure of the tapasin–ERp57 heterodimer reveals that tapasin adopts an L-shape form with its N-terminal region built up by a fusion of a seven-stranded β-barrel and an immunoglobulin (Ig)-like fold. ERp57 is a member of the PDI family and has four thioredoxin domains (a, b, b', a'), which are forming a twisted U shape[60]. The a and a' domains of ERp57 contact the N-terminal domain of tapasin.

5.6 Polymorphic MHC I heavy chains associate with the conserved light chain β_2m

The MHC I hc is a type-I membrane glycoprotein[83]. After MHC I hc is synthesized and glycosylated it forms a stable heterodimer with the light chain β_2m. The highly polymorphic hcs of the classical HLA-A, -B and -C allomorphs adopt a very similar overall structure. As mentioned above, the heavy chain comprises three domains: α1, α2, and α3. The α3 domain adopts an immunoglobulin fold. The α1 and α2 domains form the peptide-binding groove, consisting of the flanking helices α1, α2-1, and α2-2, and an eight-stranded β-sheet floor

(Fig. 4)[84]. A network of hydrogen bonds stabilizes the N and C termini of peptides in the MHC I binding pocket. Pockets stabilizing peptide residues are named A to F. The A pocket binds the N terminus, and the F pocket stabilizes the C terminus of the peptide. Residues forming the MHC I binding pocket of a particular allomorph therefore define the preference for the amino acid sequence of the bound peptides. Thereby, the different allomorphs ensure the binding and presentation of a broad spectrum of peptides.

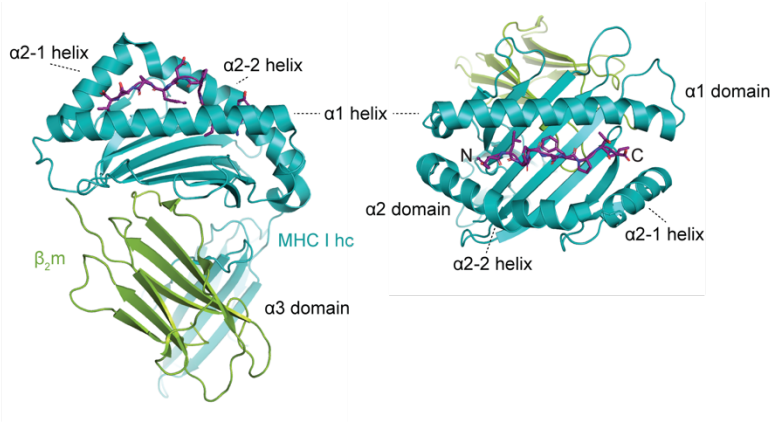

Figure 4: Structure of MHC I allomorph HLA-A02:01. Ribbon representation of the MHC I allomorph HLA-A*02:01 carrying the 9-mer peptide YLGGPDFPTI (PDB ID 5C0G). The overall view of the MHC I hc/β_2m heterodimer (left panel) shows the common structural elements of the different allomorphs. The view into the MHC I binding pocket (right panel) demonstrates the peptide-binding mode.

MHC I allomorphs show not only differences in their peptide binding preferences, but they also vary in their dependence on tapasin for optimal peptide-loading[6,16,17,19]. The most prominent examples are the allomorphs HLA-B*44:02 and HLA-B*44:05. They only differ by a single amino acid at position 116, which is located on the floor of the MHC I binding pocket but show drastic differences in their tapasin-dependence. HLA-B*44:02 has an aspartate at position 116 and is very tapasin-dependent, while HLA-B*44:05 contains a tyrosine at position 116 and is strongly tapasin-independent[70]. Crystal structures of their peptide-bound conformation are very similar[85,86]. However, MD simulations predicted major structural changes for the tapasin-dependent allomorph HLA-B*44:02 upon peptide dissociation in contrast to the tapasin-independent allomorph HLA-B*44:05 that adopts very similar conformations in the peptide-receptive and the peptide-bound states[18]. In general, the conformational plasticity of MHC I allomorphs correlates with the ability to load high-affinity peptides in the absence of tapasin[20,21,87]. Structural data explaining the promiscuity for various MHC I allomorphs of tapasin remained elusive.

5.7 The lectin-like chaperone calreticulin

The chaperone calreticulin comprises three domains, a globular domain, the P-loop, and an acidic helix (Fig. 5)[12]. The globular domain has a glycan-sensing site, which binds monoglucosylated substrates, and thereby plays an essential role for quality control in the ER[88]. It recognizes the N-linked monoglucosylated glycan of empty or suboptimally loaded MHC I hc/β_2m heterodimers and recruits them to the PLC, promoting MHC I surface expression[89,90]. By trafficking between ER and *cis*-Golgi compartments, calreticulin ensures the recycling of suboptimal loaded MHC I molecules that have been reglucosylated by UGGT1, referred to as glycoprotein quality control cycle[74].

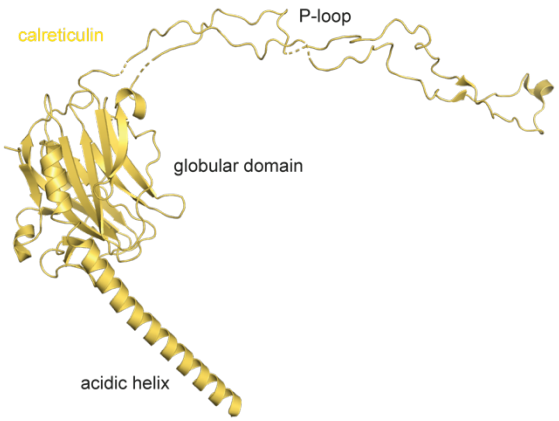

Figure 5: Structure of the chaperone calreticulin. Comic representation of calreticulin (PDB ID 6ENY). Calreticulin is composed of the globular domain, the P-loop, and the acidic helix. The acidic helix is not entirely modeled.

Furthermore, the globular domain possesses a high-affinity calcium-binding site that is important for its structural integrity[88]. The P-loop binds to the b' domain of ERp57 with micromolar affinity[22,60]. The acidic helix has a low-affinity Ca^{2+}-binding site[91] and comes in close contact with tapasin[12]. Somatic frameshift mutants of calreticulin that are associated with chronic blood tumors were recently identified[23]. Their C-terminal is lacking the ER retention signal and instead of the normal negative charge of the acidic helix, they are positively charged. The frameshift mutants were found to functionally impair the PLC and thus, lead to downregulation of MHC I surface expression[23]. Structurally, the acidic helix has not been resolved at atomic resolution, thus the interacting side chains between tapasin and calreticulin have not been identified so far.

5.8 Peptide exchange catalysis by MHC I chaperones tapasin and TAPBPR

The MHC I chaperones tapasin and its homologue TAPBPR have been shown to contact similar interfaces of MHC I, and therefore were indicated to catalyze peptide-exchange in a related manner[8–12] (Fig. 6a,b). Contrary to tapasin, TAPBPR acts beyond the PLC in the peptide-depleted environment of the *cis*-Golgi and ER-Golgi intermediate compartment (ERGIC)[13]. TAPBPR is involved in a postulated second quality control by catalyzing peptide-exchange of suboptimal-loaded MHC I complexes. In case loading of optimal peptides is not possible, TAPBPR interacts with UGGT1, identifying suboptimal pMHC I complexes for reglucosylation[75].

Human TAPBPR shares 22% sequence identity with human tapasin[92]. Crystal structures of MHC I-TAPBPR complexes revealed that TAPBPR adopts the same overall structure as tapasin[8,10–12]. The N-terminal domain of TAPBPR enfolds the α2-1 helix region of the MHC I hc and the C-terminal domain forms contacts with the α3 domain and β_2m. TAPBPR comprises a β hairpin motif, named jack hairpin, that contacts the floor of the MHC I binding pocket from below. Comparison of the peptide-bound state of MHC I and the chaperoned MHC I-TAPBPR complex shows a widened peptide-binding groove by the displacement of the α2-1 and a2-2 helices, a downward shift of the β-sheet floor of the binding pocket and a positional rearrangement of β_2m. Interestingly, residue Tyr84 of MHC I that coordinates in the peptide-bound conformation the C terminus of the peptide, is thereby swung out of the peptide-binding groove and coordinated by a conserved glutamate of TAPBPR (Fig. 6c).

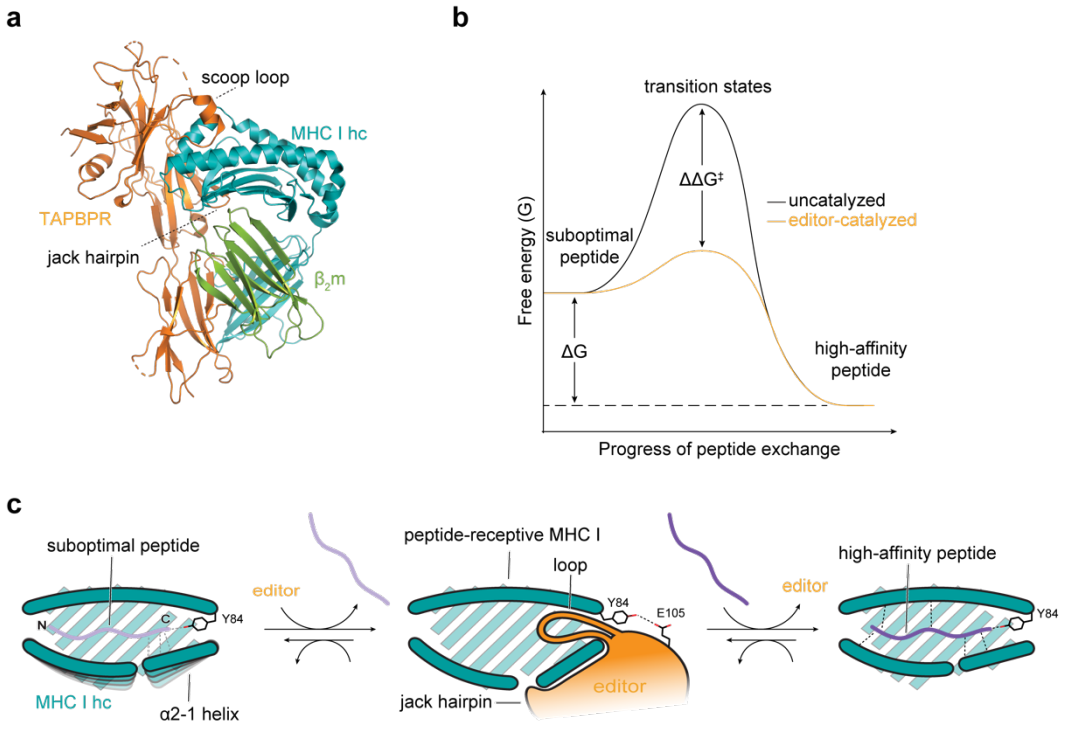

Figure 6: Peptide exchange at MHC I catalyzed by chaperones tapasin and TAPBPR[3,93]. a, Cartoon representation of MHC I-TAPBPR complex (PDB ID 5OPI). **b**, Schematic illustration of peptide exchange catalyzed by the editors tapasin and TAPBPR. Suboptimal peptide is exchanged for a high-affinity peptide by lowering the energy barrier. **c**, Schematic model of peptide exchange mediated by the MHC I-specific chaperones tapasin and TAPBPR. Suboptimal peptide is displaced by an opening of the α2-1 and a2-2 helices and stabilized by the N-terminal domain of the editor with the aid of the loop and the β-hairpin element. Further stabilization is managed by a hydrogen bond between the Tyr84 that coordinates the peptides C-terminus in a peptide-bound state and a conserved Glu residue of the editors (E105, TAPBPR; E72, tapasin). Binding of a high-affinity peptide in the MHC I binding pocket leads to the dissociation of the chaperone. It is a schematic illustration of the loop of the editor, which can be either diving in the F-pocket or placed on top. The figure is adapted from Trowitzsch and Tampé 2020, Thomas and Tampé 2017 in *Science* and *Front. Immunol.*.

The corresponding glutamate in tapasin has been shown to be important for the catalytic activity[8]. NMR studies of the MHC I-TAPBPR complex further confirmed that TAPBPR stabilizes peptide-receptive MHC I clients by widening the peptide-binding groove at the F-pocket[94]. This study proposes a negative allostery release cycle for peptide exchange. The initial contact formed by a high-affinity peptide with the A- and B-pocket leads to the closure of the α2-1 helix of MHC I and the dissociation of TAPBPR[94]. One of the MHC I-TAPBPR structures reveals a loop, which dives into the F-pocket of the peptide-binding pocket and coordinates residues that stabilize the peptide in the peptide-bound conformation of MHC I, potentially acting as a peptide-surrogate[11]. Kinetic studies identified the so-called scoop-loop to be important for the chaperone function of TAPBBR, helping to stabilize peptide-deficient MHC I clients[95]. Furthermore, studies demonstrated that the scoop loop of TAPBPR takes part

in peptide exchange by a lever mechanism[27]. Structural snapshots of MHC I with a bound short peptide corresponding to the loop of tapasin, indicate a similar peptide surrogate mechanism[28]. In contrast to the peptide surrogate theory, biophysical studies suggest that the loop of TAPBPR functions as a trap placed on top of the MHC I binding pocket, allowing moderate to high-affinity peptides to associate with MHC I-TAPBPR complexes[96]. Moreover, specific residues of the loop, such as Leu18, are identified to be essential for peptide editing[27,29,96].

While tapasin functions as the major MHC I chaperone predominantly in conjunction with ERp57 and calreticulin within the PLC, the biological role for TAPBPR, the need for a second peptide-editor for MHC I has not been fully elucidated yet[73]. The two crystal structures of the MHC I-TAPBPR complex give first insights into the peptide-loading and proofreading action of tapasin. However, high resolution structures explaining the promiscuous stabilization of peptide-deficient MHC I clients by tapasin–ERp57 have not been elucidated to date.

6 Motivation and aims

The health status of every nucleated cell is displayed at the cell surface in form of antigenic peptides loaded onto MHC I molecules. To detect and eliminate infected or cancerous cells, the adaptive immune system relies on the presentation of antigenic peptides by MHC I molecules to TCRs of $CD8^+$ T-cells[1]. MHC I molecules comprise the hc and the light chain β_2m. In humans, the polymorphic hc is encoded by the classical HLA-A, -B and -C loci located on chromosome 6. Already more than 13,000 allomorphs have been identified to date. The MHC I hc/β_2m heterodimers are synthesized and matured in the ER, before they are recruited to the PLC and loaded with antigenic peptides. Optimal loaded pMHC I complexes are released from the PLC and traffic via the secretory pathway to the cell surface for presentation to CTLs[3]. As member of the PLC, the chaperone tapasin ensures the loading of MHC I molecules and mediates the peptide proofreading by stabilizing peptide-deficient MHC I molecules and catalyzing peptide exchange by promoting peptide dissociation and association[4,6,7]. The homologue of tapasin, TAPBPR performs a second quality control step independent of the PLC in the peptide-depleted environment of the *cis*-Golgi and ER-Golgi intermediate compartment (ERGIC)[13]. Both chaperones share similar binding modes of MHC I, suggesting similar peptide exchange catalysis[3,8–11]. Nevertheless, they are located in different subcellular compartments and while TAPBPR functions independently, tapasin acts in conjunction with the oxidoreductase ERp57 and the lectin-like chaperone calreticulin within the PLC. However, the potential interaction site between tapasin and calreticulin has not been structurally characterized at high resolution to map the interactions of the side chains[12]. One part of this thesis focuses on the functional analysis of the trimeric complex especially on the potential interaction site between calreticulin and tapasin. To this end, the interaction between calreticulin and tapasin was analyzed by laser induced liquid bead ionization (LILBID) mass spectrometry and isothermal titration calorimetry (ITC).

The major peptide-editor tapasin in conjunction with ERp57 is essential for MHC I assembly and ensures high immunogenicity by altering the peptide cargo. The different MHC I allomorphs vary in their level of plasticity and exhibit different peptide-binding preferences, ensuring the presentation of a large peptide pool. For optimal peptide-loading they differ in their dependence on tapasin[16,17]. How tapasin chaperones the numerous MHC I allomorphs and stabilizes the peptide-deficient MHC I molecules has not been assessed at atomic level. To identify molecular details of MHC I recognition and structural elements essential for peptide editing by the multichaperone complex, an MHC I–tapasin–ERp57 complex should be assembled and isolated for structural analysis. To address this, a photo-triggered approach was chosen to generate peptide-deficient MHC I molecules. Various MHC I allomorphs should be screened for successful complex formation with heterodimer tapasin–ERp57 after

photocleavage of loaded peptides by size exclusion chromatography (SEC). A stable assembled MHC I–tapasin–ERp57 complex, should by structurally analyzed by X-ray crystallography. Based on the X-ray structure, interactions sites between tapasin and MHC I hc should be mutated and the resulting MHC I surface expression should be monitored in a cellular assay.

7 Materials

7.1 Chemicals

Table 1: Chemicals, listed alphabetical with respective manufacturer.

Chemical	Manufacturer
Acetonitrile (ACN)	Roth
30% Acrylamide	Roth
40% Acrylamide	Roth
2-Amino-2-(hydroxymethyl) propane-1,3-diol (Tris)	Roth
Agarose	Biozym
Ammonium persulfate (APS)	Roth
Bactoagar	Roth
Benzamidine hydrochloride monohydrate	Roth
Benzonase® nuclease (Purity > 90%)	Merck Millipore
Bovine Albumin Fraction V (7.5% solution)	Gibco Life Technologies
5-Bromo-4-chloro-3-indolyl-β-D-galactopyranoside (X-Gal)	Roth
Bromophenol blue	Roth
Calcium chloride ($CaCl_2$)	Roth
Clarity Western ECL substrate	Bio-Rad
10x CutSmart buffer	New England Biolabs
10x Cre recombinase buffer	New England Biolabs
CryoProtX kit	Molecular Dimensions
5-Cyclohexyl-1-pentyl-β-D-maltoside (CYMAL-5)	Sigma-Aldrich
Dichloromethane (DCM)	VWR
Dithiothreitol (DTT)	Sigma-Aldrich
Diethyl ether	VWR
((1,3-Dihydroxy-2-(hydroxymethyl) propan-2-yl) amino) acetic acid (Tricine)	Roth
Dimethylformamide (DMF)	VWR
Dimethyl sulfoxide (DMSO)	VWR
Dipotassium hydrogen phosphate (K_2HPO_4)	Roth
dNTP mix (10 mM)	Thermo Fisher Scientific
Ethane-1,2-dithiol (EDT)	Sigma-Aldrich
Ethanol (100%)	Roth
Ethanol	VWR
Ethidium bromide	Roth
Ethylenediaminetetraacetic acid (EDTA)	Roth
Ethylene glycol-bis(2-aminoethylether)-N, N, N', N'-tetra acetic acid (EGTA)	Roth
Ethylene glycol	Molecular Dimensions
Fmoc Glu(*t*Bu) TentaGel® S PHB resin	Rapp Polymere
Fmoc-Ile-Wang resin	Carbolution Chemicals GmbH
Fmoc-Leu-Wang resin	Carbolution Chemicals GmbH
Fmoc-Val-Wang resin	Carbolution Chemicals GmbH
Fmoc-Met-Wang resin	Carbolution Chemicals GmbH
Fmoc-Phe-Wang resin	Carbolution Chemicals GmbH
Fmoc-Val-Wang resin	Carbolution Chemicals GmbH
Fmoc-2-nitro-L-phenylalanine (2-NPA)	Sigma-Aldrich
GeneRuler 1 kb plus DNA ladder	Thermo Fisher Scientific
Glycerol (99.5%)	Roth
Glycine	Roth
10x Glycobuffer 3	New England Biolabs

(4-(2-hydroxyethyl)-1-piperazineethanesulfonic acid (HEPES)	Roth
5x HF buffer	Thermo Fisher Scientific
Hydroxy benzotriazole monohydrate (HOBt)	Acros Organics
Imidazole	Sigma-Aldrich
InstantBlue™ protein stain	Expedeon
Isopropyl alcohol (99.8%)	Roth
Isopropyl-β-D-1-thiogalactopyranoside (IPTG)	Roth
L-Arginine monohydrochloride	Roth
Magnesium chloride ($MgCl_2$)	Roth
Methanol	VWR
2-Mercaptoethanol	Roth
Milk powder	Roth
Morpheus II, buffer system 6	Molecular Dimensions
Morpheus II, LiNaK	Molecular Dimensions
Morpheus II, precipitant mix 7	Molecular Dimensions
Ni^{2+} agarose resin	Thermo Fisher Scientifc
N, N'-Diisopropylcarbodiimide	Carbolution
NucleoBond Xtra midi kit	Macherey-Nagel
NucleoSpin plasmid mini kit	Macherey-Nagel
Oxidized glutathione	Sigma-Aldrich
Oxyma	Roth
PageRuler™ prestained protein ladder	Thermo Fisher Scientific
Phenylmethanesulfonylfluoride (PMSF)	Roth
Phusion polymerase	Thermo Fisher Scientific
Pierce RIPA buffer	Thermo Fisher Scientific
Piperidine	Alfa Aesar
Polyethylene glycol (PEG) 20,000	Molecular Dimensions
Polyethylene glycol methyl ether 500 (PEG 500 MME)	Molecular Dimensions
Protease inhibitor mix HP	Serva
QIAquick® PCR extraction kit	Quiagen
Reduced glutathione	Sigma-Aldrich
S-3-(Fmoc-amino)-3-(2-nitrophenyl) propionic acid (*S*-Anp)	Santa Cruz Biotechnology
Sodium acetate	Roth
Sodium azide	Roth
Sodium cacodylate	Roth
Sodium chloride (NaCl)	Roth
Sodium dodecyl sulfate (SDS)	Roth
Sodium thiosulfate ($Na_2S_2O_3$ x 5 H_2O)	Roth
10x T4 DNA ligase buffer	Thermo Fisher Scientific
Tetramethylethylenediamine (TEMED)	Roth
tert. Butyl alcohol	Santa Cruz Biotechnology
Trifluoroacetic acid (TFA)	Roth
Triisopropylsilane (TIPS)	TCI Europe N.V.
Triton® X 100	Roth
Trypton	Roth
Tween® 20	Roth
Urea	Roth
Yeast extract	Roth

7.2 Equipment

Table 2: Used Equipment with respected manufacturer.

Equipment	Manufacturer
ACQUITY UPLC Peptide BEH C_{18} column	Waters
ACQUITY UPLC Protein BEH C_4 column	Waters
Agarose gel system	Bio-Rad
Äkta™ systems (Ettan, Go)	GE Healthcare/ Cytiva
Amicon® Ultra centrifugal filters (50K, 30K, 10K, 3K)	Merck Millipore
Avanti® J-26 XP	Beckman Coulter GmbH
Bacteria incubation shaker	HT Infors
Biometra TAdvanced Twin 48 G	Analytik Jena
Cell culture consumables	Greiner, Sarstedt
Centrifuge 5427 R	Eppendorf
Crystallization plate, sitting drop	Hampton Research
Electrophoresis power supply	Bio-Rad
FACSMelody™ Cell Sorter	BD Biosciences
Fiberlite™ F14-6 x 250y fixed-angle rotor	Thermo Fisher Scientific
Sterile workbench, laminar flow	Holten, Heraeus
FusionFX	Vilber
HPLC systems	Jasco
Insect cell incubators	HT Infors
Liberty Blue Automated Microwave Peptide Synthesizer	CEM Corporation
Liquid chromatography mass spectrometer (LC-MS) BioAccord	Waters
MicroCal iTC200	GE Healthcare
Microscope, epi-fluorescence	Leica
Mini-PROTEAN® electrophoresis system	Bio-Rad
4-20% Mini-PROTEAN TGX gels	Bio-Rad
Mosquito® crystal	SPT Labtech
Multifuge X1R TX-400	Thermo Fisher Scientific
MZ-Aqua Perfect C18	MZ-ANALYSENTECHNIK GmbH
NanoDrop-1000	PEQLAB Biotechnology
PD-10 desalting column	GE Healthcare/ Cytiva
PVDF membrane, 0.45 µm pore size	GE Healthcare
Rainin pipettes	Mettler Toledo
Slide-A-Lyzer™ dialysis cassettes (50K, 30K)	Thermo Fisher Scientific
Sorvall RC-5B Plus	Thermo Fisher Scientific
Superdex200 Increase column (3.2/300, 10/300)	GE Healthcare
Superdex75 16/60	GE Healthcare
Trans-Blot Turbo Transfer System	Bio-Rad
ThermoMixer®	Eppendorf
UV handlamp	Thorlabs
Whatman paper	Macherey-Nagel

7.3 Antibiotics

Table 3: Antibiotics. Displayed are stock and end concentrations.

Antibiotics	Stock solution	End concentration
Ampicillin (Amp)	50 mg/ml (in ddH_2O)	50 µg/ml
Chloramphenicol (Cam)	34 mg/ml (in ethanol)	34 µg/ml
Gentamycin (Gent)	10 mg/ml (in ddH_2O)	10 µg/ml
Kanamycin (Kan)	50 mg/ml (in ddH_2O)	50 µg/ml
Spectinomycin (Spec)	50 mg/ml (in ddH_2O)	50 µg/ml
Tetracycline (Tet)	10 mg/ml (in ethanol)	10 µg/ml

7.4 Enzymes

Table 4: List of commercial enzymes used in this thesis.

Enzymes	Source
Cre recombinase	New England Biolabs
EndoH	New England Biolabs
Phusion DNA polymerase	Thermo Fisher Scientific
PNGase F	New England Biolabs
T4 DNA ligase	Thermo Fisher Scientific
TEV protease	In house production

8 Methods

8.1 Molecular biology

8.1.1 DNA constructs

The plasmids encoding human β_2m and ectodomain of mouse MHC I (H2-D^b) were previously described[11]. The stabilizing mutants of ER-lumenal domain of human tapasin (tapasin$^{\Delta TMD}$; tapasin$^{\Delta TMD_SL}$) were generated using sequence and ligation independent cloning (SLIC)[97]. For flow cytometry analysis, the construct encoding full-length human tapasin was modified by the integration of an internal ribosomal entry site 2 (IRES2) followed by the enhanced green fluorescent protein (eGFP). Interaction mutations of tapasin were introduced by SLIC[97]. All vectors were validated by Sanger sequencing.

Table 5: Constructs used or generated in this thesis. aa - amino acids.

Subunit	UniprotKB	Construct	Vector	Reference
Tapasin^{IRES_eGFP}	O15533	aa 1-448	pAMI	this study
Tapasin$^{IRES_eGFP_\Delta EL}$	O15533	aa 1-448	pAMI	this study
Tapasin^{IRES_eGFP_TAPBPR_SL}	O15533	aa 1-448	pAMI	this study
Tapasin^{IRES_eGFP_L18W}	O15533	aa 1-448	pAMI	this study
Tapasin^{IRES_eGFP_K20E}	O15533	aa 1-448	pAMI	this study
Tapasin^{IRES_eGFP_E72A}	O15533	aa 1-448	pAMI	this study
Tapasin^{IRES_eGFP_S82E}	O15533	aa 1-448	pAMI	this study
Tapasin^{IRES_eGFP_R187E}	O15533	aa 1-448	pAMI	this study
Tapasin^{IRES_eGFP_Q261A}	O15533	aa 1-448	pAMI	this study
Tapasin^{IRES_eGFP_E307A}	O15533	aa 1-448	pAMI	this study
Tapasin^{IRES_eGFP_R333E}	O15533	aa 1-448	pAMI	this study
Tapasin^{IRES_eGFP_S336Y}	O15533	aa 1-448	pAMI	this study
Tapasin^{IRES_eGFP_R187E_Q261A}	O15533	aa 1-448	pAMI	this study
Tapasin^{IRES_eGFP_R333E_S336Y}	O15533	aa 1-448	pAMI	this study
Tapasin$^{\Delta TMD}$	O15533	aa 21-401/His_6-tag	pAMI	S. Trowitzsch
Tapasin$^{\Delta TMD_SL}$	O15533	aa 21-401/His_6-tag	pAMI	this study
ERp57^{C36A}	P30101	aa 1-505	pMIDK	S. Trowitzsch
Calreticulin	P27797	His_6-tag/aa 18-417	pETM	S. Trowitzsch
Calreticulin$^{\Delta acidic\ helix}$	P27797	His_6-tag/aa 18-368	pETM	S. Trowitzsch
HLA-A*02:01$^{\Delta TMD}$	P04439	aa 25-308	pET28	C. Thomas
HLA-B*44:02$^{\Delta TMD}$	P01889	aa 25-302	pET22b	S. Trowitzsch
HLA-B*44:05$^{\Delta TMD}$	P01889	aa 25-302	pET22b	S. Trowitzsch
HLA-B*08:01$^{\Delta TMD}$	P01889	aa 25-309	pET22b	C. Thomas
H2-D^b	P01899	aa 21-300	pET22b	C. Thomas[11]
β_2m	P61769	aa 21-119	pET22b	C. Thomas

8.1.2 Polymerase chain reaction

The polymerase chain reaction is a technique to amplify a selected segment of DNA. Fragments were amplified via PCR according to the pipetting scheme in Table 6 and PCR

thermocycler protocol (Table 7). PCR products were purified by agarose gel electrophoresis and the desired DNA fragments were extracted via the QIAquick® PCR extraction kit (Qiagen).

Table 6: Pipetting scheme for PCR. DMSO was used for PCR with Primers of a high GC content.

Substance	Amount
Template	100 ng
Forward primer	1 µl
Reverse primer	1 µl
dNTPs (10 mM)	2 µl
(DMSO 100%)	(3 µl)
5x HF buffer	20 µl
Phusion polymerase	1.5 µl
H_2O	Add to 100 µl

Table 7: PCR thermocycler settings. Annealing temperature needs to be adjusted for primers.

Reaction step	Time (s)	Temperature (ºC)	Cycle
Denaturation	45	98	
Denaturation	30	98	
Annealing	20	X	28 (steps 2 – 4)
Elongation	20	72	
Elongation	150	72	

8.1.3 Restriction cleavage of DNA

The restriction cleavage of DNA was performed to prepare sticky ends on 5' and 3' termini of PCR products for DNA ligation, for analytical characterization of plasmid DNA, or for preparative generation of vector backbones. For analytical scales, 500 ng of DNA were mixed with 1-10 U of restriction enzyme and 2 µl 10x CutSmart buffer (New England Biolabs) in a total reaction volume of 20 µl. Preparative cleavage reactions were usually set up in a total volume of 80 µl with 4 µg of respective DNA. Mixtures were incubated for 1.5 h at 37 °C and analyzed via agarose gel electrophoresis.

8.1.4 Agarose gel electrophoresis

Agarose gel electrophoresis separates DNA fragments according to their size. Gels of 1% agarose in TAE buffer (Table 8) were prepared and standard electrophoresis conditions (130 V) were applied. To visualize DNA molecules, gels were stained with ethidium bromide solution for 30 min and subsequently exposed to UV light. To prepare ethidium bromide solution, 1% (v/v) ethidium bromide was added to TAE buffer.

Table 8: TAE buffer.

40 mM Tris-HCl, pH 8.0
40 mM Acetic acid
20 mM EDTA

8.1.5 DNA ligation

DNA fragments were ligated using a 1:3 molar ratio of insert-to-target vector. Ligation was performed by adding 1 µl of T4 DNA ligase to 1x T4 DNA ligase buffer in a total reaction volume of 10 µl and incubation for 20 min at RT.

8.1.6 Plasmid DNA isolation

To isolate plasmid DNA for cloning purposes or transfection of mammalian cells, the NucleoSpin plasmid mini kit (Macherey-Nagel) or the NucleoBond Xtra midi kit (Macherey-Nagel) were used according to the manufacture's protocols. The concentration and purity of DNA was evaluated via NanoDrop (PEQLAB Biotechnology GmbH) by measuring the absorbance at 260 nm for the concentration and the quotient of the absorbance at 260 nm and 280 nm for purity. Typically, 260 nm / 280 nm ratio of Mini and Midi preparations were between 1.8 and 2.0 indicative for pure DNA.

8.1.7 Sequencing of DNA

All clones used or generated in this thesis were verified by Sanger sequencing. For DNA sequencing, 15 µl of each DNA sample (100 ng/µl) were sent to Microsynth Seqlab. Sequencing was performed using standard primers provided by Microsynth Seqlab (Table 9).

Table 9: Primers used for sequencing.

Primer name	Sequence
CMV-for	CGCAAATGGGCGGTAGGCGTG
FastBac-rev	CATTTTATGTTTCAGGTTCAGG
IRES-rev	TATAGACAAACGCACACCG

8.1.8 Cre-Lox recombination

The Cre recombinase reaction was used to fuse plasmids containing the LoxP element *in vitro*. The Cre-Lox recombination reaction was carried out in a total volume of 20 µl. Typically, 300 ng of Acceptor vector were mixed with 500 ng of Donor vector, 2 µl Cre recombinase buffer, 1 µl Cre recombinase and ddH_2O. Reaction mixture was incubated at 37 °C for 30 min. Subsequently, Cre recombinase was inactivation at 70 °C for 30 min. Successfully fused plasmids were selected in *E. coli* Mach1 T1 cells.

8.2 Microbiology

Bacteria suspension cultures were grown in shaker flasks using LB (Table 10) or TYP medium (Table 11) at 37 °C and 160 rpm. Selection of clones was performed on LB agar plates supplemented with the respective antibiotics. All cultivation media were sterilized at 121 °C for 20 min.

Table 10: LB media.

10% Trypton (w/v)
5% Yeast extract (w/v)
10% NaCl (w/v)

15% bactoagar (w/v) were added to prepare LB agar plates.

Table 11: TYP media.

16% Trypton (w/v)
16% Yeast extract (w/v)
5% NaCl (w/v)
1.25% K_2HPO_4 (w/v)

8.2.1 Preparation of chemical competent *E. coli* cells

A 5 ml pre-culture of either *E. coli* Mach1T1, *pir*HC or TOP10 cells was inoculated in LB media, and for Mach1T1 with the addition of the appropriate antibiotics, from a single colony. The culture was incubated overnight at 37 ºC and 180 rpm. The next day, pre-culture was diluted to 100 ml and incubated until an OD_{600} of 0.8 was reached. The cells were harvested by centrifugation at 4500 rpm for 10 min at 4 ºC, pelleted cells were resuspended in 40 ml of ice-cold solution A and centrifuged. The resulting pellet was resuspended in 40 ml of ice-cold solution B and centrifuged. 4 ml of ice-cold solution B were added to the cell pellet and cell suspension was incubated on ice for 1 h. Subsequently, 1 ml of solution C was added and 100 µl aliquots were snap-frozen in liquid nitrogen and stored at -80 ºC. Lastly, the prepared cell stocks were checked for antibiotic resistances and transformation efficiency. All solutions were sterilized for 20 min at 121 ºC.

Table 12: Solutions, used to prepare chemical competent cells.

Solution A	Solution B	Solution C
100 mM $MgCl_2$	50 mM $CaCl_2$	50% (v/v) glycerol

8.2.2 Transformation of *E. coli* cells

First, 100 µl of chemical competent *E. coli* cells were thawed on ice. Then 1 - 10 µl of DNA were added and the mixture was incubated for 20 min on ice. DNA uptake was achieved by a heat shock at 42 ºC for 1 min. Right after heat shock, cells were transferred back on ice for 5 min. Next 800 µl of LB media were added and the cell mixture was incubated for for 1 h at 37 ºC and 750 rpm. Afterwards the cell suspension was plated on LB agar plates with the appropriate antibiotics and incubated overnight at 37 ºC.

8.2.3 Bacmid preparation

To prepare Bacmid DNA for multigene expression in insect cells, DH10EMBacY cells were used. These cells carry the baculoviral genome as a bacterial artificial chromosome (BAC) and another helper plasmid encoding the Tn7 transposase. The bacmid has also a Tn7 site

embedded in a lacZ gene allowing to integrate multigene transfer plasmids via Tn7 transposition and selection of positive transformants via blue/white screening. To integrate multigene transfer plasmids into the EMBacY bacmid, 100 µl of DH10EMBacY cells were transformed with 10 µl of the transfer plasmid as described before (Chapter 8.2.2). Subsequently, cell suspension was plated on LB agar plates for blue-white screening with the antibiotics Gent, Kan, Tet, as well as IPTG and X-gal (KTGIB-plates). The plates were incubated over night at 37 ºC in the dark.

Blue-white screening distinguishes between colonies with and without the integrated transfer plasmid. This method relies on β-galactosidase which is encoded by the *lacZ* gene. Effective integration results in disruption of the *lacZ* sequence and consequently in inactivation of β-galactosidase. Cells, which express active β-galactosidase, form blue colonies on LB agar plates, while cells with an integrated transfer plasmid grow as white colonies due to disruption of the β-galactosidase gene.

Positive transformants were validated by re-streaking of typically 4 - 6 white colonies on KTGIB-plates. One blue colony was used as a negative control. The resulting white colonies were picked, transferred into 10 ml LB media supplemented with the antibiotics Kan, Tet and Gent and incubated at 37 ºC and 180 rpm overnight. The plasmid isolation was accomplished by using the NucleoSpin plasmid mini kit (Macherey-Nagel). First 4 ml of the cell suspension were centrifuged at 5000 xg for 5 min. The pellet was resuspended in 300 µl A1 buffer. Then 300 µl of A2 were added and the tube was inverted carefully. After addition of 300 µl of buffer A3 the tube was inverted carefully until the suspension turned colorless. Subsequently, lysed cell suspension was centrifuged at 13000 xg for 5 min. The supernatant was transferred to a new tube and centrifuged again. Then, the supernatant was mixed with 700 µl of 100% isopropanol and bacmid DNA was pelleted by centrifugation at maximum speed for 30 min. The resulting pellet was washed in 200 µl of 70% ethanol and centrifuged at maximum speed for 5 min. The bacmid DNA pellet was overlaid with 50 µl of 70% ethanol and subsequently used for transfection of *Sf*21 insect cells (Chapter 8.3.3).

8.2.4 Production of calreticulin in *E. coli* BL21 cells

Calreticulin constructs were produced in *E. coli* BL21. 20 - 30 ml of preculture was prepared from transformed cells and incubated overnight at 37 ºC and 160 rpm. 2 l of main culture were inoculated with overnight culture and incubated at 37 ºC and 160 rpm until an optical density at 600 nm (OD_{600}) of 0.6 was reached. After reduction of temperature to 20 ºC, cells were induced by the addition of 1 mM IPTG. The next day, cells were harvested by centrifugation at 4500 xg and 4 ºC for 15 min, cell pellets were flash-frozen in liquid nitrogen and stored at -80 ºC.

8.2.5 Production of inclusion bodies

MHC I allomorphs and β_2m were expressed as inclusion bodies in *E. coli* Rosetta(DE3)pLysS cells. Transformed cells were used to prepare 20 - 30 ml overnight culture, supplemented with ampicillin and chloramphenicol, per 2 l of main culture. Main culture was inoculated with overnight culture and incubated at 37 ºC and 160 rpm until an OD_{600} of 0.8 was reached. Temperature was reduced to 20 ºC and protein production was induced by the addition of 1 mM IPTG. After 20 h, cells were harvested by centrifugation at 4 ºC and 4500 xg for 15 min. Pelleted cells were flash-frozen in liquid nitrogen and stored at -80 ºC.

8.3 Cell Biology

8.3.1 Cell lines

All cell culture experiments were executed in a laminar-flow hood with sterile solutions, equipment, and media. *Sf*21 cells were cultured at 1 x 10^6 cells per ml in SF-900TM II SFM media at 28 ºC. HAP1 cells were maintained at about 80% confluency in Iscove Modified Dulbecco media (IMDM) supplemented with 10% fetal calf serum (FCS) at 37 ºC in a humidified atmosphere with 5% CO_2.

Table 13: Media and solution utilized for cell culture experiments.

Solution	Manufacturer
1x Dulbecco's PBS without Mg^{2+} and Ca^{2+}	Gibco Life Technologies
Fetal calf serum (FCS)	Capricorn Scientific
Iscove Modified Dulbecco media (IMDM)	Gibco Life Technologies
OPTIMEM	Gibco Life Technologies
SF-900TM II SFM	Gibco Life Technologies
1x Trypsin-EDTA (0,05 %/ 0,02 %) in Dulbecco's PBS	Gibco Life Technologies
XtremeGENE^{TM} HP	Roche

Table 14: Cell lines, used in this thesis, listed with their origin.

Name	Origin
HAP1 cells[98]	Near-haploid derived from KBM-7 cell line
HAP1$^{\Delta tapasin}$ cells[98]	Near-haploid derived from KBM-7 cell line
*Sf*21	Cell line from ovaries of *Spodoptera frugiperda*, suspension culture

8.3.2 Production of initial virus V_0 in *Sf*21 cells

To transfect of *Sf*21 insect cells, ethanol was removed from the bacmid DNA (Chapter 8.3.2) and pellet was dried for 10 min under a sterile bench. Bacmid DNA was resuspended in 25 µl of sterile water and diluted with 75 µl of Sf-900 II SFM media. 25 µl of XtremeGENE^{TM} HP transfection reagent were diluted in 75 µl of medium and mixed with the bacmid DNA. The transfection mixture was then incubated for 20 min at RT. Meanwhile, 0.2 x 10^6 cells in a total volume of 3 ml Sf-900 II SFM media were seeded per well of a 6-well plate. 100 µl of the transfection mixture were added dropwise to the cells. After incubation of 2 - 3 days at 28 ºC, transfection efficiency was monitored by YFP fluorescence. The supernatant corresponding

to virus V_0 was collected, sterile filtered and stored at 4 ºC. 3 ml of fresh media were added to each well and the cells were incubation for another 2 - 3 days at 28 ºC.

8.3.3 Production of amplified virus V_1

To amplify virus V_0, 2 ml of the initial virus were added to 25 ml of *Sf*21 insect cell suspension culture at a density of 1 x 10^6 cells per ml. A sample of 1 x 10^6 cells was taken every 24 h and analyzed for YFP fluorescence. Cells were kept at a density of 1 x 10^6 cells by dilution until proliferation arrest and YFP fluorescence was detectable. 24 h after proliferation arrest, cells were centrifuged at 1,200 x g for 5 min and the supernatant corresponding to V_1 virus was collected. The cell pellet was resuspended in fresh medium and YFP fluorescence was monitored until a plateau was reached. Cells were harvested by centrifugation at 1,200 x g for 5 min, flash-frozen in liquid N_2 and stored at -80 °C. Protein expression was analyzed by immunoblotting.

8.3.4 Transient transfection of HAP1 cells

HAP1 cells were transfected using XtremeGENE™ HP transfection reagent. Cells were seeded at a density of 0.4 x 10^5 cells in a total volume of 1 ml of IMDM media per well of a 6-well-plate and adhered for 12 h. 2 µg of plasmid DNA were diluted in 50 µl OPTIMEM media. In a separate tube, 6 µl of XtremeGENE™ HP were also diluted in 50 µl OPTIMEM media. The transfection reagent and DNA were mixed and incubated for 15 min at RT. The mixture was added dropwise to the cells. 1 ml media was added after incubation of 4-6 h at 37 ºC and 5% CO_2. After incubation of 48 h, cells were washed with 1x PBS and harvested using Trypsin-EDTA.

8.4 Protein biochemistry

8.4.1 Sample preparation from cell extracts

To check for protein production by sodium dodecyl sulfate polyacrylamide gel electrophoresis (SDS-PAGE) and/or immunoblotting, cell extracts from transfected HAP1 or infected insect cells were prepared. Media was removed and cells were washed with 1x PBS and then resuspended in 25 µl of Pierce RIPA buffer (Thermo Fisher Scientific) containing 1x Benzonase® nuclease (Merck Millipore) and 1x Protease inhibitor mix HP (Serva). After incubation for 15 min at 500 rpm and 25 °C, SDS loading buffer was added. Samples were incubated at 95 °C for 10 min and loaded onto respective gel. To follow expression of infected *Sf*21 insect cells via YFP fluorescence, 1 x 10^6 cells were harvested, resuspended in 500 µl of 1x PBS and lysed by sonication. Cell debris was removed by centrifugation (table top,

13,000 rpm, 10 min, 4 °C) and the fluorescence of the supernatant was detected using a plate reader.

Table 15: SDS loading buffer.

200 mM Tris-HCl, pH 6.8
40% (w/v) Glycerol
8% (w/v) SDS
4% (w/v) 2-Mercaptoethanol
0.08% Bromophenol blue

8.4.2 Sodium dodecyl sulfate polyacrylamide gel electrophoresis

Sodium dodecyl sulfate polyacrylamide gel electrophoreses (SDS-PAGE) is based on the separation of proteins according to their size. For the separation of tapasin$^{\Delta TMD}$, ERp57, calreticulin and MHC I allomorphs, 12% Tris-glycine or 11% Tris-tricine gels were utilized, using the BioRad Mini Protean tetra cell system. The whole cell extract from HAP1 cells was separated, using 4-20% Mini-PROTEAN TGX gels (Bio-Rad). The electrophoresis was performed either in Tris-glycine or in Tris-tricine anode and cathode buffer at 80 V for 20 min, followed by 150 V for 50 min.

Table 16: 10x Tris-glycine buffer.

25 mM Tris
192 mM Glycine
0.1% SDS (w/v)

Table 17: 10x Tris-tricine cathode buffer.

1 M Tris
1 M Tricine
1% SDS (w/v)

Table 18: 10x Tris-tricine anode buffer.

1 M Tris-HCl, pH 8.9

Table 19: 3x Gel buffer.

3 M Tris-HCl, pH 8.5
0.3% SDS

Table 20: Composition of 6% Tris-glycine stacking and 12% separation polyacrylamide gels.

Substance	6% Stacking gel (2x gels)	12% Separating gel (1x gel)
30% Polyacrylamide	2.0 ml	2.5 ml
1.5 M Tris, pH 6.8	1.3 ml	-
1.5 M Tris, pH 8.8	-	2.6 ml
H_2O	6.6 ml	2.1 ml
10% APS (w/v)	125.0 µl	62.5 µl
TEMED	14.0 µl	7.0 µl

Table 21: Tris-tricine polyacrylamide gel.

Substance	Stacking gel (1x gel)	11% Separating gel (1x gel)
40% Polyacrylamide (19:1)	0.4 ml	1.4 ml
3x Gel buffer	1.3 ml	1.7 ml
100% Glycerol	-	0.5 ml
H_2O	1.6 ml	2.2 ml
10% APS (w/v)	19.2 µl	38.5 µl
TEMED	3.9 µl	7.7µl

8.4.3 Immunoblotting and detection of chemiluminescence

For identification of proteins by immunoblotting, proteins separated by SDS-PAGE were transferred onto PVDF membranes (0.45 µm pore size, GE Healthcare) by using the Trans-Blot Turbo System (Bio-Rad). Prior to blotting, the membranes were activated by incubation in methanol. Subsequently, the membrane and three Whatman paper (Macherey-Nagel) were soaked in blotting buffer. A sandwich of 2 Whatman papers, membrane, gel, and another Whatman paper were placed into the Trans-Blot Turbo Electrophoretic Transfer Cell. Transfer was performed at 25 V for 30 min. To inhibit unspecific binding, the membrane was blocked in 5% (w/v) milk powder in TBS-T for 1 h at RT. Next, membrane was incubated with the primary antibody at 4 ºC overnight or at RT for 1 h. Membrane was washed 3x with TBS-T for 5 min, before incubation with the secondary antibody for 45 min at RT. Blot was incubated with Clarity Western ECL substrate (Bio-Rad) and chemiluminescence was detected by the FusionFX (Vilber).

Table 22: Blotting buffer.

25 mM Tris-HCl, pH 7.5
192 mM glycine
0.03% SDS
20% Methanol

Table 23: TBS-T buffer.

20 mM Tris-HCl, pH 8.0
150 mM NaCl
0.01% (w/v) Tween® 20

Table 24: Primary and secondary antibodies used for immunoblotting.

Antigen	Host and isotype	Dilution	Source
α-GAPDH, HRP conjugated	Mouse, monoclonal	1:2000	BioLegend
α-GAPDH	Rabbit, polyclonal	1:2000	Thermo Fisher Scientific
α-Tapasin (clone 7F6)	Rat IgG	1:3000	Hybridoma, in-house[99]
Secondary antibodies			
α-rabbit, HRP conjugated	Goat, polyclonal	1:20,000	Merck Millipore
α-rat, HRP conjugated	Goat, polyclonal	1:20,000	Sigma-Aldrich

8.4.4 InstantBlue™ staining

Coomassie brilliant blue staining is a common method to visualize proteins in polyacrylamide gels. The dye binds to the side chains of basic amino acids. InstantBlue™ protein stain (Expedeon) contains a Coomassie dye, ethanol, phosphoric acid, and solubilizing agents and can be used to stain proteins with a sensitivity of 5-25 ng protein per band. After electrophoreses, gels were incubated in InstantBlue™ solution from 15 min for quick inspection to overnight for complete staining of proteins.

8.4.5 Purification of proteins by immobilized metal ion affinity chromatography

Immobilized metal ion affinity chromatography (IMAC) is a common purification method for recombinant proteins that are fused to a peptide affinity tag. Characteristic for this method is a matrix of immobilized metal ions (Co^{2+}, Ni^{2+}, Cu^{2+}, Zn^{2+}), which interact with specific amino acid side chains of the protein, usually polyhistidines. The desired protein with a fused polyhistidine tag will be immobilized on the column washed and eluted by adding high amounts of imidazole or free histidine. Hexahistidine tags fused either N-terminal to tapasin$^{\Delta TMD}$ or C-terminal to calreticulin were used for purification. Tapasin$^{\Delta TMD}$–ERp57^{C36A} heterodimer was isolated from infected *Sf*21 cells, while calreticulin was purified from transformed *E. coli* BL21 DE3 cells. All purification steps were carried out at 4 ºC. Harvested cells were resuspended in lysis buffer (Table 25 or 26) and lysed by sonication. The whole cell extract was centrifuged for 30 min at 20,000 xg at 4 ºC. Supernatant was incubated with pre-equilibrated Ni^{2+}-NTA agarose beads for 1 h at 4 ºC. NTA agarose resin was washed 3x with wash buffer (Table 27) and protein complex was fraction-wise eluted with 5x bead volume of elution buffer (Table 28). Samples were taken in every step and prepared with SDS loading buffer for analysis by SDS-PAGE.

To avoid degradation of the proteins, imidazole was removed by a PD-10 desalting column (GE Healthcare/Cytiva). Subsequently, protein was concentrated by ultrafiltration using an Amicon® Ultra centrifugal filter with corresponding MW cut off. Protein concentration was determined at 280 nm by using a NanoDrop device (PEQLAB Biotechnology).

Table 25: Lysis buffer for purification of tapasin$^{\Delta TMD}$–ERp57^{C36A}.

50 mM HEPES-NaOH, pH 7.4
150 mM NaCl
25 mM Imidazole
1% PMSF
1% Benzamidine

Table 26: Lysis buffer for purification of calreticulin.

50 mM HEPES-NaOH, pH 7.4
300 mM NaCl
5 mM $CaCl_2$

25 mM Imidazole
1% PMSF
1% Benzamidine
0.5 mg/ml Lysozyme
1:10,000 (v/v) Benzonase® nuclease

Table 27: Wash buffer.

50 mM HEPES-NaOH, pH 7.4
150 mM NaCl
25 mM Imidazole

For the wash buffer for purification of calreticulin 1 mM of $CaCl_2$ was added.

Table 28: Elution buffer.

50 mM HEPES, NaOH, pH 7.4
150 mM NaCl
300 mM Imidazole

1 mM $CaCl_2$ was added to prepare the elution buffer for the purification of calreticulin.

Table 29: Exchange buffer.

50 mM HEPES-NaOH, pH 7.4
150 mM NaCl

8.4.6 Cleavage of His_6-tag by tobacco etch virus protease

The tobacco etch virus (TEV) protease is used to remove fusion tags from recombinant proteins. It recognizes highly-sequence specific the sequence Glu-Asn-Leu-Tyr-Phe-Gln/Ser(Gly) and cleaves between the residues Gln and Ser(Gly). TEV protease, used in this thesis, comprises an N-terminal His_6-tag. After buffer exchange of IMAC purified proteins tapasin$^{\Delta TMD}$–ERp57^{C36A} or calreticulin, TEV protease was added in a molar ratio of 1:20. The mixture was transferred into Slide-A-Lyzer^{TM} (30K MWCO) dialysis cassettes and dialyzed against exchange buffer (Table 29) slightly stirring, overnight at 4 ºC. For separation of TEV protease from proteins of interest, Ni^{2+}-NTA agarose beads were added after dialysis and incubated slightly stirring for 30 min at 4 ºC. The supernatant was collected, and beads were washed three times with washing buffer (Table 27). For analysis, bound proteins were eluted with elution buffer (Table 28). Supernatant was concentrated by ultrafiltration using an Amicon® Ultra centrifugal filter with appropriate MW cut off and SEC was performed for polishing of proteins (Chapter 8.4.10).

8.4.7 Dialysis

Dialysis is a separation method to remove small molecular weight substances or to exchange the buffer. Dialysis is based on diffusion, a process of thermal, random movement of molecules in solution. The movement occurs from areas of higher to lower concentration until

an equilibrium results. A semi-permeable membrane separates the sample-chamber from a second chamber. Only small molecules can pass the pores of the membrane, thereby reducing the concentration of these molecules within the sample-chamber. For buffer exchange after IMAC purification, 1-6 ml of sample were dialyzed against 2 l of exchange buffer, slightly stirring, overnight at 4 ºC. For buffer exchange before ITC experiments, up to 1 ml of pure protein solution was dialyzed against 1 l buffer either for 1 h at RT or overnight at 4 ºC.

8.4.8 Deglycosylation by Endoglycosidase H or Peptide-*N*-Glycosidase F

Tapasin$^{\Delta TMD}$ was deglycosylated using either Endoglycosidase H (Endo H) or Peptide-*N*-Glycosidase F (PNGase F). Endo H is a recombinant glycosidase and cleaves between the two N-acetylglucoseamine (GlcNAc) moieties next to the asparagine residues, thereby generating a glycoprotein with one GlcNac residue on the asparagine. PNGase F is an amidase, which generates deaminated proteins by cleaving between the GlcNAc and the asparagine residue. Endo H digest was performed to produce a more homogenous sample of tapasin$^{\Delta TMD}$–ERp57^{C36A} for crystallization trials (Chapter 8.4.21) and for LC-MS (Chapter 8.4.13). Heterodimer was mixed with Glycobuffer 3 (10x, NEB) and 2500 units of Endo H (NEB) per 4 µg protein were added. Mixture was incubated overnight at RT and deglycosylated heterodimer was purified by SEC (Chapter 8.4.10). PNGase F was also utilized for crystallization trials. Digest was carried out in the same way as for Endo H, except for the Glycobuffer 2, which was used instead of Glycobuffer 3.

8.4.9 Isolation and refolding of inclusion bodies

To isolate inclusion bodies, cell pellets (Chapter 8.2.5) were resuspended in TE buffer (Table 30) containing 1% Triton® X 100 (v/v) and ultracentrifuged at 10,000 xg for 20 min at 4 ºC. Inclusion bodies were washed five times, followed by 2 washing steps with TE buffer without Triton® X 100. Purified inclusion bodies were resuspended in TE buffer, flash-frozen in liquid nitrogen and stored at -80 ºC.

For refolding of β_2m, pure inclusion bodies from 2 l expression culture were resuspended in 50 ml denaturation buffer and incubated at RT for 1 h. Denaturized inclusion bodies were ultracentrifuged at 16,000 xg for 5 min at 4 ºC and dialyzed 2x against 2 l of 10 mM Tris-HCl, pH 8.0 for at least 9 h. Refolded β_2m was concentrated by ultracentrifugation (Amicon Ultra 3 kDa, MWCO) and further purified by size exclusion chromatography (Chapter 8.4.10).

Pure inclusion bodies from MHC I allomorphs were resuspended in denaturation buffer (Table 31) and added dropwise under constant stirring at 4 ºC to refolding buffer (Table 32) in a final concentration of 1 mM in presence of 40 mM photocleavable peptide and 2 mM of purified β_2m. Refolding mixture was incubated either stirring for 3 days at 4 ºC or 2x dialyzed

against 2 l of 10 mM Tris-HCl, pH 8.0, per 100 ml of refolding buffer, overnight at 4 ºC. Refolded peptide/MHC I/β_2m complexes were concentrated by ultracentrifugation (Amicon® Ultra 10 kDa, MWCO) and polished by size exclusion chromatography.

Table 30: TE Buffer.

20 mM Tris-HCl, pH 8.0
100 mM NaCl
10 mM DTT

Table 31: Denaturation buffer.

100 mM Tris-HCl, pH 8.0
8 M Urea

Table 32: Refolding buffer.

100 mM Tris-HCl, pH 8.0
400 mM L-Arginine monohydrochloride
5 mM reduced glutathione
0.5 mM oxidized glutathione
2 mM EDTA
1x Protease inhibitor mix HP

8.4.10 Size exclusion chromatography

Size exclusion chromatography (SEC) was performed as the last step for purification or for analysis. The corresponding fractions of the resulting peak were collected and prepared with SDS loading buffer for SDS-PAGE analysis. Tapasin$^{\Delta TMD}$–ERp57^{C36A}, calreticulin and MHC I allomorphs were polished on a Superdex200 10/300 Increase column (GE Healthcare). β_2m was purified on a Superdex75 16/60 column. All proteins were analyzed on a Superdex200 3.2/300 Increase column (GE Healthcare). Prior to SEC, samples were centrifuged at 15,000 xg and 4 ºC for 10 min and columns were pre-equilibrated in exchange buffer (Table 29).

8.4.11 Fmoc solid phase peptide synthesis

Solid phase peptide synthesis allows the fast assembly of a synthetic peptide chain. Peptide synthesis starts at the C terminus and continues towards the N terminus. The C-terminal amino acid is coupled to a solid support to a functional group of small, polymeric resin beads. The N-terminal and side chains of amino acids are protected by protecting groups such as Boc or Fmoc to prevent side reactions. The covalent attachment of the nascent peptide chain to the resin, enables the removement of unwanted side products by washing and filtration. After the first amino acid is coupled to the resin, the amine is deprotected and coupled to the acidic group of the second amino acid. The resin is washed and filtrated, before the cycle of deprotection and coupling is repeated until the desired peptide is synthesized. The crude peptide is cleaved from the resin and protecting groups are removed at the same time. The

peptide is precipitated from a unpolar solvent, such as diethyl ether. Lastly, the peptide is analyzed by reversed-phase high-pressure liquid chromatography (HPLC, Jasco) (Chapter 8.4.12) or liquid chromatography-mass spectrometer (LC-MS, BioAccord, Waters) (Chapter 8.4.13) and if required further purified by reversed-phase HPLC. The peptides were synthesized by Fmoc solid phase synthesis on a Liberty Blue Automated Microwave Peptide Synthesizer (CEM Corporation). For 9-10mer peptides, Wang resins preloaded with the specific C-terminal amino acid were used as support. Crude peptides were cleaved of resins with 95% TFA, 2.5% H_2O and 2.5% TIPS. For peptides composed of a methionine, a cleavage cocktail of 94% TFA, 2.5% water, 2.5% EDT and 1% TIPS was used. Peptides were precipitated from diethyl ether and washed 4x with diethyl ether. After removal of diethyl ether, peptides were resuspended in a mixture of tert-butanol and water (4:1) and lyophilized. Peptide identity and purity was verified by reverse-phase HPLC and Matrix-assisted laser desorption/ionization (MALDI) time of flight (TOF) or by LC-MS. For further purification, peptides were isolated by reverse-phase HPLC.

Table 33: Specific MHC I peptides, synthesized in this thesis.

Sequence	MHC I allomorph
GILGFVF(*S*-Anp)L	HLA-A*02:01 (ref.[72])
ELNRKMI(*S*-Anp)M	HLA-B*08:01 (ref.[100])
EENLLDFVRF	HLA-B*44:02/05 (ref.[101])
EEFGRAFSF	HLA-B*44:02/05 (ref.[102])
EEFG(*S*-Anp)AFSF	HLA-B*44:02/05 (ref.[102])
EEFGRA(*S*-Anp)SF	HLA-B*44:02/05 (ref.[102])
RGPGRAF(*S*-Anp)TI	H2-D^b (ref.[11])

8.4.12 Reverse-phase high-performance liquid chromatography

High-performance liquid chromatography (HPLC) is a chromatographic separation method. The sample and the solvent, the mobile phase, are pumped through a column, which is filled with the stationary phase. The components of the sample interact different with the material of the stationary phase, resulting in different flow rates and thereby separating the compounds by different elution times.

Reverse-phase (RP-)HPLC is a separation principle based on polarity. Opposed to normal-phase HPLC, the stationary phase is hydrophobic, and the mobile phase is polar. The stationary phase is composed of silica gel, which is coated with a nonpolar layer of alkenes. For the mobile phase, mixtures of polar solvents, such as water/acetonitrile (MeCN) or water/methanol are used. The pH value of the mobile phase needs to be far above or below the pI value of the analyte. Also, a highly volatile substance, such as TFA or ammonium acetate are added to the mobile phase not only to regulate the pH, but also to extend the interaction time of the analyte and the stationary phase by increasing the hydrophobicity of the analyte. The elution force increases with decreasing polarity. For isocratic separations, the

composition of the mobile phase remains the same throughout. In gradient separations, the polarity of the solvent is changed during analysis. Synthesized peptides were analyzed by reversed-phase synthesis using a MZ-Aqua Perfect C18 column (MZ-Analysentechnik GmbH) and a mixture of water/acetonitrile (0.1% TFA) for mobile phase. A standard gradient was used for analysis of 9-10mer peptides.

Table 34: Standard gradient used for analysis or purification of peptides. Eluent A: H_2O + 0.1% TFA; Eluent B: MeCN + 0.1% TFA.

Time	Solvent
0 – 5 min	100% B
5 – 9 min	100% B
9 – 10 min	5% B
10 – 16 min	5% B

8.4.13 Ultra-performance liquid chromatography

Ultra-performance liquid chromatography (UPLC) is the development of HPLC to improve speed and efficiency. UPLC systems are optimized to work at higher pressure and therefore allow the use of smaller particle sizes for the stationary phase. Intact proteins, tapasin$^{\Delta TMD}$–ERp57^{C36A} were analyzed on an ACQUITY UPLC Protein BEH C_4 Column using a linear water/acetonitrile gradient, supplemented with 0.1% formic acid.

Synthesized peptides were verified on a ACQUITY UPLC Peptide BEH C_{18} Column using a shorter gradient due to the high separation capacity. UPLC experiments were performed with a BioAccord System (Waters).

Table 35: Standard gradient UPLC. Eluent A: H_2O + 0.1% TFA; Eluent B: MeCN + 0.1% TFA.

Time	Solvent
0 – 0.5 min	2% B
0.5 – 4 min	80% B
4 – 5 min	2% B

8.4.14 Matrix-assisted laser desorption/ionization

Matrix-assisted laser desorption/ionization (MALDI) is an ionization method, which generates ions using a laser energy absorbing matrix. The analyte is cocrystallized with a matrix, which consists of small organic molecules, that strongly absorb the laser energy. High-energetic laser pulses trigger desorption of the analyte and matrix. Protonation and deprotonation lead to ionization of molecules. Ionization by MALDI generates single-charged ions. MALDI was performed by service unit Massenspektrometrie at Goethe University using a Voyager-DE™ STR Biospectrometry™ (Applied Biosystems). Purified peptides, containing a photocleavable amino acid, were cocrystallized with sinapinic acid.

8.4.15 Electrospray ionization

The technique electrospray ionization (ESI) is based on the generation of ions by electrospray. The analyte solution is passed through a metal capillary to the tip of which a voltage is applied. An electrical field is formed between the capillary and a counter electrode. The ions of the analyte solution are moving electrophoretic towards the counter electrode and an excess of homogenous charged ions occur at the tip of the capillary. To reduce the size of the droplets an inert gas is utilized, which assists in evaporation of solvent. Charge repulsion results in the formation of a Taylor-Cone and ions leave the capillary as fine aerosol. The radius of the droplets decreases, while the charge remains the same. Once the Rayleigh-limit is reached, the droplets undergo Coulomb fission and explode in many smaller, more stable droplets. Compared to ionization by MALDI, ESI can be directly connected to an LC-system. Ionization of proteins by ESI was performed using a cone voltage of 60 V and 1.5 kV capillary voltage in a positive polarity at 2 Hz. Peptides were ionized utilizing 30 V cone voltage, 550 °C desolvation temperature, 800 V capillary voltage in positive polarity at 5 Hz acquisition rate in MS^e mode.

8.4.16 Laser induced liquid bead ion desorption

Laser induced liquid bead ion desorption (LILBID) is a mass spectrometry ionization method, which ensures a soft transfer of the analytes in solution to the gas phase[103,104]. Non-covalently linked complexes remain assembled in the gas phase, allowing the determination of complex stoichiometry. A droplet generator releases microdroplets of the analyte solution into a vacuum. The droplets are separately irradiated by an IR-laser with a wavelength adjusted to the absorption maximum of water. The absorption of the energy results in the explosion of the droplet and the analyte is released into the vacuum for analysis by TOF. Purified proteins were mixed in a molar ratio of 1:1 at a concentration of 10 µM and the buffer was exchanged to 100 mM ammonium acetate using Zeba™ Spin desalting columns with appropriate cut off.

8.4.17 Time of flight mass spectrometry

Time of flight mass spectrometry is a technique, which analyzes the mass-to-charge ratio of ions by measuring their time of flight. Ionized analytes are accelerated by an electric field. Mass spectra were recorded in positive polarity at 2 Hz in full scan mode at 400 – 7000 m/z for proteins and at 50 – 2000 for peptides.

8.4.18 *In vitro* complex formation of MHC I–tapasin$^{\Delta TMD}$–ERp57^{C36A}

To assemble the transient complex of tapasin$^{\Delta TMD}$–ERp57^{C36A}/MHC I, a photocleavable peptide was engineered. First, the photocleavable peptide serves as a high-affinity peptide to ensure the proper folding of MHC I. The cleavage of the peptide's backbone results in two

low-affinity fragments, which allow tapasin$^{\Delta TMD}$–ERp57^{C36A} to associate with MHC I. Purified tapasin$^{\Delta TMD}$–ERp57^{C36A} and photocleavable peptide/MHC I complex were mixed in stoichiometric amounts and aliquots of 20 µl were exposed to UV light (365 nm, 185 mW/cm^2, 120 s). After incubation for 10 min at RT, samples were centrifuged at 15,000 xg at 4 ºC and analyzed by SEC. For crystallization, tapasin$^{\Delta TMD}$–ERp57^{C36A} and photocleavable peptide/MHC I complex were mixed in a molar ratio of 1.0/1.0 or 1.0/1.3 at a total concentration of 20 mg/ml or 10 mg/ml. After exposure with UV light, samples were directly used for crystallization trials.

8.4.19 Acidic wash to remove peptides from binding pocket of HLA-B*44:02

Acidic wash is a method to remove pMHC I hc/β_2m complexes of cell surface. Here, it was performed to remove peptides from HLA-B*44:02, which could only be refolded with high-affinity peptides without the modification of a photocleavable peptide. Tapasin$^{\Delta TMD}$–ERp57^{C36A} was either added in a molar ratio of 10/1 to 10 µM of HLA-B*44:02 in 50 µl SEC buffer either before the incubation of 750 µl of sodium citrate, pH 3.0 for 150 s or after. For neutralization, 1 ml of TRIS, pH 8.0 was added. Samples were concentrated and SEC was performed.

8.4.20 X-ray crystallography

X-ray crystallography is a technique to determine the three-dimensional molecular structure of a crystal. The crystal is exposed to an X-ray beam, which leads to the diffraction into specific directions. The diffraction pattern contains reflections, that have various intensities. Further processing provides a list of indexed reflections with corresponding intensities. Electron density can be reconstructed by Fourier Transformation, combining information of reflections and phases. Then, positions of atoms in the crystal can be calculated and an initial atomic model of the protein structure is generated. The model will be refined and rebuild until a suited match for the model and the experimental data is found.

8.4.21 Protein crystallization

To obtain protein crystals, the protein molecules of interest must arrange into a periodic lattice. For initial screenings, a solution of protein with a high concentration is used. To reduce the solubility close to spontaneous precipitation, reagents are added. In theory, crystals will grow under proper conditions for the development of nucleation sites and with slowly increasing concentration. There are several methods to grow protein crystals, such as vapor diffusion. In this technique, the protein is mixed with a crystallization cocktail, containing of precipitants, additives, detergent etc., and a droplet of this mixture is exposed to a larger reservoir with the same crystallization cocktail. As the precipitant concentration is lower in the droplet, water

evaporates from the droplet into the reservoir. The concentration of protein and precipitant in the droplet slowly increases and crystals might grow. For initial screening, 20 mg/ml of MHC I-tapasin$^{\Delta TMD}$–ERp57^{C36A} in a molar ratio of 1:1 was exposed to UV light in 20 µl aliquots and 96-well crystallization screens were set up using a mosquito® crystal (SPT Labtech). Screens were prepared at RT and transferred to 16 ºC. Fine screening was performed by varying the pH and precipitant concentration of reservoir solution 100 µM sodium cacodylate pH 6.5, 300 µM sodium acetate, 8% PEG 20,000 (v/v), 8% PEG 500 MME (v/v). Screens were set up either by sitting or hanging drop technique using 1 µl/1 µl protein/reservoir solution and 500 µl reservoir. As no crystals were obtained in hanging drop screens, sitting drop was utilized in the following screening. Concentration of protein mixture could be reduced to 10 mg/ml. To obtain higher resolution, tapasin$^{\Delta TMD}$–ERp57^{C36A} was deglycosylated by using PNGaseF or EndoH. Proteins were either deglycosylated prior to screening or glycosidases were added to protein mixture right before the screens were set up. Since resolution of crystals, containing deglycosylated heterodimer were not improved, glycosylation was not removed for further screenings. Next, constructs of H2-D^{b} and tapasin$^{\Delta TMD}$–ERp57^{C36A} without or with cleavable His_6-tag, respectively were used and molar rations of 1.1/1.0, 1.2/1.0, 1.3/1.0 of H2-D^{b}–tapasin$^{\Delta TMD}$–ERp57^{C36A} were tested. Since crystals obtained from conditions with proteins in molar ratio of 1.3/1.0 without His_6-tags showed improved morphology, these modifications were used to screen additives. 10% of additives (v/v) were added to fine screened reservoir solution of 100 µM sodium cacodylate pH 6.2, 300 µM sodium acetate, 6% PEG 20,000 (v/v), 6% PEG 500 MME (v/v). Additive screens were set up as initial 96-well screens. EDTA, EGTA and CYMAL-5 were further fine screened varying the additive concentration. As resolution could be improved for additives EGTA and CYMAL-5, both additives were separately and combined further fine screened, testing different precipitant concentrations and additive concentrations. Also, different protein/reservoir ratios of 0.8/1.2, 1.2/0.8 were tested and streak seeding using a whiskers hair, kindly provided by Samoil Sekulovski, was performed. Next, the strategy of dehydration was applied. Therefore, the precipitant concentration of the reservoir solution was increased in 0.5% steps and incubated overnight. Additionally, the solution containing crystals was exchanged with reservoir solution containing 30% ethylene glycol (v/v) and crystals were flash-frozen at different time points. After dehydration of crystals did not improve the resolution, crystals were utilized for microseed matrix screening (MMS)[24]. Therefore, crystals were crushed, transferred to a tube containing seed beads and vortexed for 5 min at RT. Seeds were used as crystallization seeds and another round of crystallization trials were performed. Initially obtained crystals from 96-well plates with a reservoir solution of 100 mM Gly-Gly, AMPD, pH 8.5 300 mM lithium sulfate, 300 mM sodium sulfate, 300 mM potassium sulfate, 20% PEG 8000 (v/v), 40% 1,5-pentanediol (v/v) and a seed/protein/reservoir of 0.3/1.0/1.0. Crystals obtained initially with MMS diffracted to the

desired resolution. Hits from MMS were further fine screened, varying pH, precipitant concentration, and seed/protein/reservoir ratio, for peptide soaking experiments. Peptides were solved in SEC buffer at a final concentration of 10 mg/ml. Volumes of 0.3 µl, 0,4 µl, 0,6 µl were added to the droplet, containing already grown crystals. After incubation times of 1 h, 1 day, 2 days, 3 days and 4 days, crystals were flash-frozen in liquid nitrogen. MMS was modified to cocrystallize the allomorph HLA-B*44:05 with tapasin$^{\Delta TMD}$–ERp57^{C36A}. To this end, screens were set up as for the H2-D^{b}–tapasin$^{\Delta TMD}$–ERp57^{C36A} complex, but the identical seeds of H2-D^{b}–tapasin$^{\Delta TMD}$–ERp57^{C36A} were applied.

For cryoprotection, different protectants of the CryoProtX kit were screened in different concentrations. Therefore, 3 µl of the corresponding reservoir containing the cryoprotectant, were added to the crystal droplet, solution was incubated for 90 s, and then removed. This step was repeated 4 times. Screening of different cryoprotectants resulted in 30% ethylene glycol to be the most prominent protectant and incubation times were further tested. Also, volatile alcohol solutions such as, 40% methanol or 40% *tert.* butyl alcohol were screened for cryoprotection by vapor diffusion[105]. To this end, crystals were transferred into the solution containing the volatile alcohol and incubated for 5s until overnight. Crystals obtained from MMS were directly flash-frozen in liquid nitrogen.

Table 36: Crystallization screens used in this thesis. All screens are manufactured by Molecular Dimensions.

Clear strategy
Hippocrates
MemAdvantage
Morpheus
Morpheus II
Structure Screen
The Morpheus Additive Screen

8.4.22 Data collection, structure determination and refinement

Crystals were measured either at beamline P13[106] or P14 operated by European Molecular Biology Laboratory (EMBL) Hamburg at the PETRA III storage ring (DESY, Hamburg, Germany) or at beamlines X06SA (PX) and X06DA (PXIII) operated by Paul Scherrer Institute (PSI) at the Swiss Light Source (SLS, Villigen, Switzerland). Collected data was indexed, integrated, and scaled using the XDS package[107]. Molecular replacement, using the coordinates of the MHC I–tapasin–ERp57 complex of the peptide-loading complex (PLC, PDB ID 6ENY)[12] within the Phenix software package[108], was performed to solve the structure. COOT[109] was utilized to build the complex manually. The refinement was done in Phenix, applying translation-liberation-screw (TLS) parameters and graphic images were created using PyMOL (Schrödinger). Further improvements were accomplished using the PDB-REDO server[110], followed by manual adjustments in COOT[109] and refinements in Phenix[108].

8.4.23 Cell staining

For analysis of surface pMHC I hc/β_2m molecules by flow cytometry, a surface staining of MHC I allomorphs using APC-conjugated antibodies was performed. All steps were carried out on ice. Transfected cells were washed with 200 µl of FACS buffer and centrifuged for 5 min at 300 xg and 4 ºC. Washed cells were blocked by 10% FcR blocking reagent, human in 50 µl of FACS buffer for 15 min. 200 µl of FACS buffer was added and cells were centrifuged for 5 min at 300 xg and 4 ºC. Then, cells were stained with 2 µl of APC anti human HLA-A/B/C antibody (clone W6/32, BioLegend), HLA-A2 antibody anti-human, APC, REAfinity™ (Miltenyi Biotec), HLA-B polyclonal antibody (Invitrogen) and purified anti-human HLA-C antibody (clone DT-9, BioLegend) in 50 µl FACS buffer for 30 min. Subsequently, cells were 2x washed with 0.2 ml FACS buffer and cells stained with conjugated antibodies were resuspended in FACS buffer for analysis by flow cytometry. Cells stained with HLA-B and HLA-C antibodies were separately incubated with goat anti-rabbit IgG (H+L) cross adsorbed secondary antibody, APC (Invitrogen) and APC goat anti-mouse IgG secondary antibody (BioLegend), respectively for 20 min. Finally, cells were 2x washed with FACS buffer and resuspended for analysis by flow cytometry.

Table 37: FACS buffer.

1x DPBS
2 mM EDTA
2% BSA
0.2% Sodium azide

Table 38: List of antibodies used for cell staining for flow cytometry.

Antigen	Conjugate	Isotype	Manufacturer
α-human HLA-A/B/C	APC	Mouse IgG2a, κ	BioLegend, W6/32
α-human HLA-A*02	APC	Recombinant human IgG1	Miltenyi Biotec, REA517
α-human HLA-B	-	Rabbit IgG	Invitrogen, PA5-35345
α-human HLA-C	-	Mouse IgG2b, κ	BioLegend, DT-9
α-rabbit	APC	Goat IgG	Invitrogen
α-mouse	APC	Goat IgG	BioLegend

8.4.24 Flow cytometry

Flow cytometry is a method to analyze single cells and particles in solution. Single particles are measured for visible light scatter and one or multiple laser fluorescent parameters. Visible light scatter is detected in forward detection, the forward scatter (FSC), and at 90º, the side scatter (SSC). While the FSC is dependent on the relative seize, the SSC depends on granularity of the cell. Fluorescent measurements are utilized for further analysis of cells. Therefore, cells can be transfected for expression of fluorescent proteins or are stained with fluorescently conjugated antibodies. Lasers function as light sources to generate both scattered and fluorescent light signals, which are measured by photodiodes or

photomultipliers. These signals are converted into electronic signals. FACSMelody™ cell sorter was utilized to record 5000 to 20,000 eGFP-positive cells and gating strategy is displayed in Figure 42.

8.4.25 Fluorescent-activated cell sorting

Fluorescent-activated cell sorting is a technique to sort single cells of a heterogenous mixture of cells based on their specific light scattering and fluorescent characteristics. The flow of suspended cells is disrupted by a vibrator and break into individual droplets, ideally containing a single cell. The droplets are given an electronic charge, which depends on the fluorescence of the cell. According to their charge, cells are attracted or repelled by deflection plates into collection tubes. To analyze the expression of the gene of interest on protein level, 10,000 to 200,000 eGFP-positive cells were sorted utilizing the FACSMelody™ Cell Sorter (BD Biosciences).

8.4.26 Isothermal titration calorimetry

The technique isothermal titration calorimetry analyses the thermodynamic parameters of an interaction. ITC is based on the generation or absorption of heat, which results from binding of two or more molecules depending on the type of reaction, which can be either endothermic or exothermic. The heat upon binding of two or more molecules in solution is measured directly and the binding affinity (k_a), binding stoichiometry (n), and enthalpy changes (ΔH) are provided. Furthermore, the changes in entropy (ΔS) and Gibbs free energy (ΔG) can be determined using the Gibbs free energy equation (ΔG=ΔH-TΔS). The instrument composes two cells, the main cell is filled with the solution of one binding partner, the second cell serves as the reference cell and contains water. Both cells are kept at the same temperature. The ligand or second molecule of interest is titrated into the main cell. Upon binding, heat is generated or consumed, causing a change in temperature relative to the reference cell. To maintain the selected temperature, the instrument gives the relevant power, which is plotted against time. The resulting heat pulses are integrated with respect to time. To analyze the interaction between tapasin$^{\Delta TMD}$–ERp57^{C36A} and calreticulin, the heterodimer was filled into the main chamber, while calreticulin was titrated in 20 steps with an injection volume of 2 µl at a constant temperature of 25 ºC. The first injection composed 0.2 µl and was deleted bevor analysis of data. The reference measurement, titration of calreticulin into buffer was subtracted from actual measurement. Protein solutions were beforehand dialyzed against the identical buffer (Chapter 8.4.7), or final SEC polishing of purified proteins was performed in the identic buffer.

9 Results

9.1 Functional and structural analysis of tapasin–ERp57/calreticulin

The PLC plays a major role in adaptive immunity, ensuring the generation of stable pMHC I complexes. Revealing assembly and interaction principles of PLC subunits are crucial to understand its mode of action. The overall architecture of native PLC was determined recently by cryo-EM[12]. In a later study, map resolution for the editing module of the PLC was improved by avoiding chemical crosslinking and utilization of lipid nanodiscs[111]. Within the PLC, calreticulin has three interaction partners[12,111]. The tip of the P-domain interacts with the b' domain of ERp57[12,22,112] , the lectin domain senses the N-core glycan at Asn[86] of MHC I[12] and the acidic C-terminal helix contacts the C-terminal domain of tapasin[12]. The interaction between the P-domain and ERp57 has been mainly characterized by solution NMR and ITC[22], whereas the contact of the lectin domain with the N-linked glycan of MHC I or the acidic helix and the C-terminal domain of tapasin was visualized by cryo-EM[111]. Due to the high flexibility of calreticulin, maps at atomic resolution could not be determined to date.

9.1.1 Intact disulfide bond present in purified tapasin–ERp57 heterodimer

For structural and functional analysis of the editing module, expression constructs for tapasin and ERp57 were established. The tapasin construct lacked the transmembrane and the cytosolic domain and carried an engineered C-terminal His_6-tag (tapasin$^{\Delta TMD}$). The ERp57 construct featured a Cys36Ala substitution (ERp57^{C36A}) that prevented the switch from an intermolecular disulfide bond with tapasin to an intramolecular disulfide bond, called escape pathway[77] . Modified MultiBac vectors of tapasin$^{\Delta TMD}$ and ERp57^{C36A} were fused by Cre-mediated recombination generating a transfer plasmid for integration into the EMBacY baculoviral genome by Tn7 transposition[113,114]. Isolated EMBacY bacterial artificial chromosomes (BACs) were utilized to transfect *Sf*21 cells to produce virus for large-scale infection of *Sf*21 cells[113–115]. Overexpressed tapasin$^{\Delta TMD}$–ERp57^{C36A} heterodimer was purified *via* IMAC, the C-terminal His_6-tag was cleaved off by TEV protease treatment, and cleaved tapasin$^{\Delta TMD}$–ERp57^{C36A} was cleaned *via* reverse IMAC. Finally, heterodimer was polished by SEC (Fig. 7).

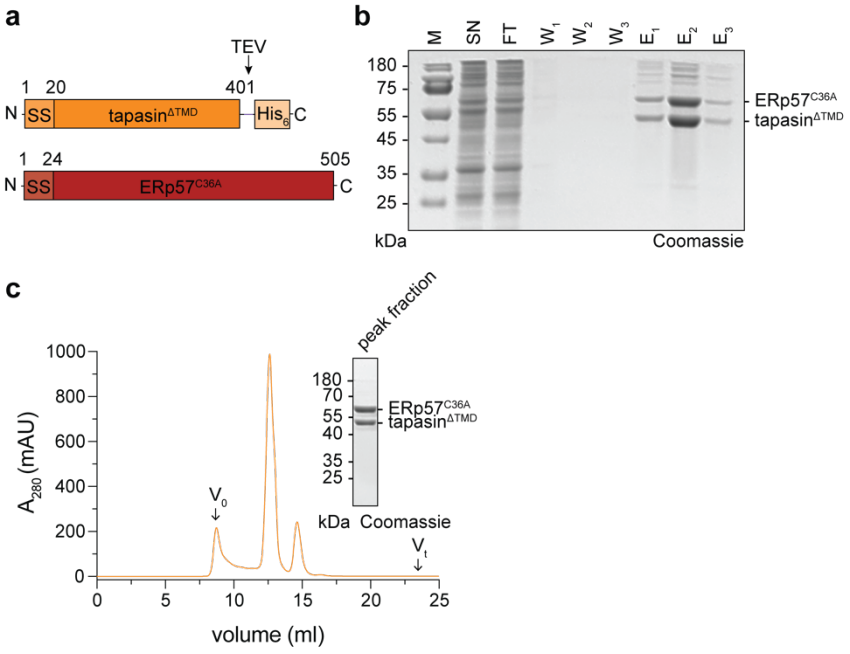

Figure 7: Purification of tapasin$^{\Delta TMD}$–ERp57^{C36A} heterodimers. a, Bar diagrams of used constructs. **b**, SDS-PAGE analysis of IMAC purification. **c**, Elution profile of a preparative SEC as final purification step and corresponding SDS-PAGE analysis of the peak fraction. 11% Tris-tricine gels were used for SDS-PAGE. SS, signal sequence; M, marker; SN, supernatant; FT, flow through; W_{1-3}, wash steps 1 - 3; E_{1-3}, elution fraction 1 - 3; kDa, kilodalton; PRE_{TEV}, sample before addition of TEV; $POST_{TEV}$, sample after addition of TEV; A_{280}, absorption at 280 nm, V_0, void volume; V_t, total volume.

Using this procedure, a stoichiometric tapasin$^{\Delta TMD}$–ERp57^{C36A} heterodimer was purified (Fig. 7). SDS-PAGE analysis of eluates from the IMAC step showed only minor impurities, as compared to the amount of heterodimer (Fig. 7b). Last polishing step by SEC revealed a small excess of tapasin$^{\Delta TMD}$, that was separated from the heterodimer by SEC (Fig. 7c). Formation of the intermolecular disulfide bond between tapasin$^{\Delta TMD}$ and ERp57^{C36A} was analyzed by SDS-PAGE and LC-MS (Fig. 8a-e). SDS-PAGE was performed with purified heterodimer either under reducing or non-reducing conditions. Under non-reducing conditions, a single narrow band with an apparent molecular mass of 110 kDa was observed corresponding to the mass of the heterodimer (Fig. 8a). That result demonstrates that the disulfide bond between tapasin$^{\Delta TMD}$ and ERp57^{C36A} is intact. Moreover, LC-MS analysis verified the presence of the mixed disulfide as shown by the detected mass of 96,369.1 Da corresponding to the heterodimer (Fig 8c). Notably, the heterodimer was treated with EndoH to generate a homogenous, tapasin$^{\Delta TMD}$ species without glycan-dependent mass differences for LC-MS analysis. Furthermore, sample quality of the heterodimer was ensured by crystallizing published crystallization conditions[8] (Fig. 8f). In summary, tapasin$^{\Delta TMD}$–ERp57^{C36A} was produced stoichiometrically as a disulfide-linked heterodimer with a sample quality that is suited for structural analysis.

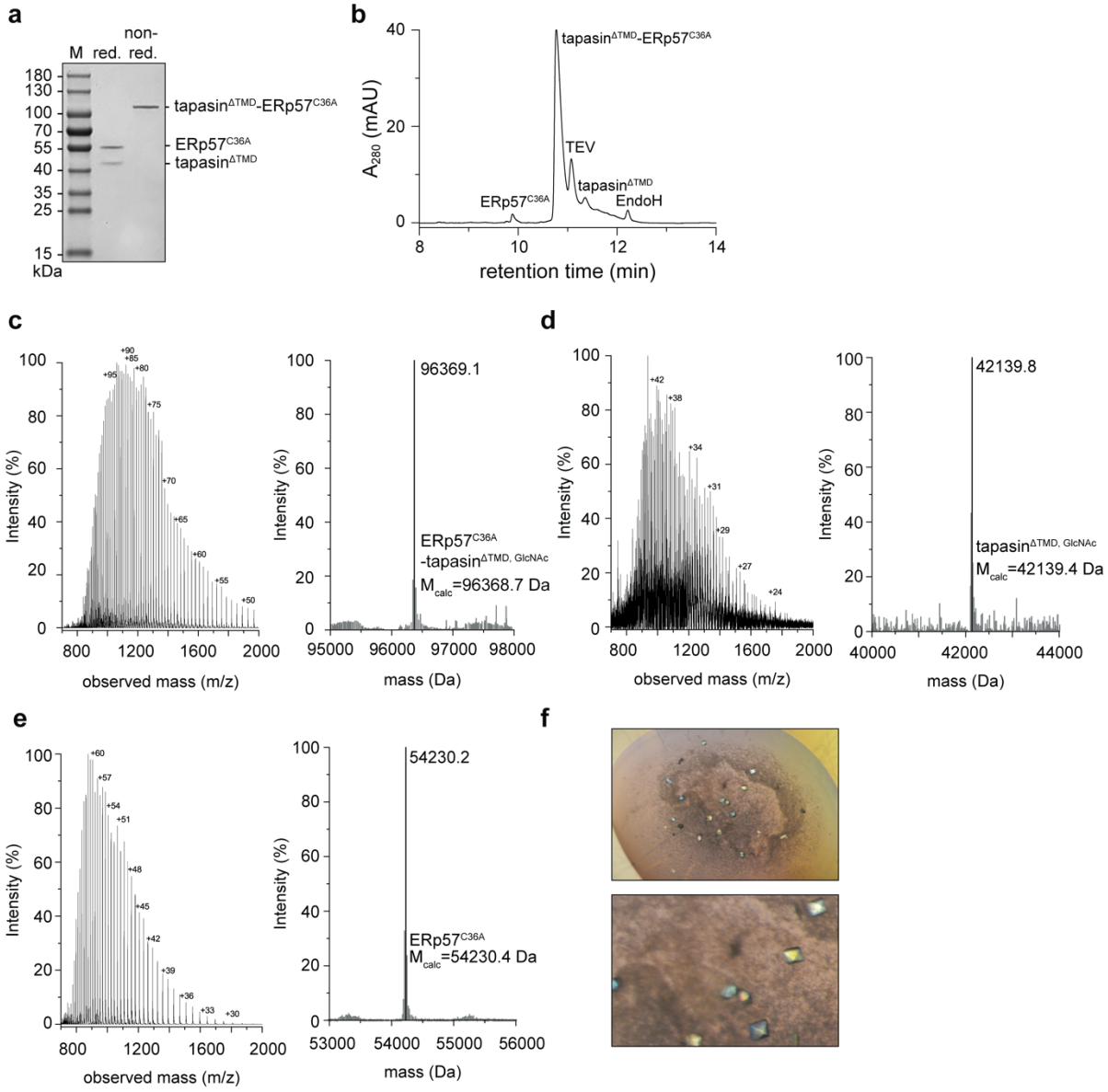

Figure 8: Intermolecular disulfide bond and sample quality of tapasin$^{\Delta TMD}$–ERp57^{C36A}. a, SDS-PAGE analysis of heterodimer in reducing and non-reducing conditions performed utilizing 11% Tris-tricine gel. **b**, RP-HPLC analysis of EndoH-deglycosylated heterodimer. **c**, ESI-MS (left) and MaxEnt1 deconvoluted (right) spectra of tapasin$^{\Delta TMD}$–ERp57^{C36A}. **d**, ESI-MS (left) and MaxEnt1 deconvoluted (right) spectra of tapasin$^{\Delta TMD}$. **e**, ESI-MS (left) and MaxEnt1 deconvoluted (right) spectra of ERp57^{C36A}. **f**, Image of 2 µl droplet, containing obtained crystals of heterodimer (top), zoom in of crystals (bottom). LC-MS measurements were performed by Christian Winter. kDa, kilodalton; M, marker; red., reducing; non red., non-reducing; A_{280}, absorption at 280 nm.

9.1.2 Tapasin$^{\Delta TMD}$–ERp57 ^{C36A} heterodimer has micromolar affinity to calreticulin

To gain further insights into the interaction between calreticulin and the tapasin$^{\Delta TMD}$–ERp57^{C36A} heterodimer, recombinant full-length (calreticulin^{WT}) and truncated calreticulin lacking the acidic helix (aa369 – aa417; calreticulin$^{\Delta acidic\ helix}$) were expressed in *E. coli* and

purified *via* an N-terminal, cleavable His_6-tag (Fig. 9a,b and c). After IMAC purification, His_6-tags were removed by TEV protease treatment and proteins were polished by SEC (Fig. 9d,e).

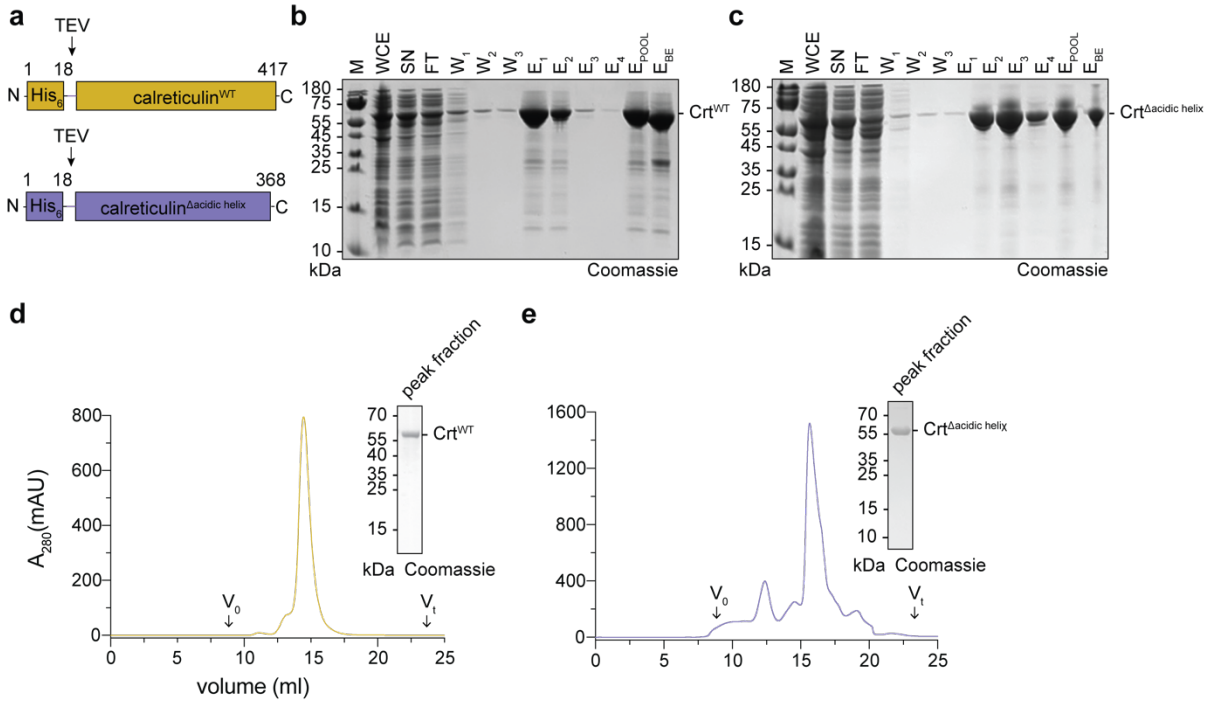

Figure 9: Purified calreticulin constructs are monodisperse. a, Schematic illustration of calreticulin constructs. b, SDS-PAGE analysis of IMAC of calreticulin^{WT}. **c**, IMAC purification of calreticulin$^{\Delta acidic\ helix}$ analyzed by SDS-PAGE. **d**, Polishing of calreticulin^{WT} by SEC and SDS-PAGE of corresponding peak fraction (inset). **e**, Elution profile of SEC of calreticulin$^{\Delta acidic\ helix}$ and SDS-PAGE analysis of the peak fraction (inset). 11% Tris-tricine gels were utilized for SDS-PAGE. crt, calreticulin; kDa, kilodalton; M, marker; WCE, whole cell extract; SN, supernatant; FT, flow through; W_1-W_3, wash steps 1-3, E_1-E_4, elution fractions 1-4; E_{POOL}, pooled eluates; E_{BE}, pooled eluates after buffer exchange; A_{280}, absorption at 280 nm, V_0, void volume; V_t, total volume.

SEC shows that both calreticulin samples were monodisperse. Full-length and C-terminally truncated calreticulin eluted as single peaks and were obtained at high protein concentrations (15-20 mg/ml) suitable for interaction studies with the tapasin$^{\Delta TMD}$–ERp57^{C36A} heterodimer.

The interaction between the P-domain of calreticulin and ERp57 was previously investigated by ITC and NMR[22]. The analysis was based on full-length ERp57 and the isolated P-domain of calreticulin comprising residues 189 to 288, which structure has been solved by NMR[116]. Similar K_D values in the micromolar range were determined at different temperatures (9.1 ± 3.0 µM at 8 °C and 18 ± 5 µM at 20 °C) with both techniques being in good agreement[22]. To investigate the impact of the acidic helix of calreticulin on the interaction with tapasin$^{\Delta TMD}$–ERp57^{C36A}, the purified calreticulin constructs were used in ITC experiments. Release of heat was measured upon titration of calreticulin^{WT} (495 µM) to tapasin$^{\Delta TMD}$–ERp57^{C36A} (19 µM) and saturation was reached (Fig. 10a).

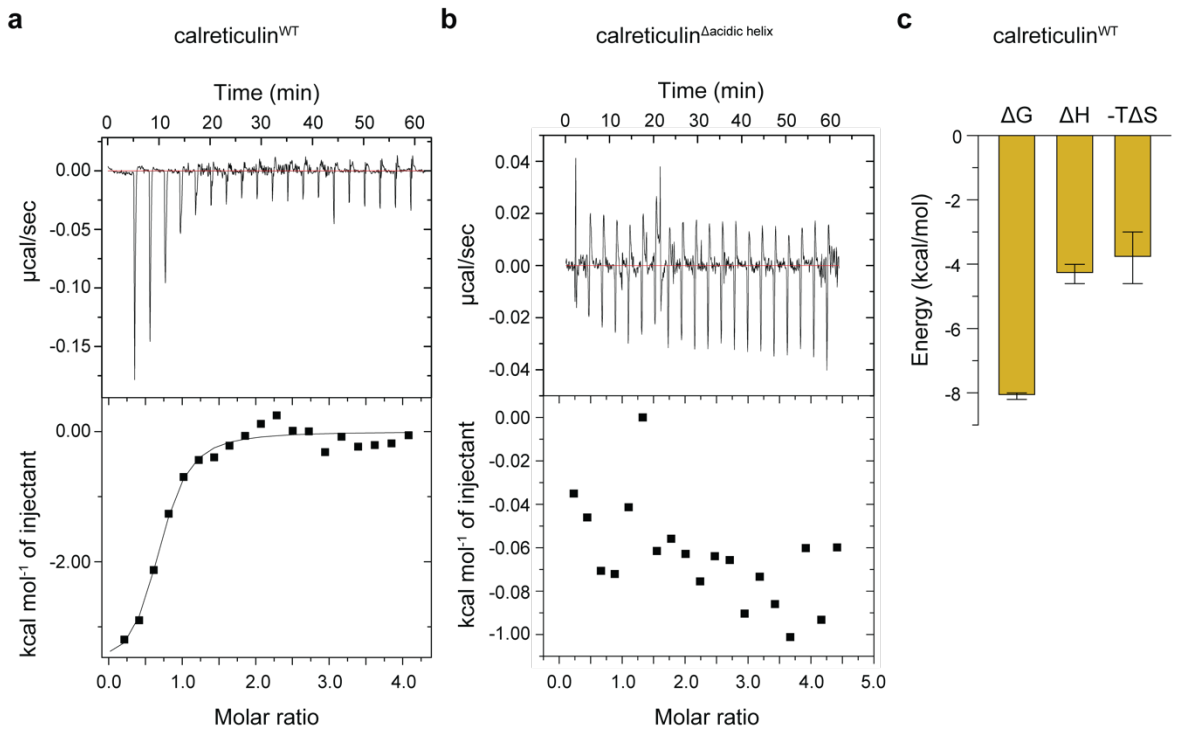

Figure 10: Interaction of tapasin$^{\Delta TMD}$–ERp57^{C36A}/calreticulin^{WT} is in the micromolar range. a, Raw data (top panel) and integrated heat peaks against molar ratio of calreticulin^{WT} (low panel) of ITC. **b**, Top panel shows raw data and low panel displays integrated heat peaks against the molar ratio of calreticulin$^{\Delta acidic\ helix}$. **c** Binding signature plot of ΔG, ΔH and -TΔS determined from ITC (a). ΔH, change of enthalpy; T, temperature; ΔS, change of entropy.

The data was background corrected by subtraction of the mean value of the integrated heat release at saturating titrant concentration and fitted using a one-site ITC binding model. A K_D value of 0.82 ± 0.09 µM with a stoichiometry (N) of 0.63 ± 0.02 sites was determined (Fig. 10a). The deviation of the stoichiometry was presumably caused by the concentration determination, which, as it turned out later, was not quite accurate for technical reasons. Based on change in enthalpy (ΔH) of -4.3 ± 0.3 kcal/mol, the change of entropy (ΔS) was calculated as 12.7 ± 2.7 cal/mol/K. The binding signature plot (Fig. 10c) demonstrates that the binding of calreticulin is comprised of hydrogen bonding and hydrophobic interactions as indicated by the negative or favorable enthalpy (ΔH) and entropy (-TΔS) factors. The binding of calreticulin to tapasin$^{\Delta TMD}$–ERp57^{C36A} is exergonic shown by a favorable ΔG value of -8.1 ± 0.1 kcal/mol.

For the calreticulin$^{\Delta acidic\ helix}$ construct, no measurable heat effect was determined upon titration to tapasin$^{\Delta TMD}$–ERp57^{C36A} using the same conditions as for the ITC experiment with calreticulin^{WT} (Fig. 10b), indicating that without the contribution of the acidic helix of calreticulin, the interaction is characterized by lower affinity. The published K_D was determined by ITC by titration of the isolated P-domain of calreticulin at a concentration of 2 mM to 200 µM ERp57[22]. However, it was not possible to concentrate full-length and C-terminally truncated

calreticulin to higher concentrations then 500 µM. In summary, the acidic helix contributes more to binding of calreticulin to tapasin$^{\Delta TMD}$–ERp57^{C36A} than the P-loop.

9.1.3 The interaction between the acidic helix of calreticulin and tapasin can be electrostatically stabilized

The acidic helix of calreticulin was shown to bind in a cleft of the C-terminal domain of tapasin[12]. However, the molecular details of this interaction have not been characterized yet. Therefore, tapasin$^{\Delta TMD}$–ERp57^{C36A} and calreticulin^{WT} were incubated in an equimolar ratio and analyzed for complex formation by SEC (Fig. 11a). SDS-PAGE analysis of the corresponding peak fraction did not show stoichiometric amounts of calreticulin^{WT}/tapasin$^{\Delta TMD}$–ERp57^{C36A} (Fig. 11a). I hypothesized that a positively charged C-terminal His_6-tag on tapasin$^{\Delta TMD}$ (tapasin$^{\Delta TMD_His6}$) may stabilize the interaction with the acidic helix of calreticulin leading to a kinetically stable complex that can be isolated by SEC. Indeed, the SEC elution profile and corresponding SDS-PAGE analysis showed that the electrostatic interaction of the His_6-tag and the acidic helix of calreticulin resulted in a kinetically stable complex (Fig. 11b). To further analyze this effect, ITC was performed as described before. The determined K_D of 2.2 ± 0.6 µM, N of 0.66 ± 0.14 sites, ΔH of -7.1 ± 2.1 kcal/mol, ΔS of -7.6± 2.5 cal/mol/K are similar to the values for tapasin without His_6-tag (Fig. 11c,d). The introduction of the C-terminal His_6-tag on tapasin$^{\Delta TMD}$ resulted in an electrostatic stabilization between the positively charged His_6-tag on tapasin$^{\Delta TMD}$ and the acidic helix of calreticulin, which was observed by SEC (Fig. 11). While the kinetic stable complex of calreticulin^{WT}/tapasin$^{\Delta TMD_His6}$–ERp57^{C36A} remained bound during the duration of the SEC, the complex of calreticulin^{WT}/tapasin$^{\Delta TMD}$–ERp57^{C36A} dissociated into the reactants calreticulin^{WT} and tapasin$^{\Delta TMD}$–ERp57^{C36A}.

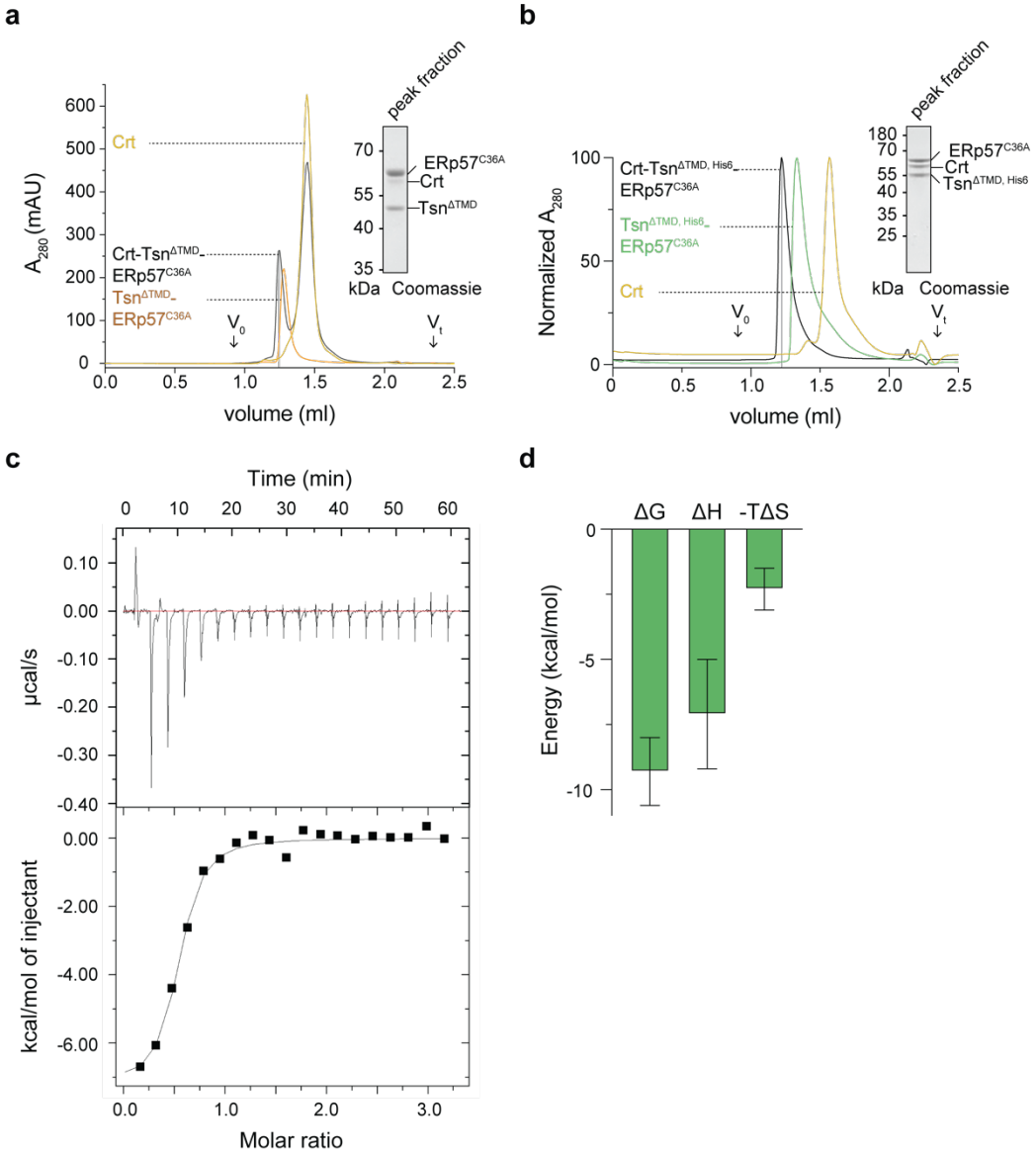

Figure 11: His$_6$-tag insertion results in electrostatically stabilization of interaction between tapasin$^{\Delta TMD}$ and calreticulin^{WT}. a, SEC analysis of calreticulin^{WT}–tapasin$^{\Delta TMD}$–ERp57^{C36A} with corresponding SDS-PAGE of peak fraction (inset). **b**, Elution profile of complex formation utilizing tapasin$^{\Delta TMD,\ His6}$ and corresponding SDS-PAGE analysis of peak fraction (inset). **c**, Raw data (top panel) and integration of heat peaks (lower panel) of ITC using tapasin^{His6}. **d**, Signature binding plot (ΔG, ΔH, -TΔS) of ITC displayed in c. 11% Tris-tricine gels were utilized for SDS-PAGE. kDa, kilodalton; A_{280}, absorption at 280 nm, V_0, void volume; V_t, total volume; ΔG, change of Gibbs energy; ΔH, change of enthalpy; T, temperature; ΔS, change of entropy.

9.1.4 Native mass spectrometry reveals a trimeric tapasin$^{\Delta TMD}$–ERp57^{C36A}/calreticulin^{WT} complex

To elucidate the oligomeric state of the recombinant tapasin$^{\Delta TMD}$–ERp57^{C36A}/calreticulin^{WT} complex and to compare it to cryo-EM structures of the native editing module[12], native mass spectrometry was performed in collaboration with the Morgner laboratory (Goethe University

Frankfurt). LILBID[104] is a soft ionization technique, which allows the analysis of intact noncovalent complexes and was therefore applied to determine the oligomeric state of the complex. Buffer of tapasin$^{\Delta TMD}$–ERp57^{C36A}/calreticulin^{WT} was exchanged to 100 mM ammonium acetate, suited for mass spectrometry. The complex of tapasin$^{\Delta TMD}$–ERp57^{C36A}/calreticulin^{WT} was found to exist as a trimeric complex (Fig. 12a). Masses corresponding to the single-, double-, triple- and quadruple-charged species of the complex were detected (mass 146 kDa; Fig. 12a). Also, a small excess of calreticulin was present, as seen by masses corresponding to single- and double-charged species of calreticulin (mass 46 kDa; Fig. 12a). The reference spectra of heterodimer displayed species up to triple charged heterodimer (mass 100 kDa; Fig. 12a). For calreticulin^{WT}, single- and double-charged species were found (Fig. 12a).

Since no interaction of calreticulin$^{\Delta acidic\ helix}$ to tapasin$^{\Delta TMD,\ His6}$–ERp57^{C36A} was observed by ITC (Fig. 10b), oligomeric state was analyzed by LILBID-MS (Fig. 12b). But no clear signal corresponding to the mass of complex was present, while calreticulin$^{\Delta acidic\ helix}$ was detected as single-charged monomer and dimer (mass 41 kDa; Fig. 12b). However, only one spectrograph of the heterdimer tapasin$^{\Delta TMD,\ His6}$–ERp57^{C36A} allowed the assignment of all masses to species of heterodimer, indicating that the heterodimer was not stable for longer durations in buffer utilized for LILBID-MS.

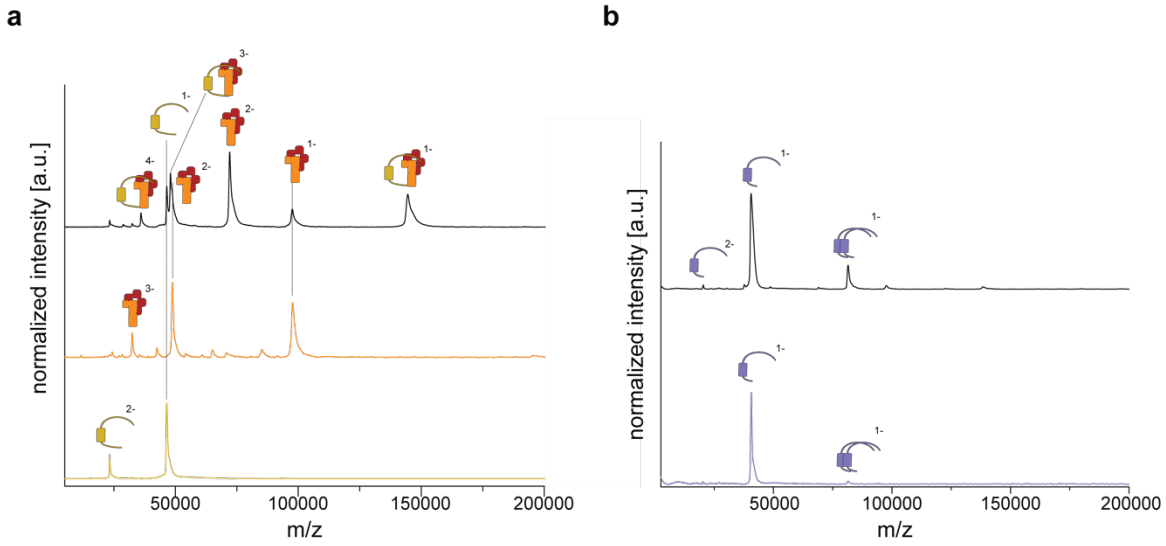

Figure 12: Tapasin$^{\Delta TMD,\ His6}$–ERp57^{C36A}/calreticulin^{WT} form a trimeric complex. a, LILBID-MS spectra of calreticulin^{WT}, tapasin$^{\Delta TMD,\ His6}$–ERp57^{C36A} and tapasin$^{\Delta TMD,\ His6}$–ERp57^{C36A}/calreticulin^{WT} (bottom to top), different complex compositions with respective charge assigned to signals with corresponding masses. **b**, LILBID-MS spectra of calreticulin$^{\Delta acidic\ helix}$ and tapasin$^{\Delta TMD,\ His6}$–ERp57^{C36A}/calreticulin$^{\Delta acidic\ helix}$ (bottom to top). Signals were assigned to complex compositions with respective charge corresponding to their size. a.u., arbitrary units; m/z, mass-to-charge ratio. LILBID-MS was performed by Dr. Janosch Martin, Morgner laboratory, Institute of Physical and Theoretical Chemistry, Goethe-University Frankfurt.

9.1.5 Crystallization of tapasin$^{\Delta TMD,\ His6}$–ERp57^{C36A}/calreticulin^{WT}

The interaction between the acidic helix of calreticulin and the C-terminal domain of tapasin has not been resolved at atomic resolution[12,111]. To gain molecular insights into the interaction of tapasin–ERp57/calreticulin, a recombinant approach was chosen to capture the trimeric complex of tapasin$^{\Delta TMD,\ His6}$–ERp57^{C36A}/calreticulin^{WT}, allowing the C-terminal His_6-tag of tapasin for stabilization. The complex was assembled *in vitro* in a 1/1/1 ratio and purified by SEC. The corresponding peak fraction was concentrated to 8.0 mg/ml and directly used for crystallization trials. Small crystals were obtained under one condition comprising 100 mM Tris-HCl, pH 8.0, 200 mM $CaCl_2$, 44% PEG 400 of as part of the MemGold 96-well plate screen (Fig. 13). However, attempts to fine screen the condition failed and a second round of 96-well plate screen did not result in crystal growth. Most likely, the binding of MHC I, occupying the third interaction site, is required to stabilize the complex of tapasin$^{\Delta TMD,\ His6}$–ERp57^{C36A}/calreticulin^{WT} for structural studies.

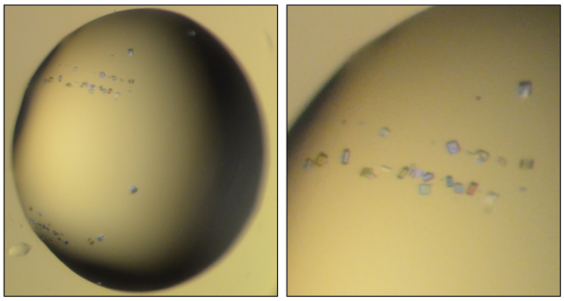

Figure 13: Crystallization trials of the tapasin$^{\Delta TMD,\ His6}$–ERp57^{C36A}/calreticulin^{WT} trimer. Image of droplet containing initially obtained crystals (left panel). Left panel shows a zoom in of crystals. Crystals grew in 100 mM Tris-HCl pH 8.0, 200 mM $CaCl_2$, 44% PEG 400. SEC purified trimer was concentrated to 8 mg/ml.

9.1.6 Calreticulin forms a trimeric complex with tapasin$^{\Delta TMD}$–ERp57 ^{C36A} with micromolar affinity

The arrangement and interaction of PLC subunits are essential for its function in peptide loading and thus in producing stable pMHC I complexes. To ensure an optimal process of peptide editing, calreticulin embraces the editing modules with three interaction sites. The tip of the P-loop was found to interact with the b' domain of ERp57[12,22,117], the glycan-binding site senses the N-core glycan of Asn^{86} of MHC I and the acidic helix was found to come in close contact with the C-terminal domain of tapasin[12]. To gain detailed insights into interaction sites of editing module subunits, the complex of tapasin$^{\Delta TMD}$–ERp57^{C36A}/calreticulin was functionally analyzed. The binding affinity of calreticulin to the tapasin$^{\Delta TMD}$–ERp57^{C36A} heterodimer was determined by ITC and a K_D of 0.82 ± 0.09 µM was observed. Hydrogen bonding and hydrophobic interactions characterize the exergonic binding of calreticulin, suggesting that the flexible acidic domain of calreticulin might be contacted via hydrogen bonds by a basic patch

located at the C-terminal domain of tapasin. Deletion of the acidic helix drastically decreased the affinity of calreticulin$^{\Delta acidic\ helix}$ to tapasin as evidenced by ITC (Fig. 10b). This contrasts with a previous study that provided K_D values in the range of 7 – 23 µM[22]. However, full-length ERp57 and the isolated P-domain of calreticulin was used in this study, which allowed the usage of higher concentrations for ITC. Comparison of the ITC data of calreticulin^{WT} and calreticulin$^{\Delta acidic\ helix}$ highlights the importance of the interaction site of the acidic helix of calreticulin and the C-terminal domain of tapasin$^{\Delta TMD}$.

The complex of tapasin$^{\Delta TMD}$–ERp57^{C36A}/calreticulin^{WT} was found to be kinetically instable in SEC. The introduction of a C-terminal His_6-tag of tapasin$^{\Delta TMD}$ lead to an electrostatic stabilization and a stoichiometric complex of tapasin$^{\Delta TMD,\ His6}$–ERp57^{C36A}/calreticulin^{WT} could be observed by SEC. Binding signature values in a similar range as for the complex without a His_6-tag for stabilization were determined by ITC. The oligomeric state of a trimer was determined by LILBID-MS in collaboration with the Morgner laboratory. For further experiments, optimal buffer conditions that are compatible for LILBID-MS with the heterodimer need to be established, enabling the investigation of possible interaction between calreticulin$^{\Delta acidic\ helix}$ and heterodimer. Moreover, assembly and disassembly of editing module subunits, involving MHC I allomorphs, can be addressed utilizing LILBID-MS in the future.

No structural data of the possible interaction site between acidic helix of calreticulin and C-terminal domain of tapasin are available at atomic resolution. Especially the extended acidic helix might be flexible. To modify proteins for further stabilization of interactions, a recombinant approach was chosen for structural analysis. Tapasin$^{\Delta TMD,\ His6}$ with a C-terminal His_6-tag was used to assemble the trimer *in vitro*. Small crystals were obtained in initial crystallization trials, but crystals could not be reproduced. For future structural analysis, the addition of MHC I with a defined monoglucosylated N-linked glycan of Asn^{86} could contribute to stabilize the interaction with calreticulin. So far, MHC I molecules were expressed in *E. coli* and refolded with a high-affinity peptide. Post-translational modifications such as glycosylation are not possible in *E. coli*, therefore, new expression and purification methods for MHC I need to be established. Recently, a leucine zippered MHC I and TAPBPR complex, in which the hc is tethered to β_2m by a GlySer-linker was coexpressed in mammalian cells[118]. The coexpression of a leucine zippered MHC I and tapasin–ERp57 construct or expression of MHC I in mammalian cells enables the production of fully glycosylated MHC I molecules, thus are important approaches for *in vitro* assembly of an editing module. Moreover, calreticulin recognizes MHC I molecules, which are monoglucosylated ($Glc_1Man_9GlcNAc_2$). To create a monoglucosylated MHC I molecule, a construct of MHC I in which the hc is tethered by a $(GGGGS)_4$-linker to β_2m could be expressed in mammalian cells. Uridine diphosphate (UDP)-glucose:glycoprotein glucosyltransferase 1 (UGGT1) was shown to re-glucosylate the N-linked glycan of MHC I client *in vitro* (Sagert *et al.*, Tampé laboratory, Institute of Biochemistry,

Goethe University, manuscript in preparation). Based on this strategy, the assembly of monoglucosylated MHC I, heterodimer tapasin–ERp57 and calreticulin could be tested by LILBID-MS, SEC and finally for crystallization.

9.2 Structural analysis of MHC I–tapasin–ERp57 complex

The presentation of antigenic peptides by MHC I molecules on the cell surface ensures the detection and elimination of infected and cancerous cells by the adaptive immune system. The MHC I-chaperone tapasin in conjunction with ERp57 plays an important role in MHC I assembly and edits the peptide repertoire for high immunogenicity. MHC I allomorphs have different peptide-binding preferences and differ in their plasticity, which relates to their dependence of tapasin for optimal peptide-loading[16–21]. Due to the transient chaperone-MHC I interaction, the molecular basis of tapasin promiscuity for different MHC I allomorphs and structural features of an MHC I–tapasin–ERp57 complex at high-resolution that are crucial for peptide-exchange catalysis have remained elusive. Here, I set out to determine the X-ray crystal structure of an MHC I–tapasin–ERp57 complex.

9.2.1 *In vitro* complex formation by photoactivation

To capture the transient complex of MHC I–tapasin–ERp57, a photocleavable approach was chosen to generate a refolded peptide-receptive MHC I[25]. The ectodomain hc of MHC I allomorphs and human β_2m were separately expressed as inclusion bodies in *E. coli* and high-affinity peptides comprising a photocleavable amino acid were synthesized. The photoreaction leads to the cleavage of the peptide backbone by UV irradiation, thereby generating a peptide-receptive MHC I hc/β_2m complex, that is receptive for its association with tapasin (Fig. 14). The modified heterodimer of tapasin$^{\Delta TMD}$–ERp57^{C36A}, co-expressed in insect cells, was utilized for the photo-triggered *in vitro* assembly of MHC I–tapasin–ERp57. Complex formation was monitored by size exclusion chromatography (SEC), since a pure stoichiometric complex is ideal for crystallography. Refolded photocleavable peptide-MHC I (p*MHC I) and heterodimer were always prepared in a molar ratio of 1/1 at a concentration of 10 µM. The approach allows a high-throughput screening for optimal MHC I allomorph that is suited for complex formation with heterodimer. The mouse MHC I allomorph H2-D^b was selected based on the crystal structure of tapasin-homologue TAPBPR in complex with H2-D^b (ref.[11]). The allomorph HLA-B*08:01 was chosen as it shows intermediate tapasin-dependence[16,17] . The HLA-A*02:01 allele is distributed worldwide and the most prominent of HLA-A*02 subtypes. Compared to HLA-B*08:01, it is rather tapasin-independent[16,17]. Additionally, the allomorphs HLA-B*44:02 and HLA-B*44:05 were investigated because they differ only in one amino acid at position 116 (02: Tyr, 05: Asp), but are shown to be on opposed sides in their dependence on tapasin[16,17].

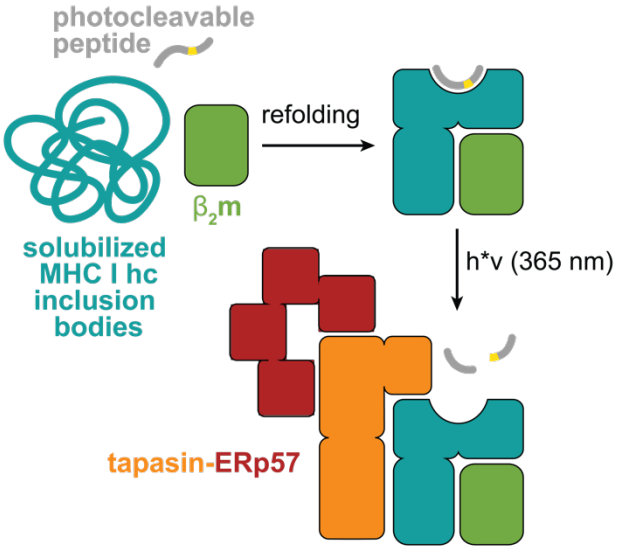

Figure 14: Schematic illustration of *in vitro* complex formation using UV irradiation[11]**.** MHC I hc inclusion bodies are solubilized, purified β_2m and a high-affinity photocleavable peptide are added for refolding. Refolded p*MHC I was UV irradiated in presence of heterodimer tapasin–ERp57. UV illumination causes cleavage of the backbone of the peptide, two low-affinity fragments result and tapasin–ERp57 can associate for stabilization and chaperoning of MHC I. hc, heavy chain. The figure is adapted from Thomas and Tampé, 2017 in *Science*.

9.2.2 Refolding of MHC I allomorphs

For MHC I assembly, the light chain β_2m was produced as inclusion bodies in *E. coli*, refolded by dialysis and polished by SEC. The β_2m sample was monodisperse (Fig. 15) and peak fractions around an elution volume of 88 ml were pooled and utilized for refolding of MHC I hc.

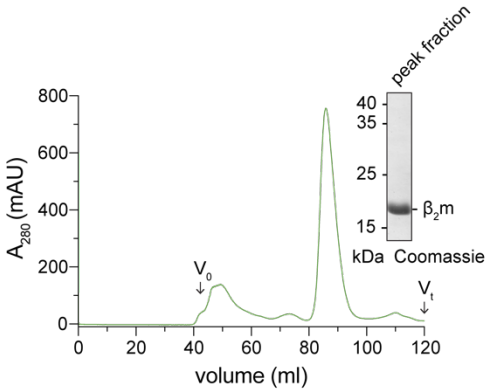

Figure 15: Production of light chain β_2m. SEC elution profile of refolded β_2m and SDS-PAGE analysis of peak fraction (inset). 8% Tris-tricine gel was utilized for SDS-PAGE. kDa, kilodalton; A_{280}, absorption at 280 nm, V_0, void volume; V_t, total volume.

Refolding MHC I necessitates the presence of high-affinity peptides besides β_2m. Since various MHC I allomorphs have different peptide-binding preferences, high-affinity peptides specific for the used allomorph were selected based on crystal structures of pMHC I

complexes. The peptides were modified with the photocleavable amino acid *S*-Anp at a position where the β-amino acid could not interfere with peptide binding (Table 33). The peptide RGPGRAF(*S*-Anp)TI synthesized for the mouse allomorph H2-D^{b} was previously utilized for assembly of the MHC I-TAPBPR complex[11]. Also for HLA-A*02:01, the photocleavable high-affinity peptide GILGFVF(*S*-Anp)L is published[72]. The photocleavable peptide ELNRKMI(*S*-Anp)M specific for HLA-B*08:01 was designed by introduction of S-Anp at position 8 as for the corresponding peptide. For allomorphs HLA-B*44:02 and HLA-B*44:05 the same peptide was used for refolding since they differ only in one amino acid at position 116 located on the floor of peptide binding pocket. Photocleavable peptide for HLA-B*44:02/05 was generated by introducing the β-amino acid *S*-Anp at position 5 (ref.[102]) leading to the sequence EEFG(*S*-Anp)AFSF. Photocleavage of this peptide results in a C-terminal 4-mer peptide, instead of a C-terminal dipeptide. The C-terminal 4-mer may remain bound to MHC I, blocking the F-pocket of MHC I and impeding association of tapasin$^{\Delta TMD}$–ERp57^{C36A}. Therefore, an additional peptide with the *S*-Anp at position 7, EEFGRA(*S*-Anp)SF, was designed. Since refolding of the highly tapasin-dependent allomorph HLA-B*44:02 was difficult, the unmodified peptides EEFGRAFSF and EENLLDFVRF which was used in a recent crystal structure[101] were also selected for refolding. All peptides were synthesized by Fmoc solid-phase synthesis, analyzed by RP-HPLC and MALDI-MS or LC-MS (Fig. 16).

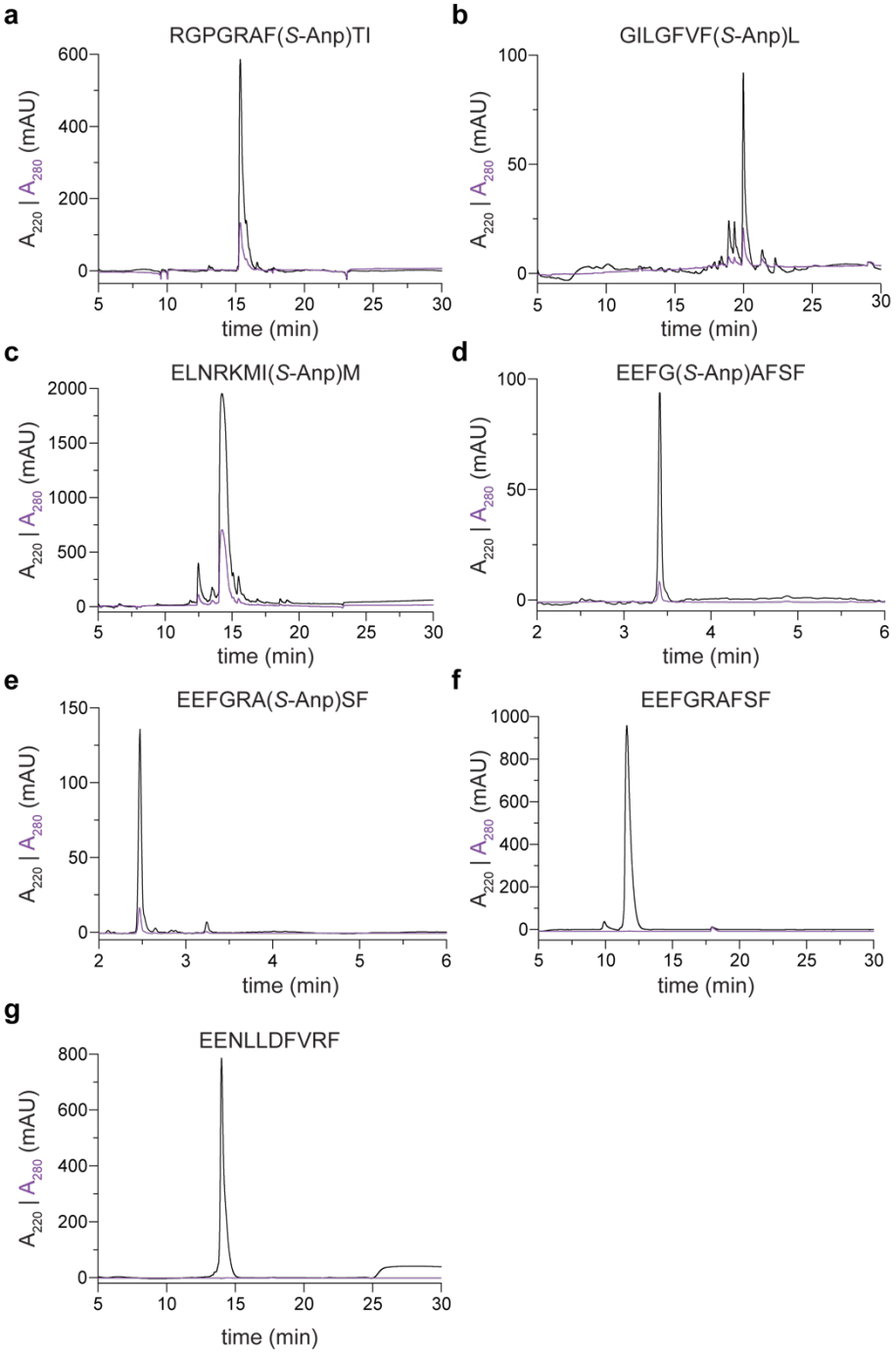

Figure 16: Synthesis of high-affinity peptides specific for the MHC I allomorphs used in this study. RP-HPLC analysis of peptides of photocleavable peptide RGPGRAF(*S*-Anp)TI specific for the H2-D^b(**a**), GILGFVF(*S*-Anp)L specific for HLA-A*02:01 (**b**), ELNRKMI(*S*-Anp)M specific for HLA-B*08:01 (**c**), EEFG(*S*-Anp)AFSF (**d**) and EEFGRA(*S*-Anp)SF specific for HLA-B*44:05 and HLA-B*44:02 (**e**), unmodified peptides EEFGRAFSF (**f**) and EENLLDFVRF synthesized for highly tapasin-dependent allomorph HLA-B*44:02. A_{280}, absorption at 280 nm; A_{220}, absorption at 220 nm.

The peptides EEFGRAFSF and EENLLDFVRF comprise three and two Phe, respectively, and thus showed no absorption at 280 nm.

Despite minor impurities of GILGFVF(*S*-Anp)L and ELNRKMI(*S*-Anp)M, refolding of all allomorphs in presence of photocleavable peptides was successful except for tapasin-dependent allomorph HLA-B*44:02 that could only be refolded with the unmodified peptide EENLLDFVRF (Fig. 17).

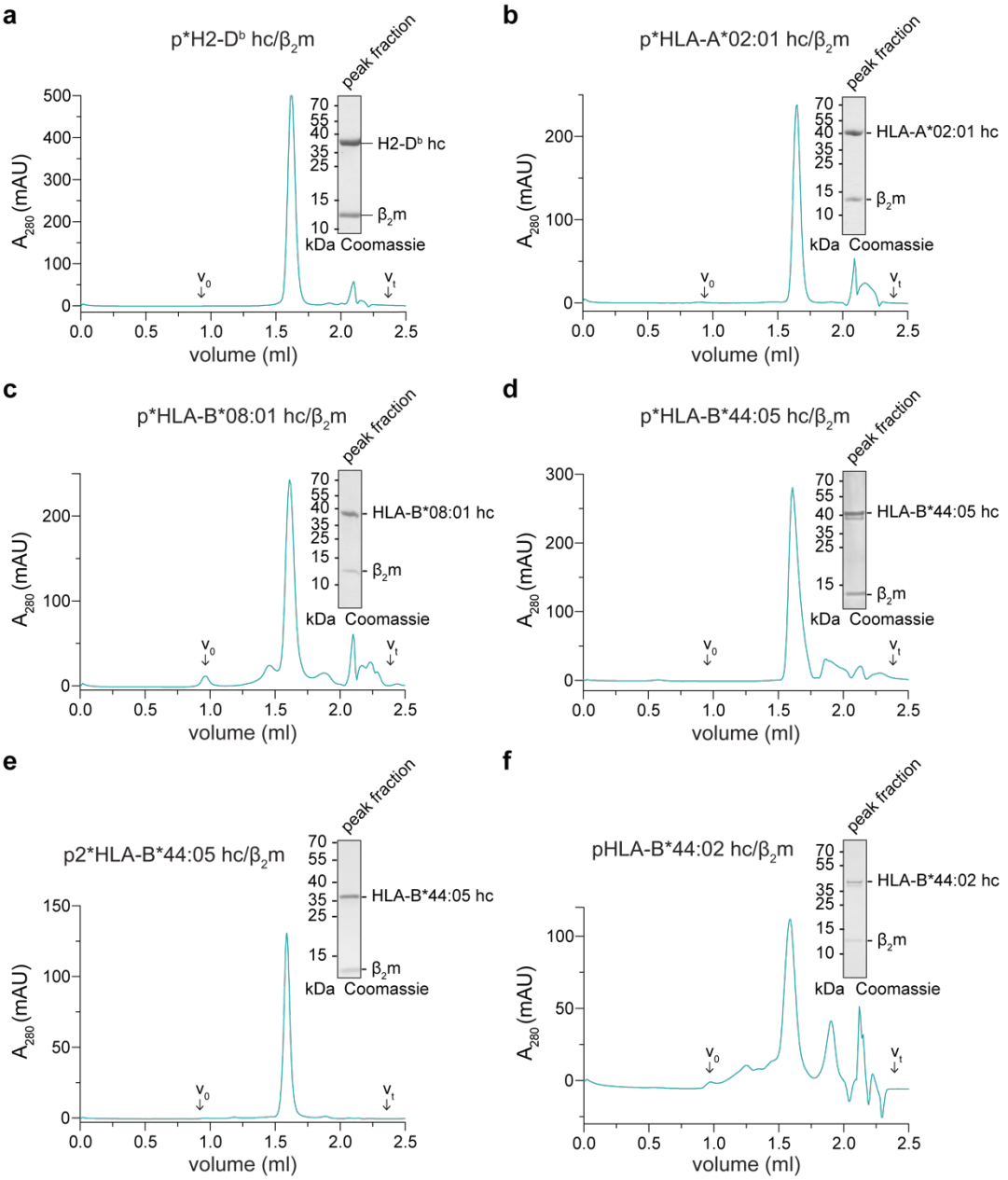

Figure 17: Refolding of MHC I allomorphs, used in this thesis. SEC and SDS-PAGE analysis (inset) of peak fraction of refolded mouse allomorph H2-D^b with peptide RGPGRAF(S-Anp)TI (p*H2-D^b hc/β_2m) (**a**), human allomorphs HLA-A*02:01 with peptide GILGFVF(*S*-Anp)L (p* HLA-A*02:01 hc/β_2m) (**b**), HLA-B*08:01 with peptide ELNRKMI(*S*-Anp)M (p* HLA-B*08:01 hc/β_2m) (**c**), HLA-B*44:05 with peptide EEFG(*S*-Anp)AFSF (p*HLA-B*44:05 hc/β_2m) (**d**), HLA-B*44:05 with EEFGRA(*S*-Anp)SF peptide (p2* HLA-B*44:05 hc/β_2m) (**e**), HLA-B*44:02 with unmodified peptide EENLLDFVRF (pHLA-B*44:02 hc/β_2m) (**f**). 11% Tris-tricine gels were utilized for SDS-PAGE. kDa, kilodalton; A_{280}, absorption at 280 nm; A_{220}, absorption at 220 nm; V_0, void volume; V_t, total volume. p* denotes peptide carrying *S*-Anp.

To ensure that UV illumination results in cleavage of the peptide backbones and dissociation of the peptide fragments from the MHC I-peptide binding pocket, the UV illuminated p*H2-D^b hc/β_2m complex was analyzed by SEC-coupled mass spectrometry. An almost complete photoinduced cleavage (> 96%) of the peptide's backbone was verified (Fig. 18). Only very small amounts of uncleaved peptide (4%) or a 6-mer peptide fragment (> 2%) were still bound to MHC I (Fig. 18). Data exemplarily shown for p*H2-D^b hc/β_2m.

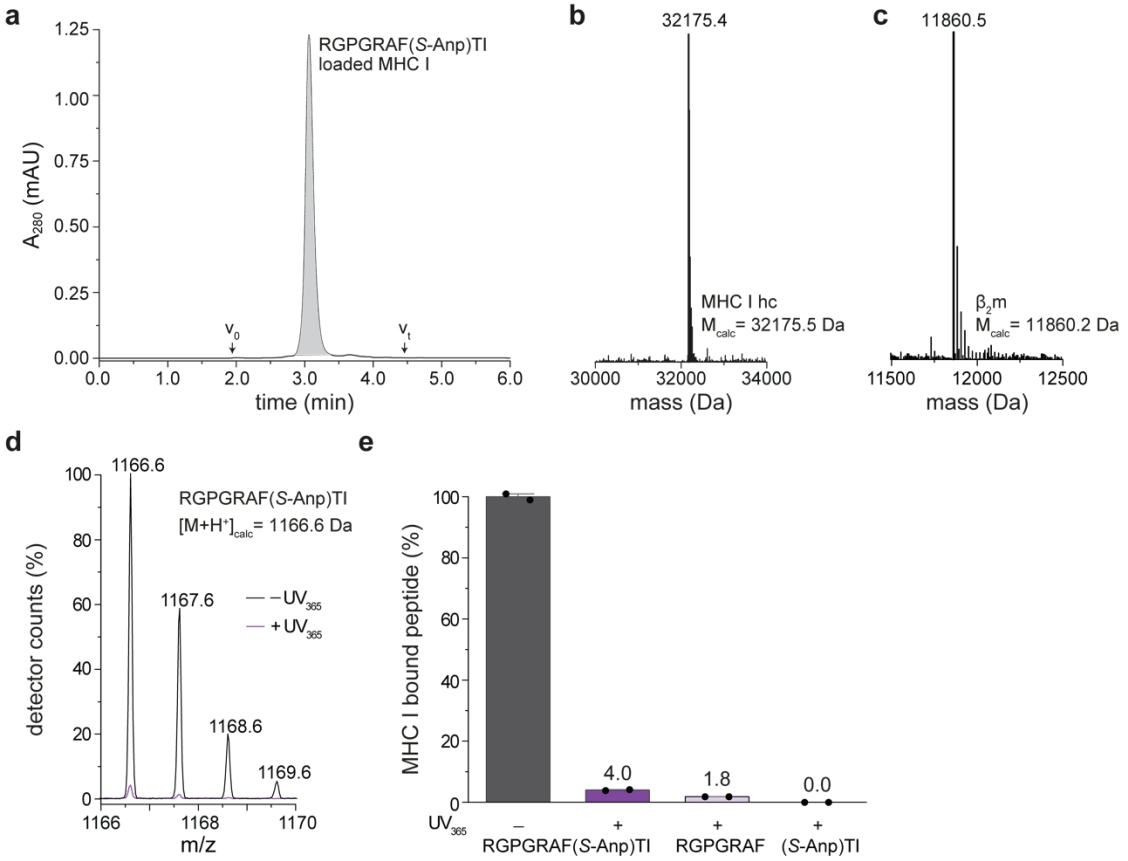

Figure 18: UV illumination of p*MHC I results in almost complete cleavage of peptide. a, SEC of RGPGRAF(*S*-Anp)TI bound MHC I. Combined ESI-MS spectra of the main peak (light grey) utilized for MS analysis displayed in (**b**-**e**). The p*MHC I complex is fragmented into individual components during the process of ionization. **b**-**d**, Intact masses for MHC I hc (**b**), β_2m (**c**), RGPGRAF(*S*-Anp)TI before UV irradiation (**d**, black line) and RGPGRAF(*S*-Anp)TI peptide after UV irradiation (**d**, purple line) were verified by ESI-MS. **e**, Quantification of MHC I-bound peptide and peptide fragments before and after UV illumination followed by SEC-MS. Quantification is based on MS detector response and normalized to non-irradiated p*MHC I. The short 3-mer fragment was not detected (n=2 biologically independent samples). A_{280}, absorption at 214 nm; M_{calc}, calculated mass. SEC-MS measurements were performed by Christian Winter.

9.2.3 Mouse MHC I allomorph H2-D^b shows partial complex formation with tapasin$^{\Delta TMD}$–ERp57^{C36A} observable by SEC

Refolded p*MHC I complexes were screened for complex formation with tapasin$^{\Delta TMD}$–ERp57^{C36A} heterodimer by SEC to find a suited candidate for structural analysis by X-ray crystallography. To this end, p*MHC I complexes were mixed in a molar ratio of 1/1 with the tapasin$^{\Delta TMD}$–ERp57^{C36A} heterodimer at a concentration of 10 µM, exposed to UV light and incubated for 10 min at room temperature before analysis by SEC. As a positive control, complex formation between p*H2-D^b hc/β_2m and TAPBPR$^{\Delta TMD}$ (kindly provided by Felix Hennig, Tampé laboratory, Institute of Biochemistry, Goethe-University Frankfurt) was successfully reproduced (Fig. 19).

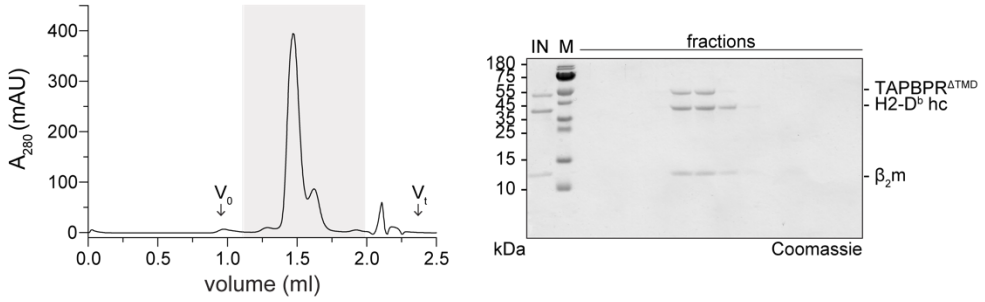

Figure 19: Complex formation of H2-D^b–TAPBPR. SEC and SDS-PAGE analysis of complex formation of tapasin homologue TAPBPR and H2-D^b hc/β_2m. 11% Tris-tricine gels were utilized for SDS-PAGE. kDa, kilodalton; A_{280}, absorption at 280 nm; A_{220}, absorption at 220 nm; V_0, void volume; V_t, total volume.

Next, tapasin$^{\Delta TMD}$–ERp57^{C36A} was tested for complex formation with refolded p*MHC I allomorphs by SEC (Fig. 20). Partial complex formation could be observed for the mouse MHC I allomorph H2-D^b and tapasin$^{\Delta TMD}$–ERp57^{C36A} (Fig. 20a). In contrast, kinetically stable complexes of the human MHC I allomorphs and tapasin$^{\Delta TMD}$–ERp57^{C36A} heterodimers were not observed (Fig. 20b-e).

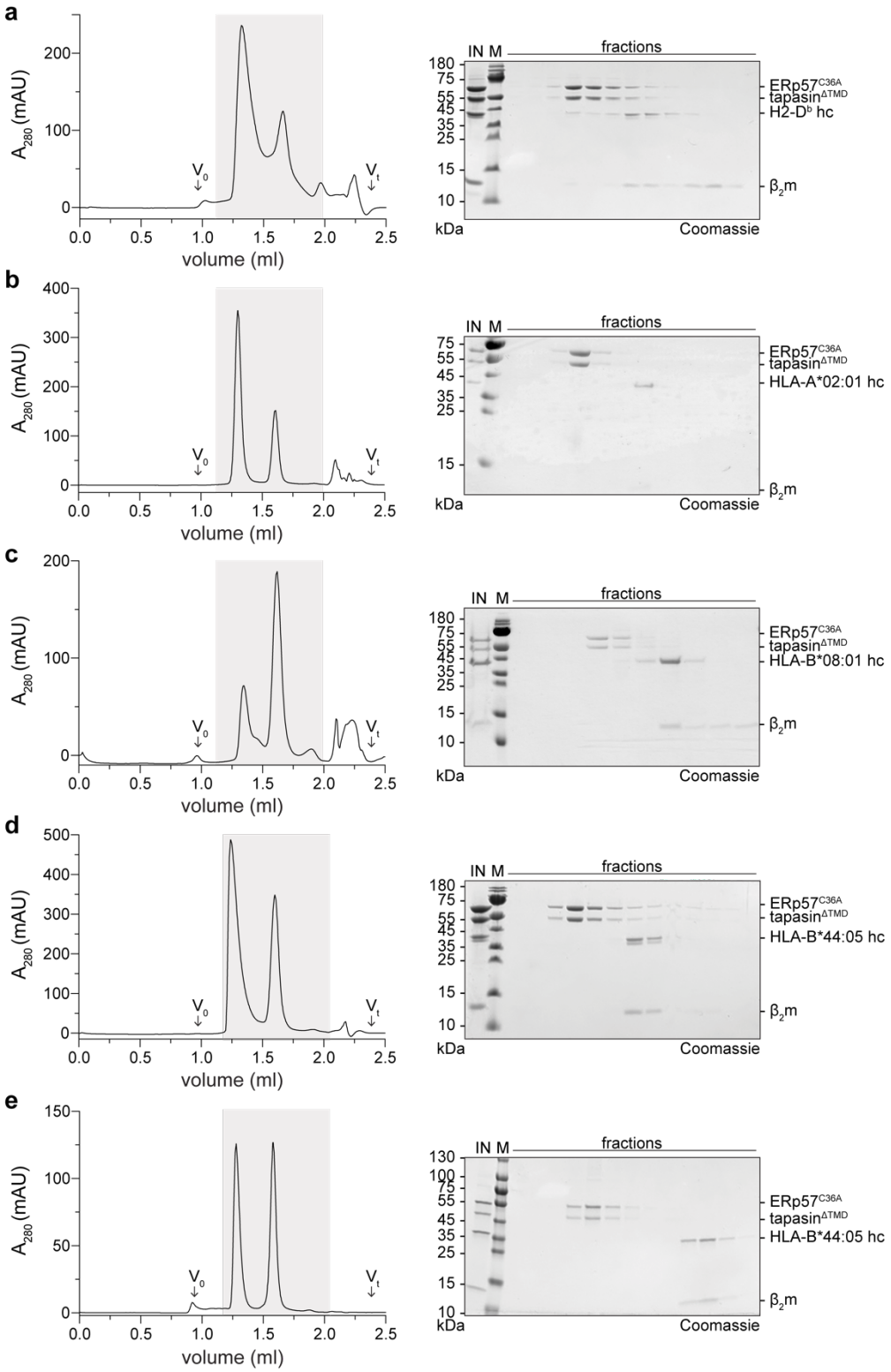

Figure 20: Mouse allomorph H2-D^{b} shows partial complex formation with tapasin$^{\Delta TMD}$–ERp57^{C36A} in SEC. SEC and SDS-PAGE analysis of screening for complex formation of heterodimer tapasin$^{\Delta TMD}$–ERp57^{C36A} with p*H2-D^{b} (**a**), p*HLA-A*02:01 (**b**), p*HLA-B*08:01 (**c**), p*HLA-B*44:05 (**d**), p2*HLA-B*44:05 complex (**e**). 11% Tris-tricine gels were utilized for SDS-PAGE. kDa, kilodalton; A_{280}, absorption at 280 nm; A_{220}, absorption at 220 nm; V_0, void volume; V_t, total volume.

Since the tapasin-dependent allomorph HLA-B*44:02 could only be refolded with the uncleavable peptide EENLLDFVR, peptide dissociation was tested under acidic conditions[119] to generate peptide-receptive MHC I molecules. The pHLA-B*44:02 sample was brought to pH 3.0 with citrate buffer and tapasin$^{\Delta TMD}$–ERp57^{C36A} was either added before or after pH shift in 10-fold molar excess. The sample was neutralized back to pH 8.0 and tested for comigration of tapasin$^{\Delta TMD}$–ERp57^{C36A} with MHC I by SEC and SDS-PAGE analysis (Fig. 21a). Oligomers formed and eluted together with tapasin$^{\Delta TMD}$–ERp57^{C36A} heterodimer around a volume of 1.1 ml and 1.3 ml for sample which was acid washed in the presence of tapasin$^{\Delta TMD}$–ERp57^{C36A} (Fig. 21a). However, HLA-B*44:02 was not found to comigrate with tapasin$^{\Delta TMD}$–ERp57^{C36A} under acidic conditions (Fig. 21). Therefore, refolding of HLA-B*44:02 was not further proceeded.

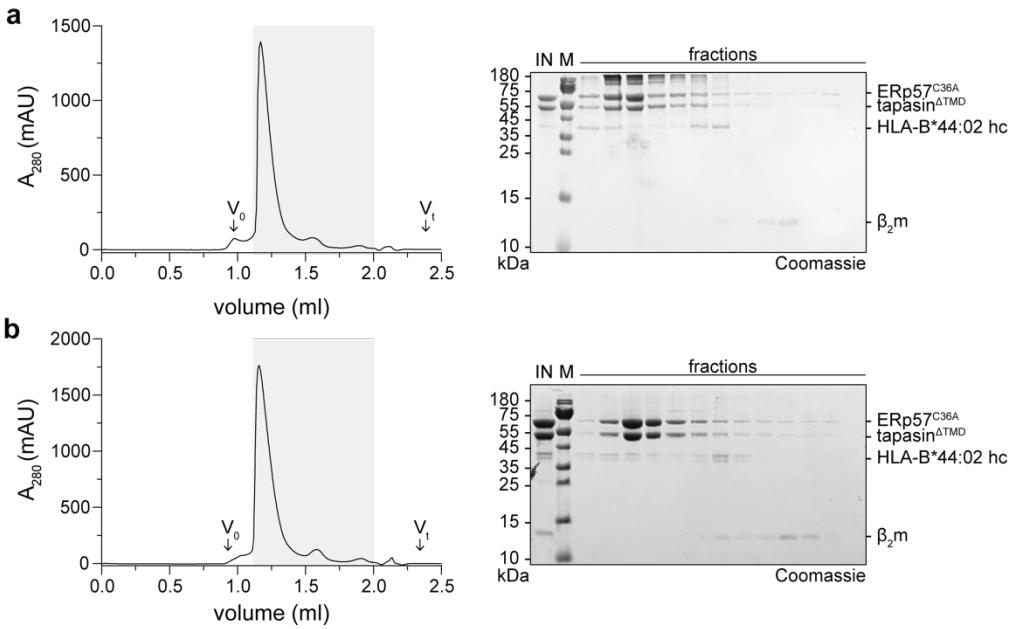

Figure 21: Tapasin$^{\Delta TMD}$–ERp57 ^{C36A} and tapasin-dependent HLA-B*44:02 did not comigrate under acidic conditions. a, Acid wash of pHLA-B*44:02 in presence of tapasin$^{\Delta TMD}$–ERp57^{C36A} analyzed by SEC and SDS-PAGE. **b**, tapasin$^{\Delta TMD}$–ERp57^{C36A} was added to acid washed HLA-B*44:02 and analyzed for complex formation by SEC and SDS-PAGE. 11% Tris-tricine gels were utilized for SDS-PAGE. kDa, kilodalton; M, marker; IN, input sample; A_{280}, absorption at 280 nm; V_0, void volume; V_t, total volume.

The screening of various MHC I allomorphs for complex formation of tapasin$^{\Delta TMD}$–ERp57^{C36A} revealed that the human MHC I molecules could not be captured in complex with tapasin$^{\Delta TMD}$–ERp57^{C36A} by SEC (Fig. 19b-e). However, the mouse MHC I hc, H2-D^b, together with human β_2m did show partial complex formation with tapasin$^{\Delta TMD}$–ERp57^{C36A} (Fig. 20a). Analysis of crystal structures of H2-D^b in complex with either human or mouse β_2m showed that the complex with human β_2m has both increased polarity and number of hydrogen bonds between β_2m and the α1/α2 domains of H2-D^b hc, which leads to an enhanced overall stability of the complex and peptide exchange capacity[26]. This stabilization enables a prolonged peptide-

receptive conformation, which might support association of tapasin in a kinetically favored fashion. Therefore, mouse H2-D^b with human β_2m was chosen as the potential candidate for structural analysis of an MHC I–tapasin–ERp57 complex.

9.2.4 Structure of HLA-B*44:05 with bound photocleaved peptide

The large amounts of refolded HLA-B*44:05 were utilized for crystallization. Microseed matrix screening[24] was performed with seeds obtained from H2-D^b–tapasin$^{\Delta TMD}$–ERp57^{C36A} crystals (Chapter 9.2.11). The screen resulted in one large crystal that diffracted to 1.3 Å in the space group $2_12_12_1$ with one molecule per asymmetric unit (Table 40). The structure of HLA-B*44:05 hc/β_2m shows the typical structural features as the peptide binding pocket flanked by the α1 and α2 helices, the β-sheets building the floor of the binding pocket and the α3 helix, that forms the large interaction interface with β_2m (Fig. 22). Interestingly, the two peptide fragments, resulting from the photocleavage, remain bound to the MHC I hc, as seen for a crystal structure of HLA-A*11:01 carrying a 4mer and 5mer peptide[120]. The study demonstrates that the peptide fragments complement each other to form a stable pMHC I complex[120]. In this case, the structure provides direct information on the photocleavage that occurs in the MHC I binding pocket, highlighting the two peptide fragments which remain tightly bound. The question arises wether the MHC I chaperone tapasin can compete the C-terminal peptide fragment out and is able to form a stable complex. However, SEC analysis did not show complex formation highlighting that tapasin$^{\Delta TMD}$ cannot compete against the remaining peptide fragments for the MHC I-peptide binding pocket (Fig. 20e). Other techniques, such as native-MS could be utilized to tackle this question.

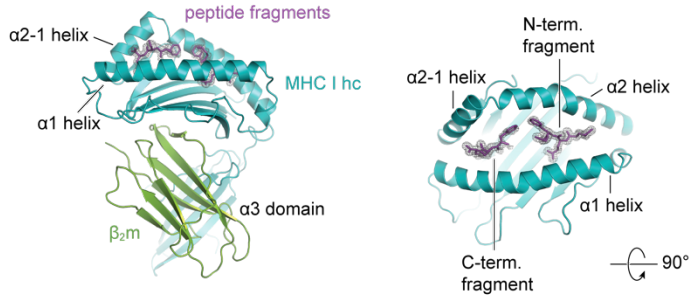

Figure 22: Crystal structure of HLA-B*44:05 reveals that cleaved peptide fragments remain bound in the MHC I binding pocket. Side and top view of HLA-B*44:05 with bound peptide fragments resulted from photocleavage in comic representation. Electron density is displayed for peptide fragments at σ-level of 1.0. hc, heavy chain; N-term., N-terminus; C-term., C-terminus.

9.2.5 Complex of H2-D^b–tapasin$^{\Delta TMD}$–ERp57^{C36A} is kinetically instable

For further analysis, components were assembled *in vitro* as described before and flow rate of SEC was set to 0.1 ml/min to extend the duration of the experiment to 4 hours. No complex

of tapasin$^{\Delta TMD}$–ERp57^{C36A}–H2-D^{b} could be observed (Fig. 23), confirming that the complex of tapasin$^{\Delta TMD}$–ERp57^{C36A}–H2-D^{b} dissociates at lower flow rate.

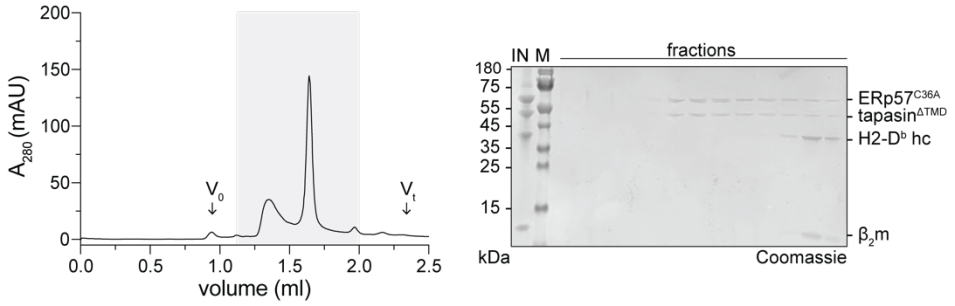

Figure 23: Complex of tapasin$^{\Delta TMD}$–ERp57^{C36A}–H2-D^{b} dissociates at lower flow rate. SEC performed over the course of 4 hours and corresponding SDS-PAGE analysis of fractions. 11% Tris-tricine gels were utilized for SDS-PAGE. kDa, kilodalton; A_{280}, absorption at 280 nm; V_0, void volume; V_t, total volume; M, marker; IN, input sample.

To find the optimal condition for photo-triggered complex formation, the concentration of each single component was increased up to 20 µM. SEC analysis and corresponding SDS-PAGE revealed an increase of tapasin$^{\Delta TMD}$–ERp57^{C36A}–H2-D^{b} complex (Fig. 24).

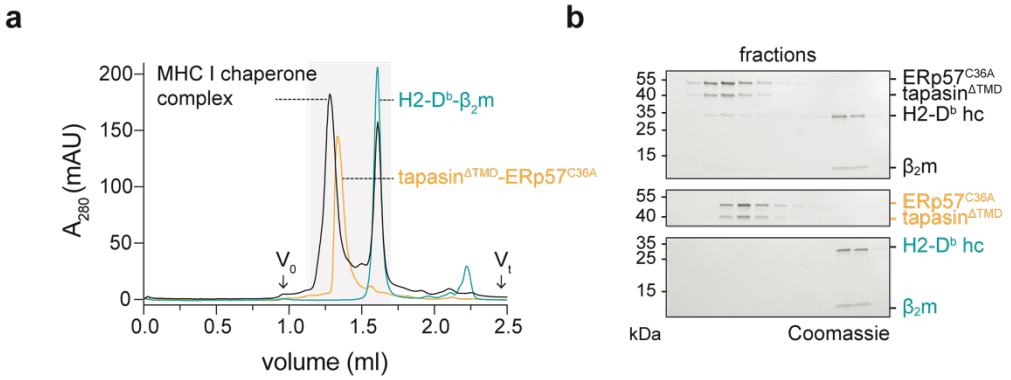

Figure 24: Photo-triggered assembly of tapasin$^{\Delta TMD}$–ERp57^{C36A}–H2-D^{b} complex. **a**, Complex formation analyzed by SEC. **b**, SDS-PAGE analysis of complex formation observed by SEC. 4-20% Mini-PROTEAN TGX gels were utilized for SDS-PAGE. kDa, kilodalton; A_{280}, absorption at 280 nm; V_0, void volume; V_t, total volume; M, marker.

9.2.6 Higher concentrations of subunits H2-D^{b} and tapasin$^{\Delta TMD}$–ERp57^{C36A} do not result in increased tapasin$^{\Delta TMD}$–ERp57^{C36A}–H2-D^{b} association

For the interaction of tapasin$^{\Delta TMD}$–ERp57^{C36A} and mouse MHC I allomorph H2-D^{b}, complex formation could be enhanced by increasing the concentration of single compounds to 20 µM (Fig. 23). Therefore, higher protein concentrations were tested to further shift the equilibrium towards the association of H2-D^{b} and tapasin$^{\Delta TMD}$–ERp57^{C36A}. To this end, concentration of H2-D^{b} was increased to 30 µM and a larger amount of H2-D^{b} was shifted to the corresponding peak fraction of tapasin$^{\Delta TMD}$–ERp57^{C36A}. Although co-migration was shown, no stoichiometric

complex formation could be observed (Fig. 25a,b). Even a 6-fold excess of H2-D^b did not result in a higher yield of formed complex (Fig. 25a,c).

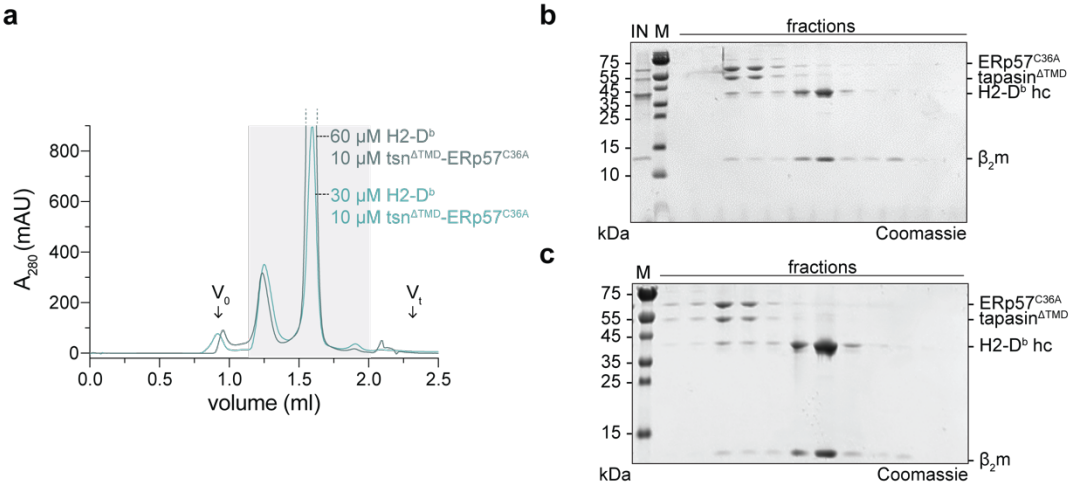

Figure 2: Higher concentration of H2-D^b and tapasin$^{\Delta TMD}$–ERp57^{C36A} do not result in increased H2-D^b–tapasin$^{\Delta TMD}$–ERp57^{C36A} association. a, Overlay of elution profiles of SEC analysis at a concentration of 30 µM (teal) or 60 µM (dark teal) of H2-D^b, while concentration of tapasin$^{\Delta TMD}$–ERp57^{C36A} was kept at 10 µM. **b**, SDS-PAGE analysis corresponding to SEC analysis of 30 µM H2-D^b. **c**, SDS-PAGE analysis corresponding to SEC analysis of 60 µM H2-D^b. 11% Tris-tricine gels were utilized for SDS-PAGE. kDa, kilodalton; A_{280}, absorption at 280 nm; V_0, void volume; V_t, total volume; M, marker; IN, input sample.

9.2.7 Higher concentrations of MHC I allomorphs and tapasin$^{\Delta TMD}$–ERp57^{C36A} does not lead to complex formation of human MHC I allomorphs with tapasin$^{\Delta TMD}$–ERp57^{C36A} heterodimer

In vitro complex formation experiments were repeated for human allomorphs at a molar ratio of 1/1 at a concentration of 20 µM. However, none of the MHC I allomorphs showed partial complex formation with tapasin$^{\Delta TMD}$–ERp57^{C36A} in SEC as it was observed for mouse allomorph H2-D^b (Fig. 26).

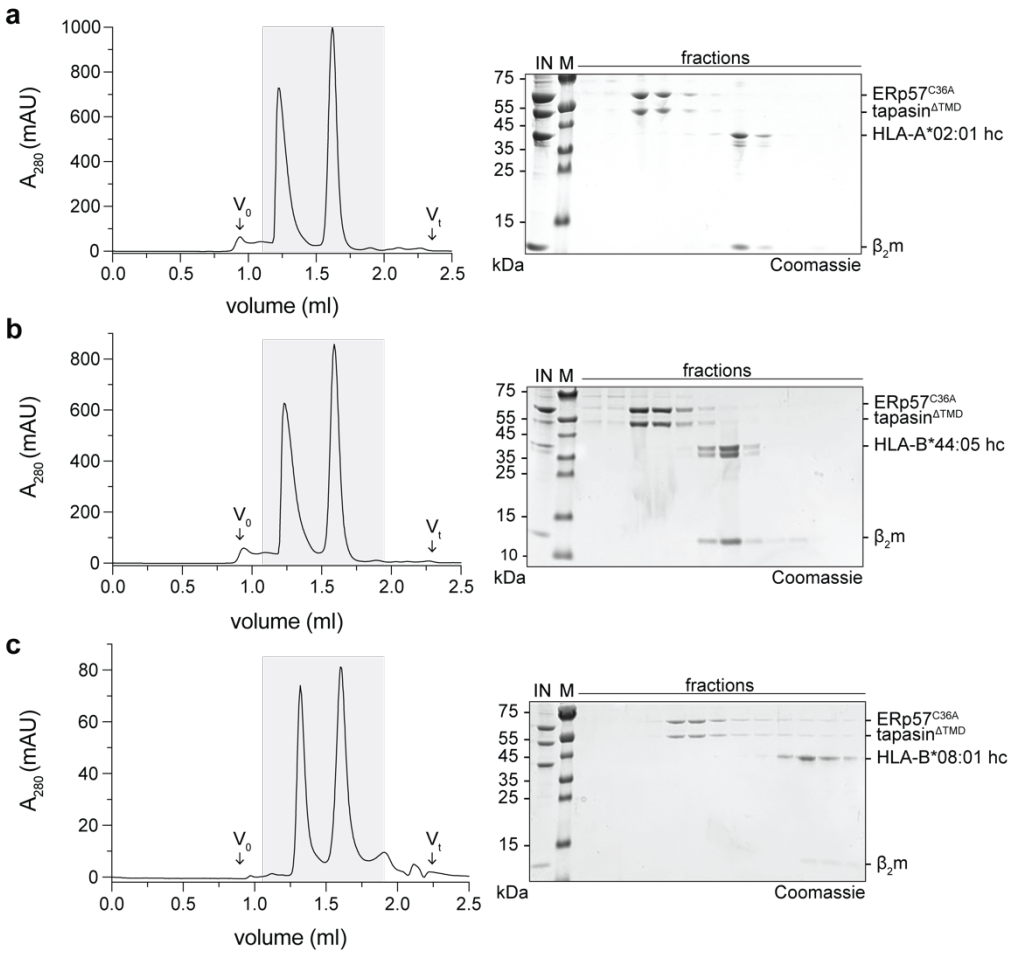

Figure 26: Increased concentrations did not result in complex formation of human MHC I allomorphs with tapasin$^{\Delta TMD}$–ERp57^{C36A}. SEC and SDS-PAGE analysis of equimolar mixtures of tapasin$^{\Delta TMD}$–ERp57^{C36A} and HLA-A*02:01 (**a**), HLA-B*44:05 (POS7) (**b**), and HLA-B*08:01 (**c**). SDS-PAGEs were conducted using 11% Tris-tricine gels; kDa, kilodalton; A_{280}, absorption at 280 nm; V_0, void volume; Vt, total volume; M, marker; IN, input sample.

9.2.8 Photocleavage of peptide leads to increased tapasin$^{\Delta TMD}$–ERp57^{C36A}–H2-D^b complex

The impact of photoactivation on complex formation was analyzed by SEC. Complex components were prepared at an equimolar ratio at 20 µM and one sample was exposed to UV light, while the second sample was kept on ice during period of UV illumination of first sample. Both samples were incubated for 10 min at RT and applied for SEC (Fig. 27). The sample that was not exposed to UV light, showed a smaller extend of complex formation, compared to the UV illuminated sample (Fig. 27). However, partial complex formation of tapasin$^{\Delta TMD}$–ERp57^{C36A}–H2-D^b in the presence of intact peptide was observable by SEC.

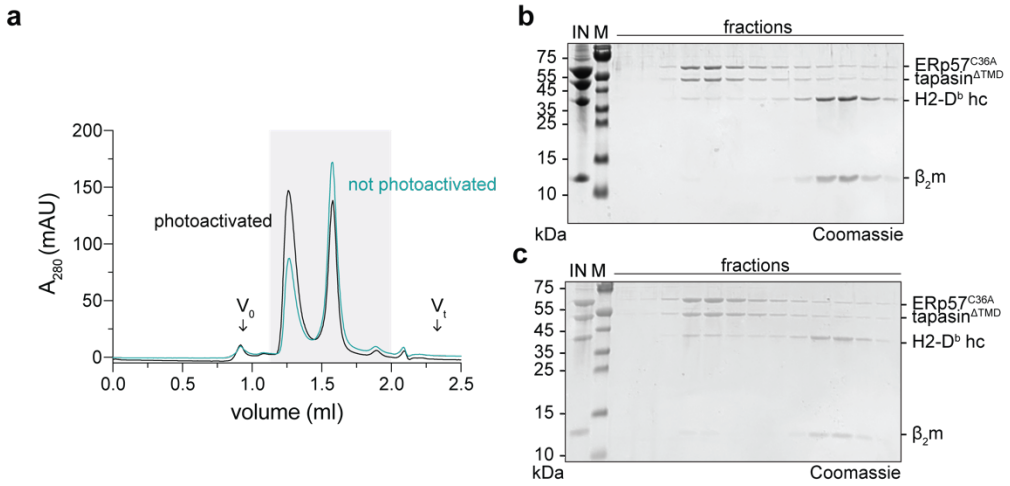

Figure 27: Complex of tapasin$^{\Delta TMD}$–ERp57^{C36A}–H2-D^{b} partially formed in the presence of intact peptide. a, Complex formation monitored before and after UV exposure by SEC. **b**, SDS-PAGE analysis of complex formation observed by SEC before photoactivation. **c**, Complex formation after UV exposure analyzed by SDS-PAGE of SEC. 11% Tris-tricine gels were utilized for SDS-PAGE. kDa, kilodalton; A_{280}, absorption at 280 nm; V_0, void volume; V_t, total volume; M, marker; IN, input sample.

9.2.9 Alternative refolding strategy of H2-D^{b} with dipeptide GL does not improve formation of tapasin$^{\Delta TMD}$–ERp57^{C36A}–H2-D^{b} complex

The photocleavage of the high-affinity peptide RGPGRAF(*S*-Anp)TI utilized for refolding of H2-D^{b} results in a 5-mer peptide and a dipeptide. The dipeptide is located at the F-pocket region of H2-D^{b}. To facilitate complex formation by avoiding the photoreaction, H2-D^{b} hc was refolded with β_2m and the dipeptide GL, based on the crystal structure of the mouse allomorph H2-K^{b} with the dipeptide GL bound in the F-pocket[28]. Refolding was performed accordingly to the protocol for refolding of MHC I allomorphs with photocleavable peptides, but instead of the photocleavable peptide in presence of 10 mM dipeptide (Fig. 28a). As compared to the refolding of p*H2-D^{b}, refolding of H2-D^{b} using the dipeptide was less efficient. Nevertheless, tapasin$^{\Delta TMD}$–ERp57^{C36A} heterodimer was added at equimolar ratio to refolded GL/H2-D^{b} (20 µM), but still no stoichiometric complex was observed by SEC (Fig. 28b). Due to the low yield of refolded GL/H2-D^{b}, the photo-triggered approach was further proceeded.

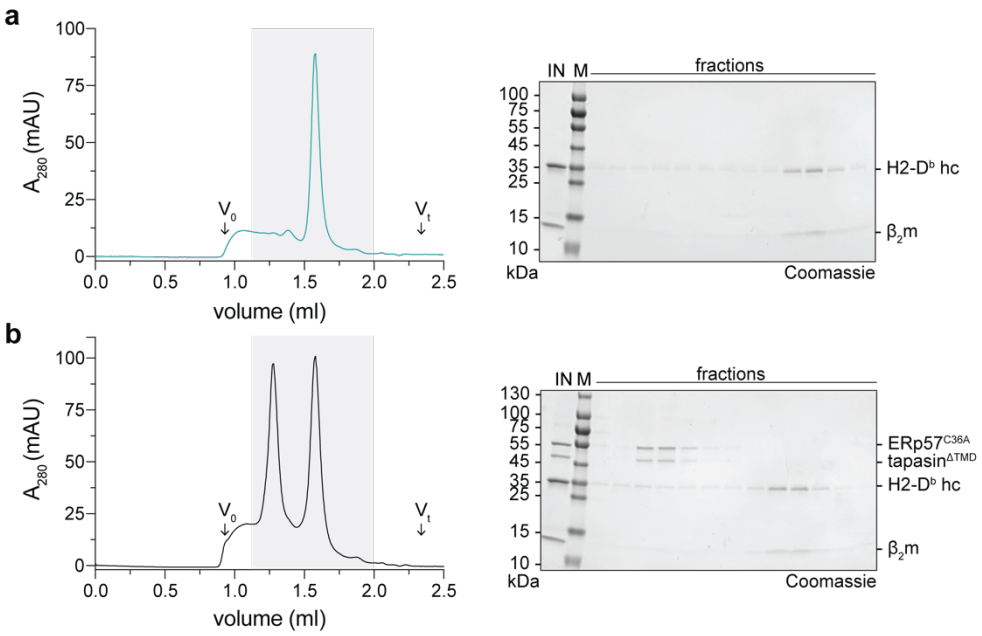

Figure 28: Utilizing dipeptide to refold H2-D^b does not improve complex formation. **a**, SEC and SDS-PAGE analysis of GL/H2-D^b. **b**, tapasin$^{\Delta TMD}$–ERp57^{C36A} and GL/H2-D^b analyzed by SEC and SDS-PAGE analysis. SDS-PAGEs were conducted using 11% Tris-tricine gels; kDa, kilodalton; A_{280}, absorption at 280 nm; V_0, void volume; V_t, total volume; M, marker; IN, input sample.

9.2.10 Substitution of the tapasin editing loop with the scoop loop of TAPBPR stabilizes a tapasin–ERp57–H2-D^b hc/β_2m complex

Based on the crystal structure of the tapasin homologue TAPBPR in complex with mouse H2-D^b hc and human β_2m[11], a stabilization mutant of tapasin was designed that carried the scoop loop of TAPBPR. In one crystal structure, the scoop loop of TAPBPR was found to interact with residues of MHC I binding pocket, acting as a peptide surrogate[11,95]. Based on these findings, the shorter editing loop of tapasin$^{\Delta TMD}$ was exchanged for the longer loop of TAPBPR (Fig. 29a). The scoop loop mutant of tapasin$^{\Delta TMD}$ was generated by exchanging the sequence Ala13 – Ala19 of editing loop of tapasin for the sequence of the scoop loop of TAPBPR (Gly27 – Asp38) (tapasin$^{\Delta TMD, SL}$) (Fig. 29b). Tapasin$^{\Delta TMD, SL}$ was co-expressed with ERp57^{C36A} and purified by IMAC from insect cells (Fig. 29c). Identities of tapasin$^{\Delta TMD, SL}$ and ERp57^{C36A} were verified by immunoblotting of IMAC elution fractions (Fig. 29d).

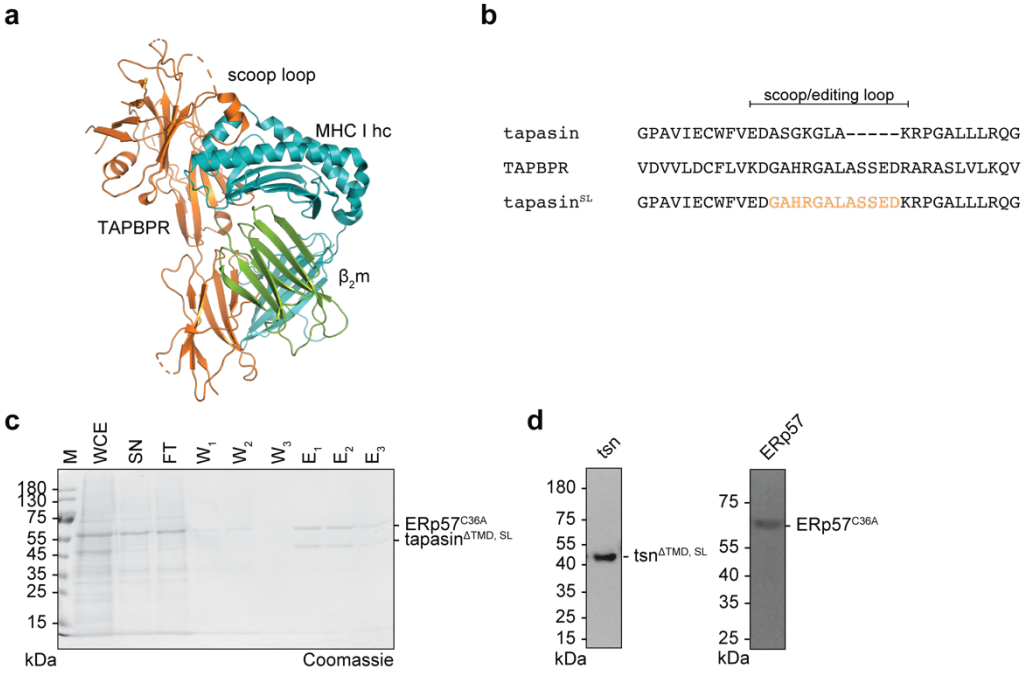

Figure 29: Design and production of scoop loop mutant of tapasin. a, Cartoon representation of MHC I–TAPBPR structure (PDB ID 5OPI). **b**, Sequence alignment of editing loop region of tapasin and TAPBPR. **c**, SDS-PAGE analysis of IMAC purification of tapasin$^{\Delta TMD,\ SL}$ co-expressed with ERp57^{C36A}. **d**, Immunoblot analysis of elution fraction of IMAC. 12% Tris-glycine gels were utilized for SDS-PAGE. kDa, kilodalton; M, marker; WCE, whole cell extract; SN, supernatant; FT, flow through; W_1-W_3, wash steps 1-3, E_1-E_3, elution fractions 1-3.

The production of scoop loop mutant tapasin$^{\Delta TMD,\ SL}$ disulfide linked with ERp57^{C36A} could be upscaled in insect cells and was tested for complex formation with UV illuminated allomorphs p*HLA-B*08:01, p*HLA-A*02:01, p2*HLA-B*44:05 and p*H2-D^b (Fig. 30). For *in vitro* assembly, tapasin$^{\Delta TMD,\ SL}$–ERp57^{C36A} heterodimer was mixed in a molar ratio of 1/1 with refolded allomorphs, followed by UV illumination and SEC, as described before. The human MHC I allomorphs showed no comigration with heterodimer during SEC (Fig. 29b-d). The longer scoop loop of TAPBPR did not stabilize the interaction of tapasin$^{\Delta TMD,\ SL}$–ERp57^{C36A} with human MHC I to the extent that it could be monitored by SEC. However, the mouse MHC I allomorph H2-D^b showed an increase in tapasin$^{\Delta TMD,\ SL}$–ERp57^{C36A}– H2-D^b complex (Fig. 30e) compared to SEC analysis using the unmodified tapasin$^{\Delta TMD}$–ERp57^{C36A} heterodimer (Fig. 20a). The introduction of the longer scoop loop of TAPBPR seems to stabilize the interaction of tapasin$^{\Delta TMD,\ SL}$–ERp57^{C36A}–H2-D^b hc/β_2m. Since mutations in the editing loop region of tapasin has been shown to be critical for the expression of tapasin (Chapter 9.2.13), the tapasin$^{\Delta TMD}$–ERp57^{C36A}–H2-D^b hc/β_2m complex formation without the scoop loop of TAPBPR was utilized for structural analysis.

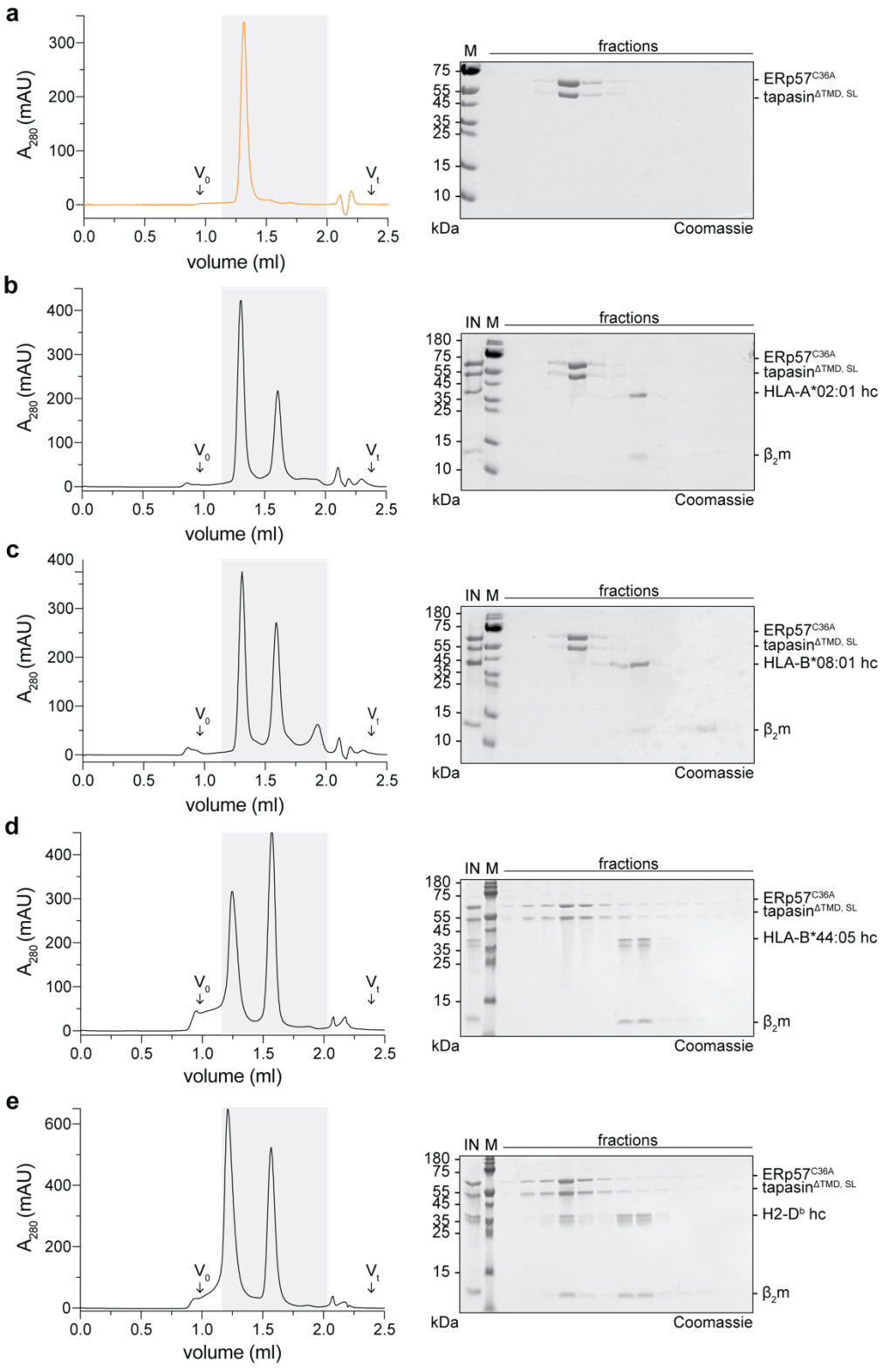

Figure 30: Introduction of scoop loop stabilizes the interaction of tapasin with mouse MHC I allomorph H2-D^{b}. a, Analytical SEC, and corresponding SDS-PAGE of fractions of tapasin$^{\Delta TMD,\ SL}$–ERp57^{C36A}. **b-e**, SEC and corresponding SDS-PAGE analysis of mixture of tapasin$^{\Delta TMD,\ EL}$–ERp57^{C36A} and HLA-A*02:01 (**b**), HLA-B*08:01 (**c**), HLA-B444:05 (POS7) (**d**) and H2-D^{b} (**e**). SDS-PAGES were carried out utilizing 11% Tris-tricine gels (**a-c**) or 4-20% Mini-PROTEAN TGX gels (**d** and **e**). kDa, kilodalton; A_{280}, absorption at 280 nm; V_0, void volume; V_t, total volume; M, marker; IN, input sample.

9.2.11 Structural analysis of tapasin$^{\Delta TMD}$–ERp57^{C36A}–H2-D^{b} complex by X-ray crystallography

For structural analysis, different MHC I allomorphs were screened for complex formation with tapasin$^{\Delta TMD}$–ERp57^{C36A} by SEC. The mouse H2-D^{b} allomorphs turned out to be the most suited MHC I hc candidate (Fig. 20a). However, a homogeneous population of a kinetically stable tapasin$^{\Delta TMD}$–ERp57^{C36A}–H2-D^{b} complex between tapasin–ERp57 and refolded MHC I hc/β_2m could not be isolated (Fig. 20a). Therefore, a photoactivated mix of refolded p*H2-D^{b}/β_2m and tapasin–ERp57 at equimolar ratio (135 µM) was directly used for initial screening. The selected concentration was much higher than for the binding assay performed by SEC, to favor the complex formation of the transient MHC I-chaperone complex. Initial 96-well screening resulted in small and flat crystals (Fig. 31a). Molar ratio of tapasin$^{\Delta TMD}$–ERp57^{C36A} and H2-D^{b} was optimized to 1/1.3 at concentrations of 67.7 µM and 88 µM, respectively. An additive screen identified EGTA, EDTA and CYMAL-5 to improve crystal growth. The crystals were cryoprotected using 30% ethylene glycol. Single crystals diffracted X-rays to a resolution of 4.0 Å in space group $P2_12_12_1$ with two heterotetrameric complexes per asymmetric unit (Fig. 31b).

To further improve the diffraction properties of the crystals, dehydration of crystals and an alternative method that utilizes vapor diffusion of volatile alcohols to cryoprotect the crystals were carried out[105]. Dehydration of crystals can improve the crystal order by removing excess solvent, which tightens packing of the molecules. For dehydration, precipitant concentration of reservoir was serial increased and crystals were harvested after 8 – 48 hours. Cryoprotecting the crystals by vapor diffusion of volatile alcohols was tested to prevent crystal damage due to handling and osmotic stress[105]. The volatile alcohols 40% methanol or 40% *tert.* butanol was used. Both methods, dehydration and cryoprotection using vapor diffusion of volatile alcohols did not lead to an improved resolution.

Microseed matrix screening (MMS) is based on the theory that crystal nucleation and growth do not require the same condition[24]. Previously obtained crystals were crushed and used as seeds in a screening for optimal growth condition. Crystals grew thicker with a changed morphology (Fig. 31c). They diffracted to a resolution of 2.7 Å in space group $P22_12_1$ with one complex in the asymmetric unit. Data and refinement statistics are listed in Table 39.

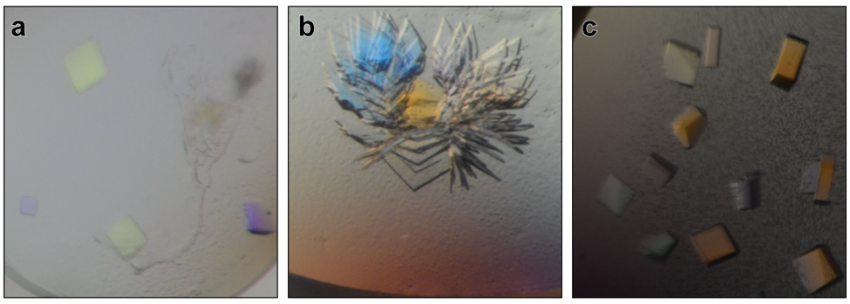

Figure 3: Microseed matrix screening improved morphology of crystals. a, Photograph of crystals obtained in first 96-well screening. **b**, Crystals improved by fine and additive screening. **c**, Image of crystals obtained by microseed matrix screening.

Table 39: Data collection and refinement statistics. Highest-resolution shell statistics are given in parentheses.

	MHC I–tapasin–ERp57 complex
Wavelength	1.033
Resolution range (Å)	48.0 - 2.7 (2.8 - 2.7)
Space group	$P22_12_1$
Unit cell dimensions (Å)	a = 74.76, b = 168.53, c = 187.05
Total reflections	388317 (38711)
Unique reflections	65668 (6488)
Multiplicity	5.9 (6.0)
Completeness (%)	99.76 (99.86)
Mean I/sigma(I)	14.90 (1.02)
Wilson B-factor	87.61
R-merge	0.07144 (1.507)
R-meas	0.0784 (1.65)
R-pim	0.03178 (0.6626)
CC1/2	0.998 (0.443)
CC*	1 (0.783)
Reflections used in refinement	65719 (6488)
Reflections used for R-free	3284 (324)
R-work	0.1983 (0.3229)
R-free	0.2289 (0.3445)
CC(work)	0.959 (0.666)
CC(free)	0.959 (0.561)
Number of non-hydrogen atoms	9726
macromolecules	9635
ligands	39
solvent	52
Protein residues	1214
RMS(bonds)	0.009
RMS(angles)	1.36
Ramachandran favored (%)	95.00
Ramachandran allowed (%)	5.00
Ramachandran outliers (%)	0.00
Rotamer outliers (%)	4.19
Clashscore	5.46
MolProbity score	1.64

Average B-factor	106.17
macromolecules	106.23
ligands	128.14
solvent	79.25
Number of TLS groups	21

The four domains of ERp57 are found in the characteristic twisted U form and tapasin presents the known L-shaped form (Fig. 32a)[8,12]. The N-terminal domain of tapasin is formed by a seven-stranded β barrel and an Ig-like fold and is contacted by the a and a' domains of ERp57[8] (Fig. 32a). The disulfide bond of Cys95 of tapasin and Cys33 of ERp57, which is required for the escape pathway[77], could only be modeled in its reduced form contrary to the client-free tapasin–ERp57 structure[8,77] (32b-d). However, the intramolecular disulfide bond is formed in the purified heterodimer (Fig. 32b-d) and SDS-PAGE analysis showed that reduction of the disulfide bond is not due to the UV illumination performed for photocleavage of the peptide, but more likely facilitated by X-ray radiation or might be involved in the MHC I-editing process.

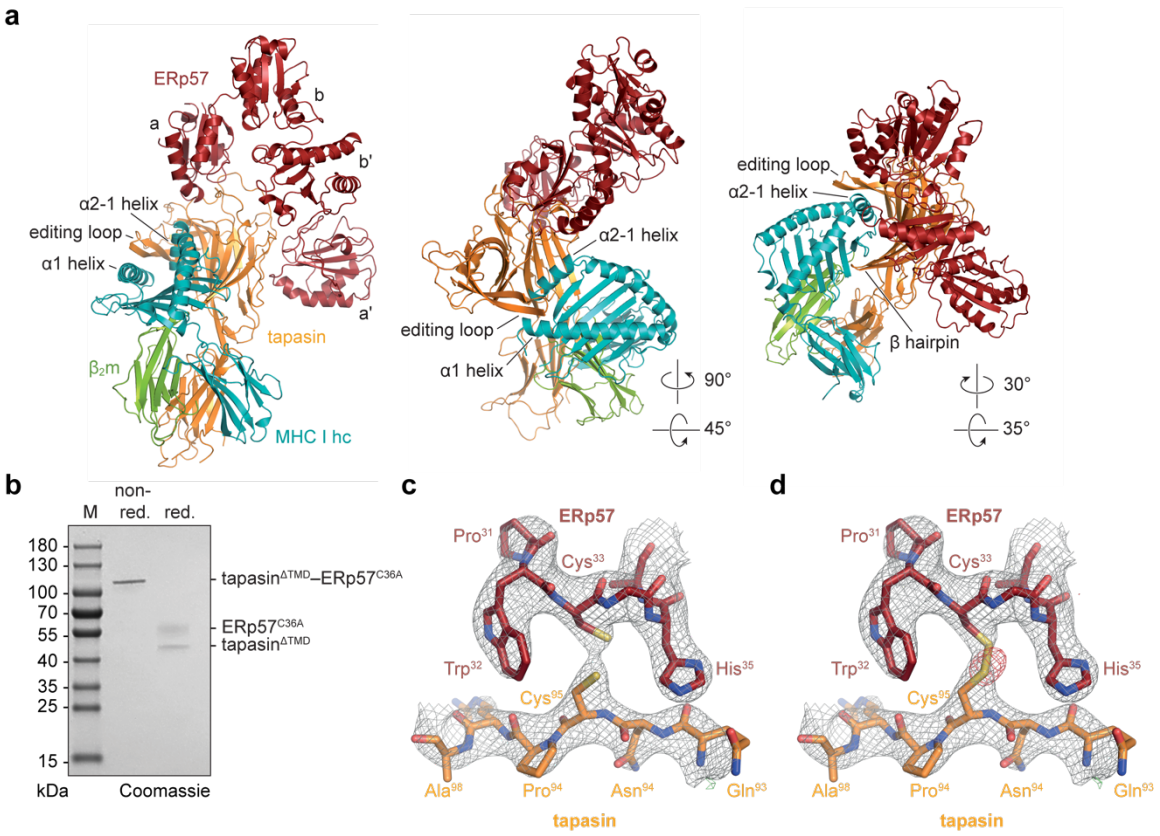

Figure 32: Structural overview of tapasin$^{\Delta TMD}$–ERp57^{C36A}–H2-D^{b} complex. a, Cartoon representation of peptide-receptive MHC I in complex with heterodimer tapasin$^{\Delta TMD}$–ERp57^{C36A} in different orientations. **b**, SDS-PAGE analysis of heterodimer after photoactivation. **c**, Stick representation of nearby residues of Cys95 of tapasin (orange) and Cys33 of ERp57 (firebrick) with the $2F_o$-F_c map (grey mash) displayed at the 2 σ level and the F_o-F_c difference map (red mesh) displayed at -4 σ level. **d**, Same representation as in (f) but with a modeled disulfide bond between Cys95 of tapasin and Cys33 of ERp57 calculated. 4-20% Mini-PROTEAN gel were utilized for SDS-PAGE. a, a', b and b' thioredoxin-like domains of ERp57.

9.2.12 Binding of MHC I induces conformational changes within the MHC I–chaperone complex

The interface between tapasin and MHC I forms a total surface aera of 4,381 Å^2 (hc: 74%; β_2m: 26%) (Fig. 33), whereof the N-terminal domain of tapasin covers 2,657 Å^2 (Fig. 33). The concave binding site of tapasin embraces the α2-1 helix region of MHC I hc (Fig. 32a). A loop composed of residues Glu11-Lys20, called editing loop, is placed on top of the F-pocket of MHC I peptide-binding groove, and a β hairpin contacting the floor of the peptide-binding pocket is flanking the N-terminal interaction site of tapasin (Fig. 34a-c).

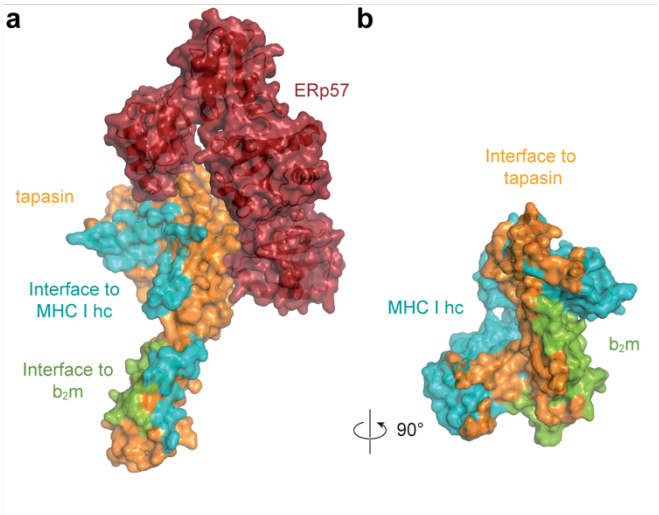

Figure 4: Interaction interfaces of the MHC I chaperone complex. a, Surface representation of tapasin–ERp57 with contact regions of MHC I (teal) and β_2m (splitpea). **b**, Contact regions of tapasin (orange) on MHC I and β_2m. hc, heavy chain; β_2m, β_2-microglobulin.

Superposition of client-free tapasin–ERp57 structure and peptide-bound MHC I reveals molecular rearrangement of several domains. Structure of MHC I in complex with tapasin–ERp57 shows a widened F-pocket based on the repositioning of α1 and α2-1 helices (Fig. 34a), which is stabilized by a hydrogen bond network between His70 and Glu72 of tapasin, attracting the side chain of Tyr84 of MHC I hc (Fig. 35a,b). Additionally, side chain of Lys20 of tapasin supports the positioning of Tyr84 by a hydrogen bond with the main chain oxygen (Fig. 35b). Remarkably, Glu72 of tapasin structurally corresponds to Glu105 of TAPBPR and is found to interact with Tyr84 of MHC I hc similar[10,11]. Also, β-strands β5-7 of the floor of the peptide-binding pocket of MHC I are disformed upon engagement of tapasin–ERp57 (Fig. 34b). The β hairpin of tapasin positions towards the α2-1 region of MHC I hc (Fig. 34c) as seen in TAPBPR-MHC I structures[10,11]. Moreover, C-terminal domain of tapasin is shifted towards the α3 domain of MHC I hc and β_2m (Fig. 34d), resulting in an interaction interface with a buried surface area of 1,724 Å^2 (hc: 55%; β_2m: 45%) (Fig. 33).

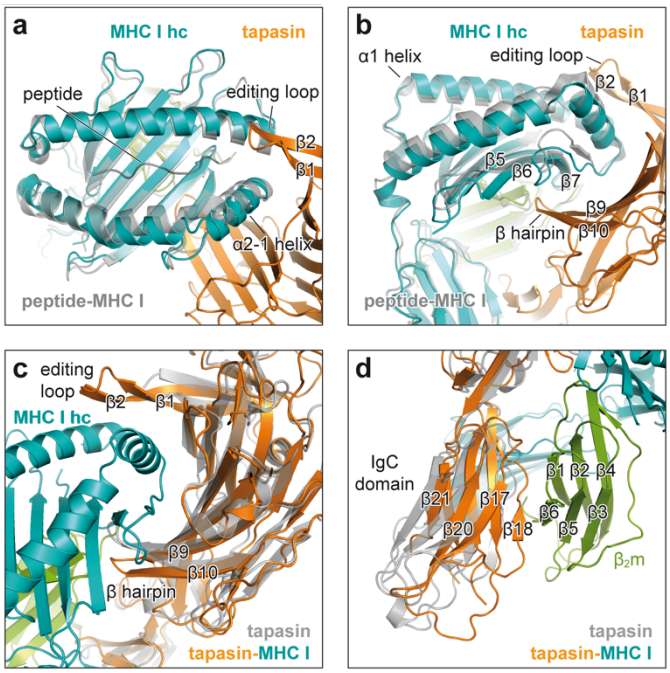

Figure 34: Molecular rearrangements upon engagement of MHC I chaperone complex. a, Top view of superposition of peptide-receptive MHC I of the chaperone complex (teal) with peptide-bound H2-D^b (grey, PDB ID 2F74) in cartoon representation. **b**, Side view of superposition of (**a**). **c**, View onto N-terminal domain of tapasin in superposition of tapasin in the chaperone complex (orange) with unbound tapasin (grey, PDB ID 2F8U). **d**, View onto C-terminal domain of tapasin in superposition as in (c). β_2m, β_2-microglobulin.

9.2.13 Editing loop of tapasin promotes widening of F-pocket of MHC I

The editing loop of client-free heterodimer tapasin–ERp57 was not modeled due to the lack of electron density[8]. However, clear density for most of the residues of the editing loop in the MHC I–tapasin–ERp57 structure at the 1.5 σ level is clearly visible, suggesting that the editing loop is disordered without its client MHC I and rigidifies upon binding (Fig. 35a-e). The editing loop is stabilized by hydrogen bonding of side chain of Asn80 of MHC I with backbone-carbonyl oxygen of Lys16 of tapasin (Fig. 35d). Also, side chain of Asp12 of the editing loop forming a salt-bridge with the ε-amino group of Lys[146] of MHC I adds to stabilization of widened peptide-binding pocket and rigidification of the editing loop (Fig. 35d). Moreover, residue Leu18 points into the F-pocket, mimicking a C-terminal hydrophobic side chain of the peptide, and thereby contributing to a groove widening. Consistent with the findings that Leu18 has been shown to be crucial for MHC I surface expression[27–29], exchange of Leu18 for the bulky hydrophobic side chain Trp did not affect MHC I surface expression in a flow-cytometry based cellular assay (Fig. 35e,f). In contrast to *in vitro* peptide-loading assays[8], the inhibition of the hydrogen bond between Tyr84 of MHC I and Glu72 of tapasin did not decrease surface MHC I level compared to wildtype (WT) tapasin (Fig. 35e). The mutation of Lys20 to Glu, which facilitated the positioning of α1 helix of MHC I by a hydrogen bond to backbone-carbonyl

oxygen of Tyr84 (Fig. 35a,b), did not majorly decrease MHC I surface expression 72±10% (Fig. 35e). This finding indicates that the editing loop stabilizes the empty F-pocket predominantly by hydrophobic interactions. Furthermore, the replacement of the editing loop with three glycine residues or the scoop loop of TAPBPR (Fig. 35g) resulted in a reduction of MHC I surface expression to 60±4% and 71±2%, respectively (Fig. 35h,i). These findings indicate that the intact editing loop of tapasin is essential for MHC I surface expression and that the longer scoop loop of TAPBPR cannot compensate for the editing loop of tapasin. However, the expression levels of the loop mutants are rather low compared to WT therefore, it could not exclude that the reduced surface MHC I was due to lower expression levels (Fig. 35i). Contrary to one of the MHC I-TAPBPR structures, the residues Thr143, Lys146 and Trp147 of the MHC I binding groove, which coordinate the residues of the bound peptides C-terminus, are involved in interactions with tapasin and its editing loop (Fig. 35a,b and Fig. 38a), suggesting that the editing loop of tapasin functions in a dual way, opening the peptide-binding groove and stabilizing the empty F-pocket of MHC I hc.

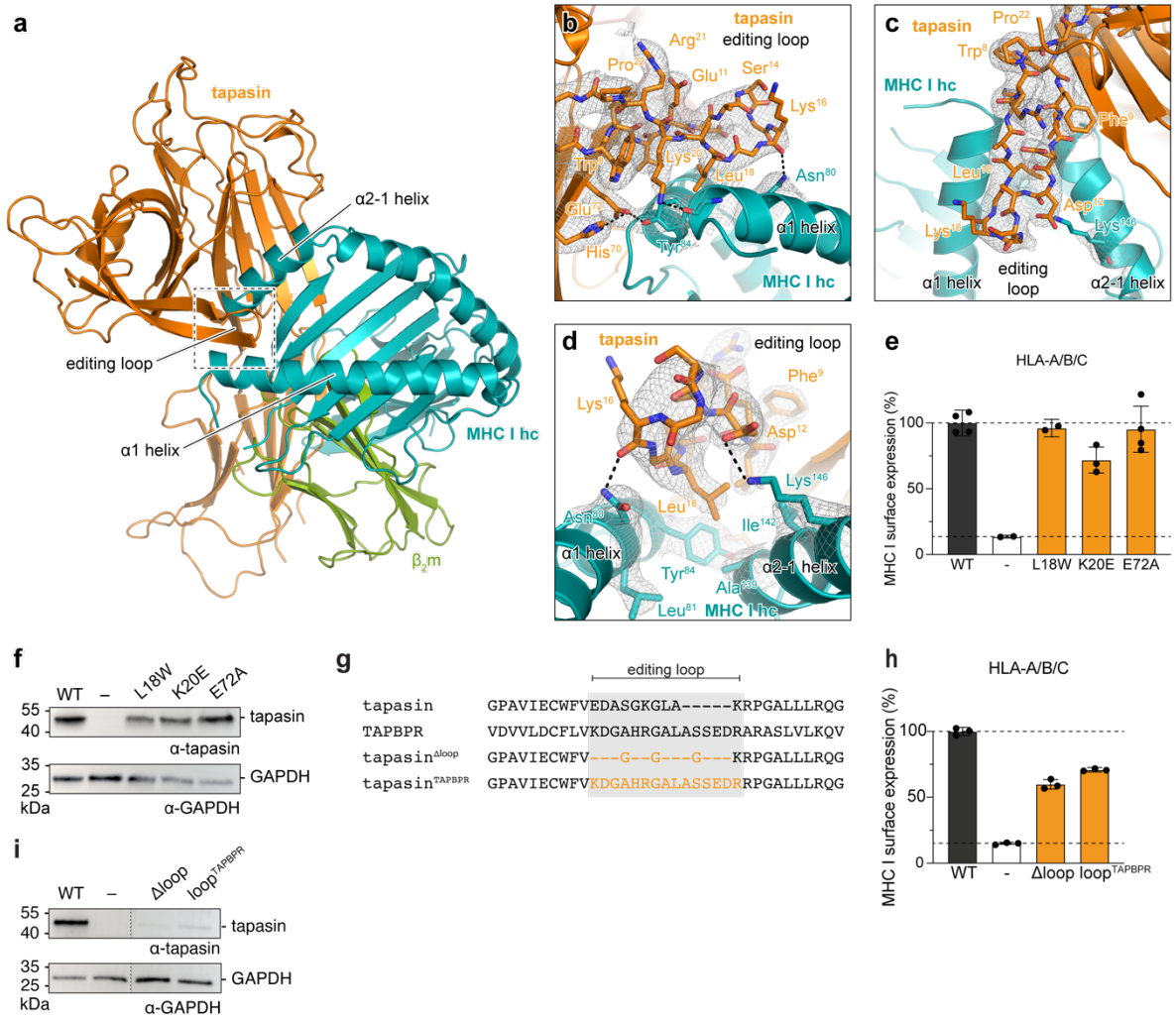

Figure 35: Editing loop assists in widening of MHC I peptide-binding pocket. a, Cartoon representation of the MHC I-chaperone complex. Dashed boxes indicate regions displayed in **b**-**d**. For clarity, ERp57 is not shown. **b**, Side view onto editing loop in stick representation with corresponding electron density map at 1.5 σ level. **c**, Top view onto the editing loop with corresponding electron density map as shown in (**b**). **d**, Zoom into F-pocket of MHC I with electron density map shown in (**b**). **e**, Surface expression of MHC I of tapasin-deficient HAP1 cells, expression wildtype (WT) and various interaction mutants of tapasin. Flow-cytometry was conducted using an APC-labeled HLA-A/B/C-specific antibody (W6/32). The lower dashed line represents the level of MHC I surface expression of cells transfected with a vector devoid of gene of interest. The upper dashed line represents MHC I surface expression level of cells transfected with wildtype tapasin (± SD; n=4 biological independent samples; K20E, n=3 biological independent samples; L18W and mock-transfected, n=2 biological independent samples). The gating strategy is provided in Fig. 41 – see appendix. **f**, Whole cell extracts of eGFP positive cells, that express wildtype and interface mutants of tapasin, analyzed by SDS-PAGE and immunoblotting. **g**, sequence alignment of loop region of tapasin, TAPBPR and loop mutants. **h** MHC I surface expression of tapasin-deficient HAP1 cells, expressing wildtype (WT) and loop mutants of tapasin. Flow cytometry was performed using an APC-labeled HLA-A/B, C-specific antibody (W6/32). The upper dashed line represents the MHC I surface level of cells, expressing wildtype tapasin. The lower dashed line represents MHC I surface expression of cells transfected with a vector devoid of gene of interest (mock). The mean fluorescent intensities were normalized wildtype tapasin (± SD; n=3 biologically independent samples). The gating strategy is provided in Fig. 41 – see appendix. **i**, SDS-PAGE and immunoblot analysis of whole cell extracts of eGFP positive cells, expressing wildtype and loop mutants of tapasin. 4-20% Mini-PROTEAN gel were utilized for SDS-PAGE.

9.2.14 Interaction sites at tapasin–MHC I interface essential for MHC I surface expression

The interface loop region of tapasin does not form specific interactions with the α2-1 helix of MHC I and thus has a minor impact on MHC I surface expression (Fig. 36a). Contrary to the nearby Gln261, which mutation to alanine, inhibiting several hydrogen bonds with the α2-1 helix of MHC I decreases surface MHC I to 65±6% compared to WT (Fig. 36b,f and g). The interaction between β hairpin of tapasin and the α_2-domain of MHC I has a stronger effect on MHC I surface expression (R187E; 55±13% compared to WT) (Fig. 36c,f). Mutating residues of interface loop and β hairpin led to a synergistical reduction of surface MHC I to 46±4% (Fig. 36f). In the interface between the IgC domain of tapasin and α3 domain of MHC I, two intermolecular contact sides were identified (Fig. 36d). Disrupting the hydrogen bond between Arg333 of tapasin and Glu229 of MHC I, resulted in a reduced MHC I surface expression to 37±3% (Fig. 36f). This interaction site between the CD8-recognition loop of MHC I and IgC domain of tapasin has previously been described by the cryo-EM structure of the PLC[12]. Mutation of Ser336 of tapasin to prevent the contact site with Thr225 of MHC I did not reduce surface MHC I (Fig. 36d,f). The repositioned IgC domain of tapasin is additionally stabilized by backbone interactions between Ile92 and Lys94 of β_2m and Leu329 of tapasin and by side chain hydrogen bonding of Ser88 of β_2m and Glu307 of tapasin (Fig. 36e). The mutation of Glu307 to alanine, disrupting the hydrogen bond between Ser88 of β_2m and Glu307 of tapasin resulted in a reduced MHC I surface expression of 46±1% (Fig. 36e,f and h), though the expression level of mutant tapasin was also lowered compared to WT (Fig. 36h).

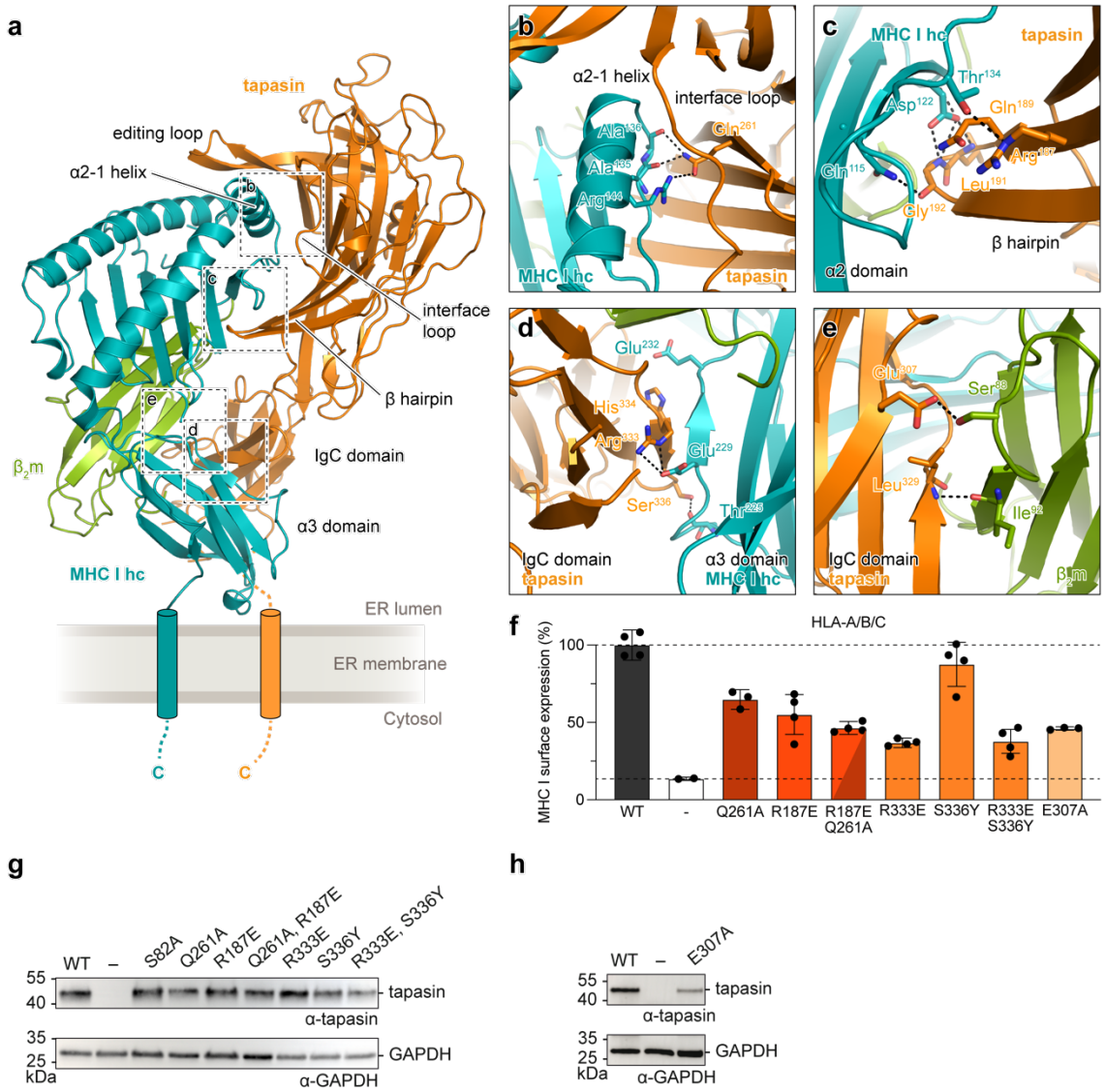

Figure 36: Interaction sites at the MHC I–tapasin interface influence MHC I surface expression. a, Cartoon representation of chaperone complex. The regions displayed in **b**-**e** are indicated by dashed boxes. ERp57 is not shown for reasons of clarity. Schematic illustration of C-terminal (C) transmembrane helices of MHC I and tapasin. **b**, Close up view of the interaction site between α2-1 helix of MHC I (teal) and the interface loop of tapasin (orange). Hydrogen bonds are shown as dashed black lines. **c**, Interface between the α2 domain of MHC I and β hairpin of tapasin. **d**, Zoom into the α3 domain of MHC I and the IgC domain of tapasin. **e**, Interface formed between β_2m and C-terminal domain of tapasin. **f**, MHC I surface expression of tapasin-deficient HAP1 cells expression interface mutants of tapasin monitored by flow cytometry. Mean fluorescent intensities of cells stained with APC conjugated HLA-A/B/C antibody (W6/32) normalized to cells expressing wildtype tapasin (upper dashed line). The lower dashed line represents the MHC I surface level of mock transfected cells. (±SD, n=4 biological independent samples; Q261A, R333E/S336Y, n=3 biological independent samples; mock transfection, n=2 biological independent samples). Dark orange, interface loop region; orange, β hairpin interface; light orange, α3 interface. The gating strategy is provided in Fig. 41 – see appendix. **g**, Whole cell extracts of eGFP positive cells, expressing wildtype and interface mutants of tapasin, analyzed by SDS-PAGE and immunoblotting. **h**, SDS-PAGE and immunoblot analysis of whole cell extracts of eGFP positive cells, that express wildtype and β_2m interface mutant of tapasin. 4-20% Mini-PROTEAN gels were utilized for SDS-PAGE. WT, wildtype; -, mock transfection.

9.2.15 Editing loop fulfills two functions during peptide exchange catalysis

It has been proposed that tapasin and its homologue TAPBPR have distinct preferences for specific MHC I allomorphs[24,72,121]. Nevertheless, the structure of the MHC I–tapasin–ERp57 structure reveals that binding interfaces for client recognition for both chaperones are similar and there are only minor differences for single residues (Fig. 37).

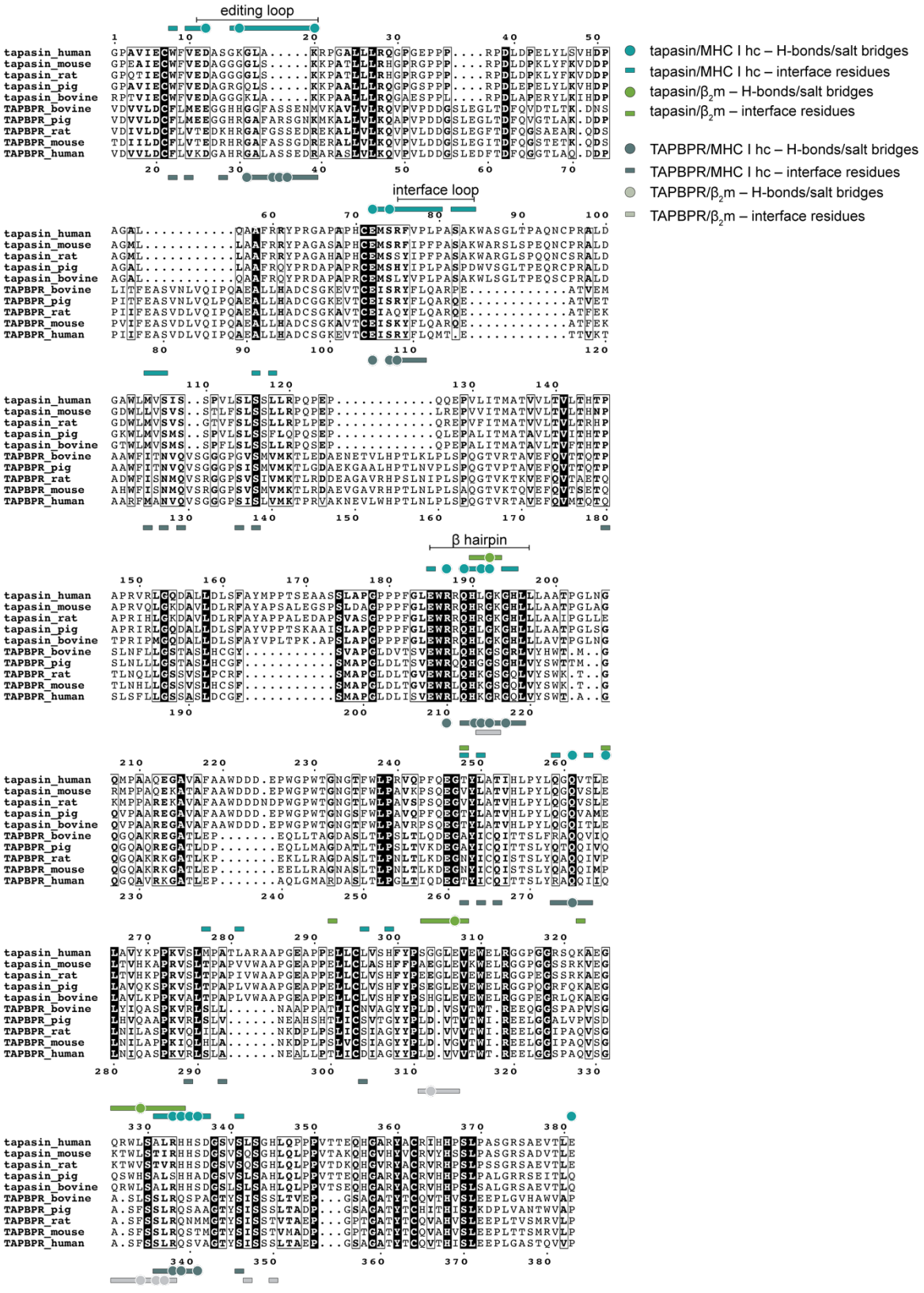

Figure 37: Sequence alignment of tapasin and TAPBPR based on the structure. Conserved residues are highlighted in black and physiochemically related residues are displayed in bold letters. Residues that are involved in interactions with MHC I are marked with teal (MHC I) and green (β_2m) for tapasin and dark (MHC I) and light (β_2m) bars and dots for TAPBPR. The dots represent specific interactions such as hydrogen bonds and salt bridges. hc, heavy chain.

The structure of TAPBPR in complex with MHC I shows a slightly increased widening of the peptide-binding pocket by a stronger rearrangement of the α2-1 helix of MHC I (Fig. 38b). In the MHC I–tapasin–ERp57 structure, the editing loop is located on top if the F-pocket of MHC I and in the client-free pMHC I structure, the side chains of residues Asn80 and Lys146 are orientated into the F-pocket and coordinate the bound peptides C-terminus (Fig. 38a). In an intermediate state, where peptide and chaperone are bound to MHC I, the carbonyl group of Gly15 of the editing loop may acts as a hydrogen-bond acceptor that could shield the peptide-bound MHC I F-pocket. Therefore, the editing loop supposedly has two contrasting tasks. It promotes the widening of a peptide-receptive MHC I F-pocket, while during peptide-loading the editing loop shields the C-terminus of the bound peptide. This theory could also be applied for TAPBPR, because NMR studies showed that the loop can be observed as lid on top of the F-pocket[96], while in one of the MHC I-TAPBPR structures, the loop dives into the binding pocket and stabilizes the peptide-receptive binding cleft by acting as a peptide surrogate[11,95].

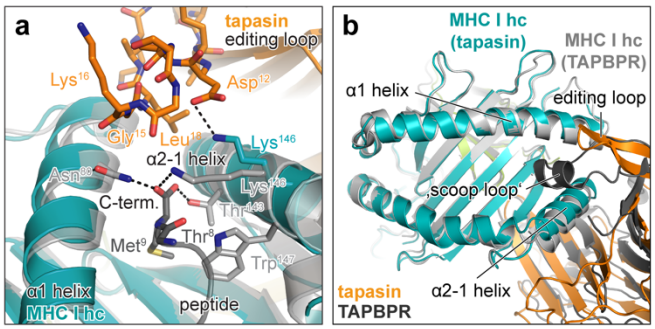

Figure 38: The editing states of MHC I induced by the chaperones tapasin or TAPBPR. a, Overlay of the peptide-receptive MHC I in complex with tapasin–ERp57 with the peptide bound H2-D^b (grey, PDB ID 2F74). Hydrogen bonds are highlighted by dashed lines. **b**, Comparison of the tapasin (orange)-ERp57-MHC I (teal) complex with the TAPBPR-MHC I complex (grey PDB ID 5OPI). C-termin., C terminus.

9.2.16 MHC I allomorphs have the structural prerequisites to interact with the chaperone tapasin regardless of their dependence on tapasin

Sequence alignments of classical MHC I molecules reveal that the interaction sites for tapasin are conserved for tapasin-dependent and tapasin-independent allomorphs (Fig. 39). Also, the interaction sites are similar for both chaperones tapasin and TAPBPR, except for residue Trp73 of H2-D^b (Fig. 39).

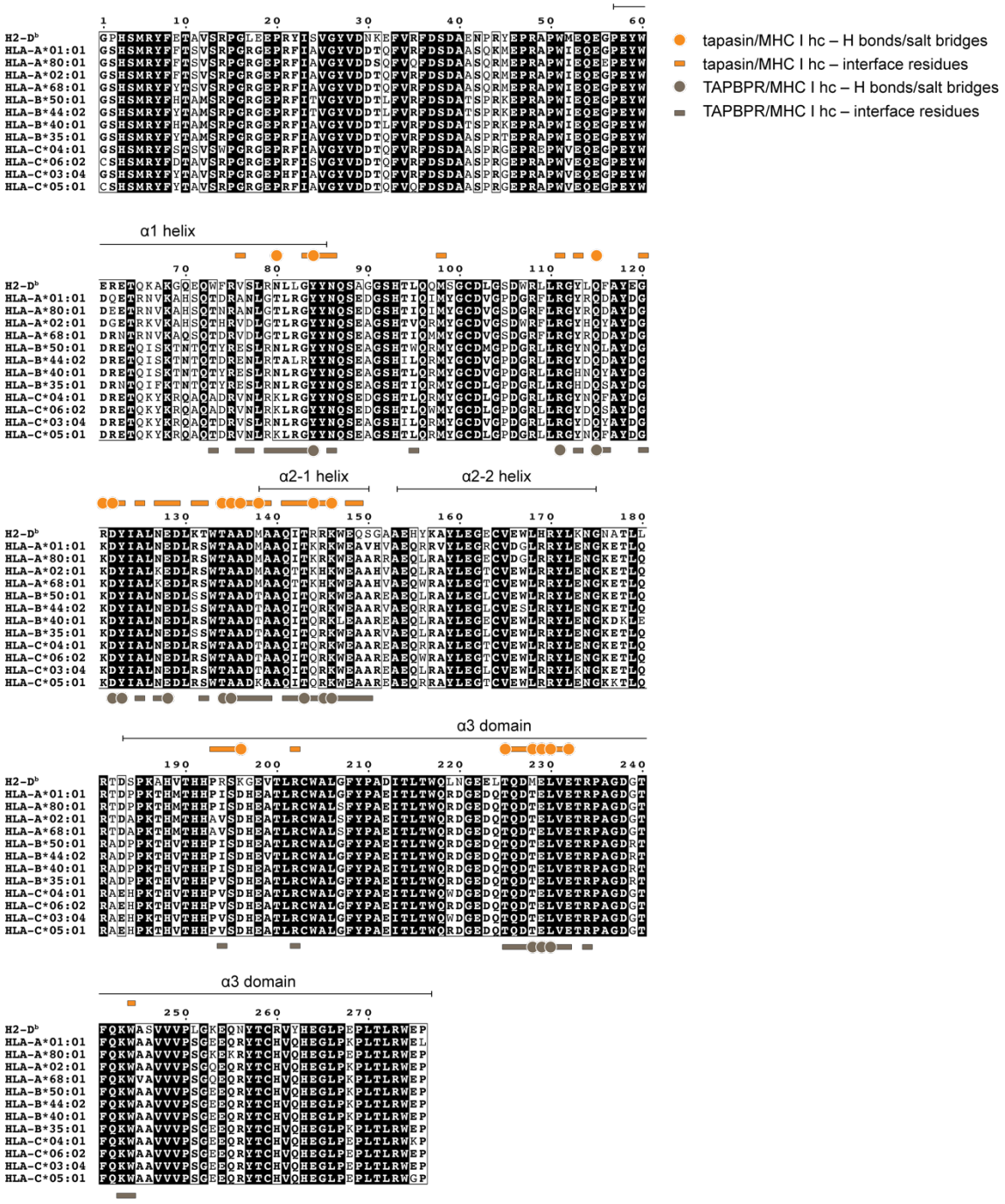

Figure 39: Multiple sequence alignment of classical MHC I allomorphs. Interaction sites with tapasin or TAPBPR are marked with orange or brown bars and dots, respectively. The dots represent direct interactions such as hydrogen bonds or salt bridges. hc, heavy chain.

For non-classical MHC I molecules HLA-E, -F and -G not all potential interface sites are conserved. Most of the alternative residues are still able to form hydrogen bonds (Fig. 40).

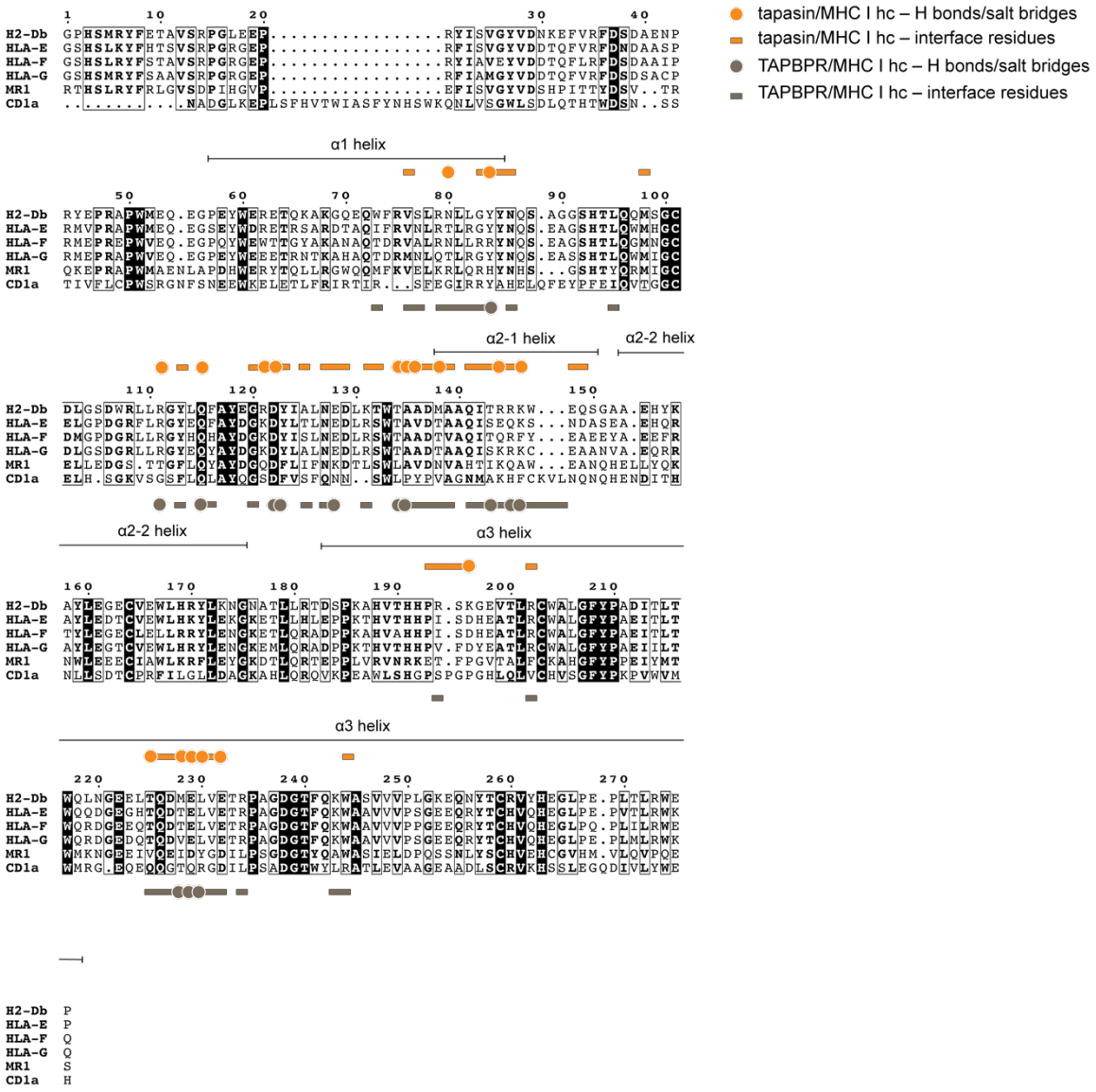

Figure 40: Multiple sequence alignment of non-classical and MHC I-related molecules. Orange and brown dots and bars represent interaction sites with tapasin and TAPBPR, respectively. The dots highlight specific interactions such as hydrogen bonds and salt bridges.

Taken together, the crystal structure of the MHC I chaperone complex MHC I–tapasin–ERp57 shows that tapasin-dependent and -independent allomorphs have the structural prerequisites to interact with tapasin. These findings suggest that their level of plasticity and thus their ability to accommodate high-affinity peptides determines the association that is facilitated by key structural elements of the chaperone tapasin (Fig. 40). Further structural and functional investigation is required to understand how e.g., C-terminally extended peptides, protruding

from the MHC I F-pocket are proofread by tapasin or TAPBPR. Tapasin functions within the editing module of the PLC. Therefore, the association with ERp57 might not only be essential to coordinate calreticulin but the molecular dynamics of this interaction may facilitate unlocking tapasin for MHC I engagement and peptide editing catalysis (Fig. 41).

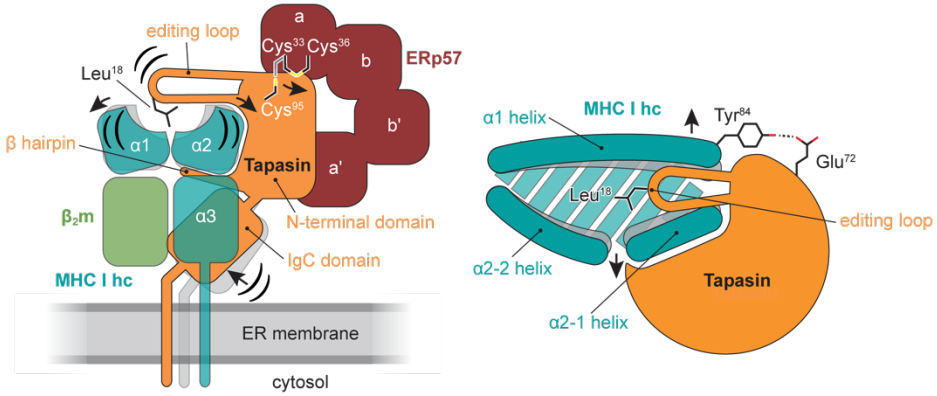

Figure 41: Mechanistic model of peptide-editing function of tapasin. Domain movements upon association of tapasin–ERp57 heterodimer results in stabilized peptide-receptive MHC I allomorphs. Movements are indicated by black arrows and dotted lines represents polar interactions between tapasin and MHC I. ERp57 is not displayed in the right panel for clear focus on interactions in the F-pocket region. hc, heavy chain; ER, endoplasmic reticulum.

10 Conclusion

During this thesis, the complex of MHC I–tapasin–ERp57 was captured by a photo-triggered approach. Various selected MHC I allomorphs were screened for stable complex formation with tapasin–ERp57 by SEC, identifying the mouse allomorph H2-D^b as a suited client. Initially fine-screened crystals diffracted X-rays to 4.0 Å with two heterotetrameric complexes per asymmetric unit belonging to the space group $P2_12_12_1$. Microseed matrix-screening[24] resulted in crystals with an improved resolution of 2.7 Å in space group $P22_12_1$ and one complex in the asymmetric unit.

The MHC I–tapasin–ERp57 complex reveals two peptide-editing features. A loop, referred to as editing loop, is located on top of the F-pocket of MHC I. Combining the structural data with functional data of a flow cytometry-based cellular assay, suggest that the editing loop functions in a dual fashion. In a peptide-receptive state, the loop is involved in stabilizing a widened F-pocket, while in an intermediate peptide-chaperone-bound state, the loop might shield the peptides C-terminus during the process of loading. A similar peptide-editing function might be possible for TAPBPR, as NMR studies showed that the longer loop of TAPBPR can be observed as lid located on top of the F-pocket[96] The second structural feature is a β hairpin motif is shifted upwards beneath the β-sheets of the MHC I binding pocket, similar as seen for TAPBPR[11].

Overall, the structure of MHC I–tapasin–ERp57 shows that the binding interfaces for stabilization of peptide-deficient MHC I molecules are comparable for the two MHC I-specific chaperones with slight differences in specific residues. The opening of the α2-1 helix of MHC I is slightly stronger when bound to TAPBPR, which might be essential for peptide-editing in a peptide-depleted environment where TAPBPR occurs, and more time is needed until an optimal peptide can be loaded onto MHC I. The position of β_2m in relation to the MHC I hc in the tapasin–ERp57–MHC I structure remains similar to the peptide-bound state, while the binding of TAPBPR to MHC I results in a rearrangement of β_2m. Sequence alignments of classical MHC I allomorphs demonstrate that the interaction sites for tapasin are conserved among tapasin-dependent and -independent MHC I allomorphs. Furthermore, the interaction sites are shared between tapasin and TAPBPR, except for residue Trp^{73} of H2-D^b. Interestingly, two studies with different readouts to measure the MHC I-specific editors' functionality, TAPBPR and tapasin were on opposite sites on the dependence of HLA-A allomorphs[17,73,121]. However, depletion of TAPBPR leads to a minor decrease of MHC I surface compared to the loss of tapasin[7,14,24,73], excluding that certain MHC I allomorphs are exclusively edited by either tapasin or TAPBPR. How the two MHC I-specific chaperones work together to shape the epitope repertoire of MHC I allomorphs for high immunogenicity needs to be addressed in the future.

All in all, the MHC I–tapasin–ERp57 structure highlights that both tapasin-dependent and -independent MHC I allomorphs have the structural prerequisites to interact with the editor, proposing that their level of plasticity and hence their capability to harbor a high-affinity peptide defines the association that is stabilized by key structural elements of tapasin. Further structural and functional studies are required to understand how *e.g.*, C-terminally extended peptides, which protrude from the MHC I F-pocket are edited by tapasin or TAPBPR.

Since tapasin acts primarily within the PLC multichaperone network, the theory wether the association of ERp57 with tapasin is not only necessary for association of the glycan-chaperone calreticulin, but that the molecular dynamics of this interaction also assists in unlocking tapasin for MHC I engagement and peptide proofreading catalysis needs to be tackled in the future.

This study provides further insights into the mechanistic basis for MHC I recognition of tapasin and reveals how the various MHC I allomorphs are stabilized during peptide loading and editing to ensure the generation of optimal pMHC I complexes for adaptive immunity.

11 References

1. Blum, J. S., Wearsch, P. A. & Cresswell, P. Pathways of antigen processing. *Annu Rev Immunol* **31**, 443–473 (2013).
2. Neefjes, J., Jongsma, M. L. M., Paul, P. & Bakke, O. Towards a systems understanding of MHC class I and MHC class II antigen presentation. *Nat Rev Immunol* **11**, 823–836 (2011).
3. Trowitzsch, S. & Tampé, R. Multifunctional chaperone and quality control complexes in adaptive immunity. *Ann Rev Biophys* **49**, 135–161 (2020).
4. Chen, M. & Bouvier, M. Analysis of interactions in a tapasin/class I complex provides a mechanism for peptide selection. *EMBO J* **26**, 1681–1690 (2007).
5. Wearsch, P. A. & Cresswell, P. Selective loading of high-affinity peptides onto major histocompatibility complex class I molecules by the tapasin-ERp57 heterodimer. *Nat Immunol* **8**, 873–881 (2007).
6. Fleischmann, G. *et al.* Mechanistic basis for epitope proofreading in the peptide-loading complex. *J Immunol* **195**, 4503–4513 (2015).
7. Ortmann, B. *et al.* A critical role for tapasin in the assembly and function of multimeric MHC class I-TAP complexes. *Science* **227**, 1306–1309 (1997).
8. Dong, G., Wearsch, P. A., Peaper, D. R., Cresswell, P. & Reinisch, K. M. Insights into MHC Class I peptide loading from the structure of the tapasin-ERp57 thiol oxidoreductase heterodimer. *Immunity* **30**, 21–32 (2009).
9. Hermann, C., Strittmatter, L. M., Deane, J. E. & Boyle, L. H. The binding of TAPBPR and tapasin to MHC class I Is mutually exclusive. *J Immunol* **191**, 5743–5750 (2013).
10. Jiang, J. *et al.* Crystal structure of a TAPBPR–MHC I complex reveals the mechanism of peptide editing in antigen presentation. *Science* **358**, 1064–1068 (2017).
11. Thomas, C. & Tampé, R. Structure of the TAPBPR-MHC I complex defines the mechanism of peptide loading and editing. *Science* **358**, 1060–1064 (2017).
12. Blees, A. *et al.* Structure of the human MHC-I peptide-loading complex. *Nature* **551**, 525–528 (2017).
13. Boyle, L. H. *et al.* Tapasin-related protein TAPBPR is an additional component of the MHC class i presentation pathway. *PNAS* **110**, 3465–3470 (2013).
14. Garbi, N. *et al.* Impaired immune responses and altered peptide repertoire in tapasin-deficient mice. *Nat Immunol* **3**, 234–238 (2000).
15. Grandea Iii, A. G. *et al.* Impaired assembly yet normal trafficking of MHC class I molecules in tapasin mutant mice. *Immunity* **13**, 213–222 (2000).
16. Rizvi, S. M. *et al.* Distinct assembly profiles of HLA-B molecules. *J Immunol* **192**, 4967–4976 (2014).
17. Bashirova, A. A. *et al.* HLA tapasin independence: broader peptide repertoire and HIV control. *Proc Natl Acad Sci U S A* **117**, 28232–28238 (2020).
18. Sieker, F., Straatsma, T. P., Springer, S. & Zacharias, M. Differential tapasin dependence of MHC class I molecules correlates with conformational changes upon peptide dissociation: A molecular dynamics simulation study. *Mol Immunol* **45**, 3714–3722 (2008).
19. van Hateren, A., Bailey, A., Werner, J. M. & Elliott, T. Plasticity of empty major histocompatibility complex class I molecules determines peptide-selector function. *Mol Immunol* **68**, 98–101 (2015).
20. Bailey, A. *et al.* Selector function of MHC I molecules is determined by protein plasticity. *Sci Rep* **5**, 14928 (2015).
21. Abualrous, E. T. *et al.* The carboxy terminus of the ligand peptide determines the stability of the MHC class I molecule H-2Kb: A combined molecular dynamics and experimental study. *PLoS One* **10**, e0135421 (2015).
22. Frickel, E.-M. *et al.* TROSY-NMR reveals interaction between ERp57 and the tip of the calreticulin P-domain. *Proc Natl Acad Sci U S A* **99**, 1954–1959 (2002).

23. Arshad, N. & Cresswell, P. Tumor-associated calreticulin variants functionally compromise the peptide loading complex and impair its recruitment of MHC-I. *J Biol Chem* **293**, 9555–9569 (2018).
24. D'Arcy A, Villard V & Marsh M. An automated microseed matrix-screening method for protein crystallization. *Acta Crystallogr D Biol Crystallogr* **63**, 550–554 (2007).
25. Rodenko, B. *et al.* Generation of peptide-MHC class I complexes through UV-mediated ligand exchange. *Nat Protocols* **1**, 1120–1132 (2006).
26. Achour, A. *et al.* Structural basis of the differential stability and receptor specificity of H-2Db in complex with murine versus human β2-microglobulin. *J Mol Biol* **356**, 382–396 (2006).
27. Ilca, F. T. *et al.* TAPBPR mediates peptide dissociation from MHC class I using a leucine lever. *eLife* **7**, (2018).
28. Hafstrand, I. *et al.* Successive crystal structure snapshots suggest the basis for MHC class i peptide loading and editing by tapasin. *Proc Natl Acad Sci U S A* **116**, 5055–5060 (2019).
29. Lan, H. *et al.* Exchange catalysis by tapasin exploits conserved and allele-specific features of MHC-I molecules. *Nat Commun* **12**, 4236 (2021).
30. Parkin, J. & Cohen, B. An overview of the immune system. *Lancet* **357**, 1777–1789 (2001).
31. Takeuchi, O. & Akira, S. Pattern recognition receptors and inflammation. *Cell* **140**, 805–820 (2010).
32. Hoebe, K., Janssen, E. & Beutler, B. The interface between innate and adaptive immunity. *Nat Immunol* **5**, 971–974 (2004).
33. Antoniou, A. N., Powis, S. J. & Elliott, T. Assembly and export of MHC class I peptide ligands. *Curr Opin Immunol* **15**, 75–81 (2003).
34. Rock, K. L. & Goldberg, A. L. Degradation of cell proteins and the generation of MHC class I-presented peptides. *Annu Rev Immunol* **17**, 739–79 (1999).
35. Yewdell, J. W., Antón, L. C. & Bennink, J. R. Defective ribosomal products (DRiPs): a major source of antigenic peptides for MHC class I molecules? *J Immunol* **157**, 1823–1826 (1996).
36. Rock, K. L. *et al.* Inhibitors of the proteasome block the degradation of most cell proteins and the generation of peptides presented on MHC class I molecules. *Cell* **78**, 761–771 (1994).
37. Cascio, P., Hilton, C., Kisselev, A., Rock, K. & Goldberg, A. 26S proteasomes and immunoproteasomes produce mainly N-extended versions of an antigenic peptide. *EMBO J* **20**, 2357–2366 (2001).
38. Bard, J. A. M. *et al.* Structure and function of the 26S proteasome. *Annu Rev Biochemi* **87**, 697–724 (2018).
39. Murata, S., Takahama, Y., Kasahara, M. & Tanaka, K. The immunoproteasome and thymoproteasome: functions, evolution and human disease. *Nat Immunol* **19**, 923–931 (2018).
40. Abele, R. & Tampé, R. Moving the cellular peptidome by transporters. *Front Cell Dev Biol* **6**, 1–13 (2018).
41. Abele, R. & Tampé, R. The ABCs of immunology: Structure and function of TAP, the transporter associated with antigen processing. *Physiology* **19**, 216–224 (2004).
42. Meyer, T. H., van Endert, P. M., Uebel, S., Ehring, B. & Tampé, R. Functional expression and purification of the ABC transporter complex associated with antigen processing (TAP) in insect cells. *FEBS Lett* **351**, 443–447 (1994).
43. Koch, J., Guntrum, R., Heintke, S., Kyritsis, C. & Tampé, R. Functional dissection of the transmembrane domains of the transporter associated with antigen processing (TAP). *J Biol Chem* **279**, 10142–10147 (2004).
44. Blees, A. *et al.* Assembly of the MHC I peptide-loading complex determined by a conserved ionic lock-switch. *Sci Rep* **5**, 17341 (2015).

45. Hulpke, S., Baldauf, C. & Tampe, R. Molecular architecture of the MHC I peptide-loading complex: One tapasin molecule is essential and sufficient for antigen processing. *FASEB J* **26**, 5071–5080 (2012).
46. Koch, J., Guntrum, R. & Tampé, R. The first N-terminal transmembrane helix of each subunit of the antigenic peptide transporter TAP is essential for independent tapasin binding. *FEBS Lett* **580**, 4091–4096 (2006).
47. van Endert, P. M. *et al.* A sequential model for peptide binding and transport by the transporters associated with antigen processing. *Immunity* **1**, 491–500 (1994).
48. Androlewicz, M. J. & Cresswell, P. Human transporters associated with antigen processing possess a promiscuous peptide-binding site. *Immunity* **1**, 7–14 (1994).
49. Koopmann, J.-O., Post, M., Neefjes, J. J., Hämmerling, G. J. & Momburg, F. Translocation of long peptides by transporters associated with antigen processing (TAP). *Eur J Immunol* **26**, 1720–1728 (1996).
50. Uebel, S. *et al.* Requirements for peptide binding to the human transporter associated with antigen processing revealed by peptide scans and complex peptide libraries. *J Biol Chem* **270**, 18512–18516 (1995).
51. Uebel, S. *et al.* Recognition principle of the TAP transporter disclosed by combinatorial peptide libraries. *Proc Natl Acad Sci U S A* **94**, 8976–8981 (1997).
52. Momburg, F. *et al.* Selectivity of MHC-encoded peptide transporters from human, mouse and rat. *Nature* **367**, 648–651 (1994).
53. Hammer, G. E., Gonzalez, F., James, E., Nolla, H. & Shastri, N. In the absence of aminopeptidase ERAAP, MHC class I molecules present many unstable and highly immunogenic peptides. *Nat Immunol* **8**, 101–108 (2007).
54. York, I. A. *et al.* The Er aminopeptidase ERAP I enhances or limits antigen presentation by trimming epitopes to 8-9 residues. *Nat Immunol* **3**, 1177–1184 (2002).
55. Serwold, T., Gonzalez, F., Kim, J., Jacob, R. & Shastri, N. ERAAP customizes peptides for MHC class I molecules in the endoplasmic reticulum. *Lett Nature* **419**, 480–483 (2002).
56. Hulpke, S. & Tampé, R. The MHC I loading complex: A multitasking machinery in adaptive immunity. *Trends Biochem Sci* **38**, 412–420 (2013).
57. Dempski, R. E. & Imperiali, B. Oligosaccharyl transferase: Gatekeeper to the secretory pathway. *Curr Opin Chem Biol* **6**, 844–850 (2002).
58. Bai, L., Wang, T., Zhao, G., Kovach, A. & Li, H. The atomic structure of a eukaryotic oligosaccharyltransferase complex. *Nature* **555**, 328–333 (2018).
59. Springer, S. Transport and quality control of MHC class I molecules in the early secretory pathway. *Curr Opin Immunol* **34**, 83–90 (2015).
60. Frickel, E. M. *et al.* ERp57 is a multifunctional thiol-disulfide oxidoreductase. *J Biol Chem* **279**, 18277–18287 (2004).
61. Peaper, D. R. & Cresswell, P. Regulation of MHC class I assembly and peptide binding. *Ann Rev Cell Dev Biol* **24**, 343–368 (2008).
62. Solheim, J. C., Harris, M. R., Yu, Y. Y. L., Kindle, C. S. & Hansen, T. H. Calreticulin and calnexin interact with different protein and glycan determinants during the assembly of MHC class I. *J Immunol* **160**, 5404–5409 (1998).
63. Hammond, C., Braakman, I. & Helenius, A. Role of N-linked oligosaccharide recognition, glucose trimming, and calnexin in glycoprotein folding and quality control. *Proc Natl Acad Sci U S A* **91**, 913–917 (1994).
64. Williams, D. B. Beyond lectins: The calnexin/calreticulin chaperone system of the endoplasmic reticulum. *J Cell Sci* **119**, 615–623 (2006).
65. del Cid, N. *et al.* Modes of calreticulin recruitment to the major histocompatibility complex class I assembly pathway. *J Biol Chem* **285**, 4520–4535 (2010).
66. Vassilakos, A., Michalak, M., Lehrman, M. A. & Williams, D. B. Oligosaccharide binding characteristics of the molecular chaperones calnexin and calreticulin. *Biochem* **37**, 3480–3490 (1998).

67. Peaper, D. R. & Cresswell, P. The redox activity of ERp57 is not essential for its functions in MHC class I peptide loading. *Proc Natl Acad Sci U S A* **105**, 10477–10482 (2008).
68. Trowitzsch, S. & Tampé, R. ABC transporters in dynamic macromolecular assemblies. *J Mol Biol* **430**, 4481–4495 (2018).
69. Wearsch, P. A., Peaper, D. R. & Cresswell, P. Essential glycan-dependent interactions optimize MHC class I peptide loading. *Proc Natl Acad Sci U S A* **108**, 4950–4955 (2011).
70. Williams, A. P., Peh, C. A., Purcell, A. W., McCluskey, J. & Elliott, T. Optimization of the MHC class I peptide cargo is dependent on tapasin. *Immunity* **16**, 509–520 (2002).
71. Fisette, O., Wingbermühle, S., Tampé, R. & Schäfer, L. V. Molecular mechanism of peptide editing in the tapasin-MHC I complex. *Sci Rep* **6**, 19085 (2016).
72. Morozov, G. I. *et al.* Interaction of TAPBPR, a tapasin homolog, with MHC-I molecules promotes peptide editing. *Proc Natl Acad Sci U S A* **113**, 1006–1015 (2016).
73. Hafstrand, I., Aflalo, A. & Boyle, L. H. Why TAPBPR? Implications of an additional player in MHC class I peptide presentation. *Curr Opin Immunol* **70**, 90–94 (2021).
74. Helenius, A. & Aebi, M. Roles of N-linked glycans in the endoplasmic reticulum. *Ann Rev Biochem* **73**, 1019–1049 (2004).
75. Neerincx, A. *et al.* TAPBPR bridges UDP-glucose:glycoprotein glucosyltransferase 1 onto MHC class I to provide quality control in the antigen presentation pathway. *eLife* **6**, (2017).
76. Thomas, C. & Tampé, R. MHC I assembly and peptide editing — chaperones, clients, and molecular plasticity in immunity. *Curr Opin Immunol* **70**, 48–56 (2021).
77. Dick, T. P., Bangia, N., Peaper, D. R. & Cresswell, P. Disulfide bond isomerization and the assembly of MHC class I-peptide complexes. *Immunity* **16**, 87–98 (2002).
78. Sadasivan, B. & Lehner, P. J. Roles for calreticulin and a novel glycoprotein, tapasin, in the interaction of MHC class I molecules with TAP. *Immunity* **5**, 103–114 (1996).
79. Howarth, M., Williams, A., Tolstrup, A. B. & Elliott, T. Tapasin enhances MHC class I peptide presentation according to peptide half-life. *Proc Natl Acad Sci U S A* **101**, 11737–11742 (2004).
80. Purcell, A. W. *et al.* Quantitative and qualitative influences of tapasin on the class I peptide repertoire. *J Immunol* **166**, 1016–1027 (2001).
81. Myers, N. B. *et al.* Kb, Kd, and Ld molecules share common tapasin dependencies as determined using a novel epitope tag. *J Immunol* **165**, 5656–5663 (2000).
82. Walker, K. W. & Gilbert, H. F. Scanning and escape during protein-disulfide isomerase-assisted protein folding. *J Biol Chem* **272**, 8845–8848 (1997).
83. Madden DR. The three-dimensional structure of peptide MHC complexes. *Annu. Rev. Immunol* **13**, 587–622 (1995).
84. Garrett, T. P., Saper, M. A., Bjorkman, P. J., Strominger, J. L. & Wiley, D. C. Specificity pockets for the side chains of peptide antigens in HLA-Aw68. *Nature* **342**, 692–6 (1989).
85. Macdonald, W. A. *et al.* A naturally selected dimorphism within the HLA-B44 supertype alters class I structure, peptide repertoire, and T cell recognition. *J Exp Med* **198**, 679–691 (2003).
86. Zernich, D. *et al.* Natural HLA class I polymorphism controls the pathway of antigen presentation and susceptibility to viral evasion. *J Exp Med* **200**, 13–24 (2004).
87. van Hateren, A. & Elliott, T. The role of MHC I protein dynamics in tapasin and TAPBPR-assisted immunopeptidome editing. *Curr Opin Immunol* **70**, 138–143 (2021).
88. Kozlov, G. *et al.* Structural basis of carbohydrate recognition by calreticulin. *J Biol Chem* **285**, 38612–38620 (2010).
89. Gao, B. *et al.* Assembly and antigen-presenting function of MHC class I molecules in cells lacking the ER chaperone calreticulin. *Immunity* **16**, 99–109 (2002).
90. Stepensky, D., Bangia, N. & Cresswell, P. Aggregate formation by ERp57-deficient MHC class I peptide-loading complexes. *Traffic* **8**, 1530–1542 (2007).

91. Bakshs, S. & Michalakg, M. Expression of calreticulin in Escherichia coli and identification of its Ca2+ binding domains. *J Biol Chem* **266**, 21458–21465 (1991).
92. Teng, M. S. *et al.* A human TAPBP (TAPASIN)-related gene, TAPBP-R. *Eur J Immunol* **32**, 1059–1068 (2002).
93. Thomas, C. & Tampé, R. Proofreading of peptide-MHC complexes through dynamic multivalent interactions. *Front Immunol* **8**, 65 (2017).
94. McShan, A. C. *et al.* Peptide exchange on MHC-I by TAPBPR is driven by a negative allostery release cycle. *Nat Chem Biol* **14**, 811–820 (2018).
95. Sagert, L., Hennig, F., Thomas, C. & Tampé, R. A loop structure allows TAPBPR to exert its dual function as MHC I chaperone and peptide editor. *eLife* **9**, (2020).
96. McShan, A. C. *et al.* TAPBPR promotes antigen loading on MHC-I molecules using a peptide trap. *Nat Commun* **12**, (2021).
97. Li, M. Z. & Elledge, S. J. Harnessing homologous recombination in vitro to generate recombinant DNA via SLIC. *Nat Methods* **4**, 251–256 (2007).
98. Jongsma, M. L. M. *et al.* The SPPL3-defined glycosphingolipid repertoire orchestrates HLA class I-mediated immune responses. *Immunity* **54**, 132–150 (2021).
99. Hulpke, S. *et al.* Direct evidence that the N-terminal extensions of the TAP complex act as autonomous interaction scaffolds for the assembly of the MHC I peptide-loading complex. *Cell Mol Life Sci* **69**, 3317–3327 (2012).
100. Smith, C. *et al.* Molecular imprint of exposure to naturally occurring genetic variants of human cytomegalovirus on the T cell repertoire. *Sci Rep* **4**, 3993 (2014).
101. Archbold, J. K. *et al.* Natural micropolymorphism in human leukocyte antigens provides a basis for genetic control of antigen recognition. *J Exp Med* **206**, 209–219 (2009).
102. Macdonald, W. *et al.* Identification of a dominant self-ligand bound to three HLA B44 alleles and the preliminary crystallographic analysis of recombinant forms of each complex. *FEBS Lett* **527**, 27–32 (2002).
103. Morgner, N., Barth, H. D. & Brutschy, B. A new way to detect noncovalently bonded complexes of biomolecules from liquid micro-droplets by laser mass spectrometry. *Aust J Chem* **59**, 109–114 (2006).
104. Peetz, O. *et al.* LILBID and nESI: Different native mass spectrometry techniques as tools in structural biology. *J Am Soc Mass Spectrom* **30**, 181–191 (2019).
105. Farley, C. & Juers, D. H. Efficient cryoprotection of macromolecular crystals using vapor diffusion of volatile alcohols. *J Struct Biol* **188**, 102–106 (2014).
106. Cianci, M. *et al.* P13, the EMBL macromolecular crystallography beamline at the low-emittance PETRA III ring for high- and low-energy phasing with variable beam focusing. *J Synchroton Radiat* **24**, 323–332 (2017).
107. Kabsch, W. XDS. *Acta Crystallogr D Biol Crystallogr* **66**, 125–132 (2010).
108. Liebschner, D. *et al.* Macromolecular structure determination using X-rays, neutrons and electrons: Recent developments in Phenix. *Acta Crystallogr D Struct Biol* **75**, 861–877 (2019).
109. Emsley, P., Lohkamp, B., Scott, W. G. & Cowtan, K. Features and development of Coot. *Acta Crystallogr D Biol Crystallogr* **66**, 486–501 (2010).
110. Joosten, R. P., Long, F., Murshudov, G. N. & Perrakis, A. The PDB-REDO server for macromolecular structure model optimization. *IUCrJ* **1**, 213–220 (2014).
111. Domnick, A. *et al.* Molecular basis of MHC I quality control in the peptide loading complex. *Nat Commun* **13**, 4701 (2022).
112. Zhang, W., Wearsch, P. a, Zhu, Y., Leonhardt, R. M. & Cresswell, P. A role for UDP-glucose glycoprotein glucosyltransferase in expression and quality control of MHC class I molecules. *Proc Natl Acad Sci U S A* **108**, 4956–4961 (2011).
113. Sekulovski, S. *et al.* Assembly defects of human tRNA splicing endonuclease contribute to impaired pre-tRNA processing in pontocerebellar hypoplasia. *Nat Commun* **12**, 5610 (2021).

114. Trowitzsch, S., Bieniossek, C., Nie, Y., Garzoni, F. & Berger, I. New baculovirus expression tools for recombinant protein complex production. *J Struct Biol* **172**, 45–54 (2010).
115. Berger, I., Fitzgerald, D. J. & Richmond, T. J. Baculovirus expression system for heterologous multiprotein complexes. *Nat Biotechnol* **22**, 1583–1587 (2004).
116. Ellgaard, L. *et al.* NMR structure of the calreticulin P-domain. *Proc Natl Acad Sci U S A* **98**, 3133–3138 (2001).
117. Zhang, Y. *et al.* ERp57 does not require interactions with calnexin and calreticulin to promote assembly of class I histocompatibility molecules, and it enhances peptide loading independently of its redox activity. *J Biol Chem* **284**, 10160–10173 (2009).
118. O'Rourke, S. M., Morozov, G. I., Roberts, J. T., Barb, A. W. & Sgourakis, N. G. Production of soluble pMHC-I molecules in mammalian cells using the molecular chaperone TAPBPR. *Protein Eng Des Sel* **32**, 525–532 (2019).
119. Vigneron, N., Peaper, D. R., Leonhardt, R. M. & Cresswell, P. Functional significance of tapasin membrane association and disulfide linkage to ERp57 in MHC class I presentation. *Eur J Immunol* **39**, 2371–2376 (2009).
120. Huan, X., Zhuo, Z., Xiao, Z. & Ren, E. C. Crystal structure of suboptimal viral fragments of Epstein Barr Virus Rta peptide-HLA complex that stimulate CD8 T cell response. *Sci Rep* **9**, (2019).
121. Ilca, F. T., Drexhage, L. Z., Brewin, G., Peacock, S. & Boyle, L. H. Distinct polymorphisms in HLA class I molecules govern their susceptibility to peptide editing by TAPBPR. *Cell Rep* **29**, 1621–1632 (2019).

12 Appendix

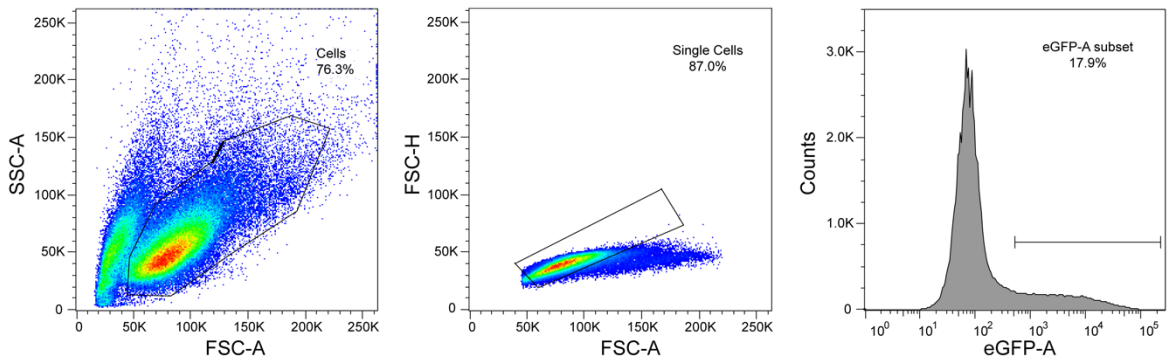

Figure 42: Gating strategy of flow cytometry experiments. Transfected tapasin-deficient HAP1 cells were first gated based on their size and granularity (SSC-A/FSC-A), duplets were discriminated (FSC-H/FSC-A), and final gate was set based on eGFP fluorescence (histogram).

Table 40: Data collection and refinement statistics. Highest-resolution shell statistics are given in parentheses.

	HLA-B*44:05
Wavelength	0.976
Resolution range (Å)	54.8 - 1.3 (1.4 - 1.3)
Space group	$P2_12_12_1$
Unit cell dimensions (Å)	a = 50.70, b = 81.95, c = 109.95
Total reflections	177025 (1233)
Unique reflections	88539 (619)
Multiplicity	2.0 (2.0)
Completeness (%)	81.0 (6.0)
Mean I/sigma(I)	16.50 (1.04)
Wilson B-factor	14.57
R-merge	0.02755 (0.6323)
R-meas	0.03896 (0.8942)
CC1/2	0.999 (0.407)
CC*	1 (0.761)
Reflections used in refinement	88537 (618)
Reflections used for R-free	4389 (27)
R-work	0.1519 (0.2494)
R-free	0.1877 (0.3152)
CC(work)	0.969 (0.760)
CC(free)	0.957 (0.547)
Number of non-hydrogen atoms	3634
macromolecules	3150
ligands	4
Protein residues	382
RMS(bonds)	0.006
RMS(angles)	0.85
Ramachandran favored (%)	99.00
Ramachandran allowed (%)	1.30
Ramachandran outliers (%)	0.00

Rotamer outliers (%)	1.2
Clashscore	3.1
Average B-factor	21.32
macromolecules	18.56
ligands	164.41
solvent	38.23

13 Abbreviations

Å	Ångström
ABC	ATP-binding cassette
APS	ammonium persulfate
BCR	B-cell receptor
BiP	binding immunoglobulin protein
β_2m	β_2-microglobulin
C	Celsius
CTL	cytotoxic T lymphocyte
Crt	calreticulin
CYMAL-5	5-cyclohexyl-1-pentyl-β-D-maltoside
DC	dendritic cell
ddH_2O	purified water
DMF	dimethylformamide
DMSO	dimethyl sulfoxide
DNA	deoxynucleoside triphosphate
DRiPs	defective ribosomal products
eGFP	enhanced green fluorescent protein
E	eluate
ESI	electrospray ionization
EDTA	ethylenediaminetetraacetic acid
EGTA	ethylene glycol-bis(2-aminoethylether)-N, N, N', N'-tetra acetic acid
EM	electron microscopy
Endo H	Endoglycosidase H
ER	endoplasmic reticulum
ERAP	ER-associated amino peptidase
ERp57	ER thiol oxidoreductase
ERGIC	ER-Golgi intermediate compartment
FACS	fluorescent-activated cell sorting
FCS	fetal calf serum
FT	flow through
Glc	glucose
GlcNAc	N-acetylglucoseamine
h	hour
hc	heavy chain
HEPES	(4-(2-hydroxyethyl)-1-piperazineethanesulfonic acid
HLA	human leucocyte antigen
HOBt	hydroxy benzotriazole monohydrate
HPLC	high-performance liquid chromatography
Ig	immunoglobulin
IMAC	immobilized metal ion affinity chromatography
IMDM	Iscove Modified Dulbecco media
IPTG	isopropyl-β-D-1-thiogalactopyranoside
IRES2	internal ribosomal entry site 2
ITC	isothermal titration calorimetry
kDa	kilo Dalton
LB	Luria-Bertani

LC	liquid chromatography
LILBID	laser induced liquid bead ion desorption
M	molar
MALDI	matrix-assisted laser desorption/ionization
Man	mannose
MHC	major histocompatibility complex
MW	molecular weight
µ	micro
min	minute
ml	milliliter
MMS	microseed matrix screening
MS	mass spectrometry
NBD	nucleotide binding domain
NK cell	natural killer cells
NMR	nuclear magnetic resonance
2-NPA	Fmoc-2-nitro-L-phenylalanine
OD	optical density
OST	oligosaccharyltransferase
PAGE	polyacrylamide gel electrophoresis
PAMP	pathogen-associated molecular pattern
PBS	phosphate-buffered saline
PCR	polymerase chain reaction
PDB	protein data bank
PDI	protein disulfide isomerase
PEG	polyethylene glycol
PEG 500 MME	polyethylene glycol methyl ether 500
PLC	peptide loading complex
pMHC I	peptide bound MHC I
PMSF	phenylmethanesulfonylfluoride
PNGase F	Peptide-*N*-Glycosidase F
PRRs	pattern recognition receptors
RP	reverse-phase
RT	room temperature
S-Anp	*S*-3-(Fmoc-amino)-3-(2-nitrophenyl) propionic acid
SDS	sodium dodecyl sulfate
SEC	size exclusion chromatography
*Sf*21	*Spodoptera frugiperda 21*
SLIC	sequence and ligation independent cloning
SN	supernatant
TAE	Tris-acetate-EDTA
TAP	transporter associated with antigen processing
TAPBPR	TAP-binding protein related
TCR	T-cell receptor
TEMED	tetramethylethylenediamine
TEV	tobacco etch virus
TFA	trifluoroacetic acid
TIPS	triisopropylsilane
TMD	transmembrane domain

TOFMS	time of flight mass spectrometry
Tricine	((1,3-dihydroxy-2-(hydroxymethyl) propan-2-yl) amino) acetic acid
Tris	2-amino-2-(hydroxymethyl) propane-1,3-diol
Tsn	tapasin
UGGT1	uridine diphosphate (UDP)-glucose:glycoprotein glucosyltransferase 1
UPLC	ultra-performance liquid chromatography
UPS	ubiquitin proteasome system
UV	ultraviolet
v/v	volume/volume
W	wash sample
WCE	whole cell extract
w/v	weight/volume
X-Gal	5-bromo-4-chloro-3-indolyl-β-D-galactopyranoside
YFP	yellow fluorescent protein

14 Danksagung

An erster Stelle danke ich meinem Doktorvater Prof. Dr. Robert Tampé für die Chance an diesem spannenden und interessanten Projekt mit arbeiten zu dürfen. Insbesondere bedanke ich mich für die zielorientierte Unterstützung, die es mir ermöglicht hat, mich rasch einzufinden und meine Potenziale zu entwickeln.

Bei meiner Zweitgutachterin Prof. Dr. Nina Morgner bedanke ich mich sowohl für die Evaluierung meiner Arbeit, als auch für das Monitoring im Rahmen von CLiC und für die schöne Zusammenarbeit.

Mein besonderer Dank gilt Dr. Simon Trowitzsch, der mir kein besserer Begleiter hätte sein können. Ich bedanke mich vor allem für die geduldige und ausgezeichnete fachliche Unterstützung in der Theorie und in der Praxis an der Bench.

Weiterhin bedanke ich mich bei den Mitarbeiter*innen des Europäischen Laboratoriums für Molekularbiologie (EMBL) innerhalb des Deutsch Elektronen-Sychrotron (DESY, Hamburg, Germany) und denen des Paul-Scherrer-Institutes (PSI) an der Synchrotron Lichtquelle Schweiz (SLS, Villigen, Switzerland) für die Unterstützung während der Messzeiten.

Ich bedanke mich auch bei Dr. Robbert M. Spaapen für die Bereitstellung der Wildtyp und der Tapasin-defizienten HAP1 Zellen.

Renate Guntrum danke ich für den täglichen Austausch, der nicht ausschließlich die Arbeit beinhaltete, sondern auch sehr persönlich war.

Ich danke Dr. Christoph Thomas und Dr. Lukas Susac für ihre fachlich wertvollen Ratschläge und Lukas Susac besonders für seine Positivität im Laboralltag.

Bei allen aktuellen und ehemaligen Mitarbeiter*innen der Arbeitsgruppe bedanke ich mich für die schöne produktive gemeinsame Zeit. Bei Christian Winter, dem „Peptid-Flüsterer“, möchte ich mich für die große Hilfsbereitschaft, die Unterstützung bzw. Reparaturen an dem Melody und die zahlreichen LC-MS Messungen bedanken.

Gerne bedanke ich mich bei Lina Sagert, meiner Lieblingskollegin Linii, für die schöne und unkomplizierte Zusammenarbeit und Unterstützung.

Bei Max Löffler bedanke ich mich für sein stets offenes Ohr, seine fachlichen Ratschläge insbesondere bezüglich der weiten Welt der Peptide und nicht zuletzt für die Einführung in das Züchten von Tomaten.

Des Weiteren danke ich den Mitgliedern des Labors 123, den Immunogirls, Jamina Brunnberg und Martina Barends, und Sami, Samoil Sekulovski, für eine tolle Nachbarschaft und ihre

fachlichen Ratschläge. Bei Jamina Brunnberg bedanke ich mich außerdem für ihren Einsatz, das Melody zu reparieren und in dem Zusammenhang für die vielen gemeinsamen Stunden am Melody.

Weiterhin bedanke ich mich bei meinen Mitstreitern Holger Heinemann, auch bekannt als Holgi, und Alexander Domnick für die schöne gemeinsame Zeit.

Nicht zu vernachlässigen sind Dr. Sunesh Sethumadhavan, Dr. Andreas Blees, Dr. Stefan Brüchert, Dr. Heike Krüger, Phil Höllthaler, Bianca Hetzert, Dr. Tim Diederichs, und Michael Urban deren Erfahrungsreichtum ebenfalls unverzichtbar für mich war.

Außerdem danke ich Kerstin Zehl für die persönliche Unterstützung.

Bei Andrea Pott und Inga Nold bedanke ich mich für ihren Beistand bei bürokratischen Angelegenheiten und einer immer offenen Tür.

Zu guter Letzt bedanke ich mich herzlich bei meiner Familie und meinem Freund Dusti für die großartige und bedingungslose Unterstützung während der großen Reise durch die Promotion.